A PARAMETRIC STUDY OF VORTEX-INDUCED VIBRATION OF A LONG FLEXIBLE MARINE RISER

ANUP GHIMIRE

A
Parametric Study
of
Vortex-Induced Vibration
of
A Long Flexible Marine Riser

By
© Anup Ghimire

A thesis submitted to the School of Graduate Studies
in partial fulfillment of the requirements for the degree of
Master of Engineering

Faculty of Engineering and Applied Science
Memorial University of Newfoundland

March 2008

St. John's Newfoundland Canada

Abstract

This thesis describes a parametric study of vortex induced vibration (VIV) on a marine riser, subjected to uniform and sheared flow. Raman-Nair and Baddour (2003), has developed a program that simulates the riser dynamics based on a time domain analysis. A parametric study was carried out, taking the code as a bench mark. The riser was simulated using lumped masses, connected by springs that model the riser's properties. This study proceeds by validating the code against the analytical proof and the experimental results.

Force coefficients, drag and lift force primarily, were taken as the important parameters to study their effect upon the riser structural responses in terms of maximum bending moment, tension, tensile stress, and displacements. Other factors such as internal fluid flow and movement of riser top-end were also considered for the case where riser was subject to sheared flow. A certain configuration of riser was chosen with certain material properties. A steel catenary riser with an un-stretched length of 3000 meters was pinned at both ends and immersed in 2500 meters water depth with an outer and inner diameter of 0.5m and 0.4 m respectively.

Design of Experiment (DOE) methodology was adopted for this parametric study. Full factorial and half fractional factorial designs were carried out for uniform and sheared flow respectively. Studies showed the drag force coefficients affected the in-line displacement and the lift force coefficient affected the cross-flow displacement. The maximum tension and maximum tensile stress on riser segments, all were affected by the internal fluid flow. The change in the position of the top end of riser reduced the bending moment and increased the tension and tensile stress. After identifying the significant parameters, magnitudes of the parameters were changed within the expected ranges, to determine if responses of the riser were varied by significant amount which would help in the riser analysis and design.

Acknowledgements

I would like to take this opportunity to thank my supervisors, Dr. Neil Bose, Dr. Wayne Raman-Nair and Dr. Wei Qiu for providing me guidance during the research period. Also, I am grateful to my brother Sandesh Ghimire and friends especially, Doris Hans as well as colleagues for their support and guidance directly and/or indirectly. Finally, I would like to thank my family, who constantly encourages me in every step.

CONTENTS

List of Figures

List of Tables

List of Symbols

a	horizontal length of the cable
b	vertical height of the cable
A_e	cross-sectional area of cylinder
D	diameter of the cylinder
C_D	drag force coefficient
C_{Dmean}	mean drag force coefficient
C_{DN}	normal drag force coefficient
C_{Do}	oscillating drag force coefficient
C_d	damping coefficient
C_L	lift force coefficient
C_m	added mass coefficient
C_M	inertia coefficient
C_{DT}	tangential drag force coefficient
E	modulus of elasticity
f	forcing force frequency
$f(s)$	load component
f_s	shedding frequency
F_d	total drag force
$F_{drag\ N}$	normal drag force
$F_{drag\ T}$	tangential drag force
F_L	total lift force
f_n	Strouhal natural frequency
g	acceleration due to gravity
H	horizontal load

I	moment of inertia
kL	flexibility factor
l	length of riser segments
L	total deformed length of cable
m	mass of the cable
n	number of lumped masses
n_1, n_2, n_3	unit vectors
$\vec{n}$	unit normal vector
P_0	bottom end of the riser
P_n	top end of the riser
R	radius of curvature
Re	Reynolds number
s	arc length of the cable
S	Strouhal frequency
$\vec{t}$	unit tangential vector
T	top-end tension on the riser
U	flow velocity
V	vertical load
V_n	normal velocity of velocity
V_t	tangential component of velocity
w	self weight of the catebary riser
$d\theta$	angle between arcs
ω_s	angular frequency
ds	arc length
σ_k	bending stiffness of the cable
$w\cos\theta$	component of self weight on catenary riser
$\dot{v}$	cylinder acceleration
ϕ	cylinder diameter
v	cylinder velocity

ζ	damping ratio
$\dot{u}$	fluid acceleration
ρ	fluid mass density
u	fluid velocity
υ	kinematic viscosity
V_r	reduced velocity
ϕ	phase angle between force coefficient and displacement of structure
σj	spring stiffness

Chapter 1

Introduction and Overview

1.1 Introduction

A major aim of the oil and gas industry is to deliver fluids from subterranean sources to the surface at the lowest costs while remaining compatible with the constraints imposed by technology and the environment. Despite many continuing developments, these constraints are somewhat related, which leads to the need of addressing complex and poorly understood problems. Those problems have direct and/or indirect effects on the design of the structures and the effective cost of the whole operating system.

One of the challenges of the offshore industry has been identified in underwater and riser systems. The most important challenges are to effectively predict the dynamical response of offshore marine-risers and under-sea pipelines to fluid dynamic forces. These slender structures experience both current flow and top-end vessel motion, and the internal fluid carried by the pipe. The flow-structure relative motion produces oscillatory drag and lift forces on the structures. When the frequency of vortex shedding approaches the structural natural frequency of the risers (this synchronization of frequencies is called 'lock-in'), vortex-induced vibration occurs with possible high dangerous amplitudes that may lead to the failure of the risers. For a fixed rigid circular cylinder, the vortex shedding frequency is a function of the Reynolds number only. For a flexible and/or moving cylinder like a marine riser, the fluid interacts strongly with the riser motion, and the vortex shedding frequency is controlled by the body frequency over a wider range of flow speed [Bearman, 1984].

Marine risers are widely used in various offshore activities such as ocean thermal energy conversion (OTEC), deep-sea exploration, and oil exploration and production. As the ocean resource developments are moving toward much deeper seas, the dynamics of a long slender marine riser is now becoming more important than ever. These slender and

long marine risers for ultra-deep water developments may be highly flexible due to the increased length to diameter ratio, so their dynamic motions induced by various external loads become more complex. Thus it is necessary to carry out more exact dynamic analyses and experiments for understanding the behavior of a long flexible marine riser.

Vortex-induced vibration of marine risers has been receiving increasing interest from industry and academics. Due to the large demand for crude oil in the world, offshore oil and gas exploration has been moving into deeper water regions. This requires greater length of marine risers. As a result, they encounter a complex environment of high velocity and non-uniform currents, large and non-uniform tension forces and vortex induced vibration caused by the current forces and high tension. In addition, VIV of a structure is one of the most important dynamic responses caused by the flow past it, and results in wide dynamic behaviors [Panton, 1996]. This underlines the importance of understanding vortex dynamics that give rise to the different body responses. Regular vortices are formed in the wake, which interact with the cylinder motion and form the main sources causing cylinders (elastically mounted) to vibrate due to vortex dynamics, when shed from the cylinder.

Deepwater risers are especially susceptible to VIV for the following reasons:

1) Currents can be higher in deepwater areas than the shallower areas
2) Natural frequency is lowered with the increase in the length of the riser, which in turn reduces the magnitude of current required for VIV
3) Deepwater platforms are usually floating, so there are no other structures adjacent to the riser to which it could be clamped (figure 1.2 a).

Since deepwater currents usually change their magnitude and direction with depth, a possibility may exist that multiple modes of riser can be excited into VIV. This makes deepwater riser prediction more complex than that of the short riser spans, typical of fixed platforms in shallow water.

1.2 Vortex-induced vibration prediction

An accurate estimation of the fatigue life of a deepwater riser experiencing vortex induced vibration depends critically upon an accurate estimation of the response amplitude and frequencies (or mode numbers). Accurate estimations of the response amplitude and mode numbers are, in turn, dependent upon several 'basic' parameters, which include:

a) the current profile, both magnitude and shape variation with depth
b) the frequency and magnitude of the lift force imparted to the riser by vortex shedding
c) the excitation and correlation length (defined below) of the lift forces and vortex shedding
d) the hydrodynamic damping and
e) the structural properties of the riser including damping, mass, tension, bending stiffness and the cross sectional geometry (including surface roughness)

These parameters, in turn, define other useful parameters including the vortex shedding frequency (defined as $f_s = \frac{U * S}{D}$, where f_s is the vortex shedding frequency, U is the local current velocity, D is the riser outside diameter, and S is a proportionality constant called the Strouhal number which is dependent upon other parameters but is generally about 0.2). Other parameter includes the Reynolds number (defined as $Re = \frac{U * D}{\upsilon}$ where υ is the kinematic viscosity) and the reduced velocity ($V_r = \frac{U}{f_n * D}$ where f_n is the Strouhal natural frequency). Basic parameters are in turn, affected by each other. For example, the lift force is dependent upon parameters such as Re, the free stream turbulence, the correlation of the vortex shedding, and the surface roughness. Vortex shedding in the turbulent wake regime (i.e. Re>200) occurs in cells along the length of the cylinder. Shedding does not occur uniformly along the length of the cylinder, but

rather in cells as shown in figure 1.1. Consequently, the maximum resultant force (as cells along the length of the cylinder are out of phase) acting on the cylinder over its total length may be smaller (or larger depending upon location of cell) than the force acting on the cylinder over the length of a single cell [Fredsoe and Sumer, 1997]. The average length of the cells may be termed the *correlation length*. The lift force is highly dependent upon the cylinder amplitude and mode(s) of response, making VIV prediction a non-linear process requiring iteration between the lift force description and the response.

Figure 1.1: Formation of shedding in a cell in turbulent wake

VIV is perhaps more sensitive to the current profile than any other parameter [Allen, 1998]. For short riser spans, the current magnitude determines whether or not VIV will occur (including other factors such as reduced mass, damping and structural frequency) and determines whether the response is in-line or transverse to the flow direction (or both). For deepwater risers, a very low current will at least theoretically produce some VIV due to the low natural frequency of the riser in bending. The variation of the current along the riser span (i.e. with the depth) then determines which modes will be present in the response. In general, current profile is varied during the analysis to determine the sensitivity of the results to current profile shape. It is possible that even if numerous modes are potentially excited by a current profile (typically of a deepwater riser in a significant current), a single mode (or a small number of modes) can dominate the response due to 'lock-in' in which the vortex shedding tends to adjust to the vibration frequency within certain limits (dependent upon mass ratio and Reynolds number). Allen (1998) discovered that even in a highly sheared current, it is possible for a single mode (or small number of modes) to dominate the response.

The hydrodynamic damping, which is of course dependent upon the current profile, can be very large, relative to the structural damping, for a deepwater riser. This is especially

true when the excitation length is only a fraction of the riser length. Accurate estimation of hydrodynamic damping (and for that matter, added mass) for VIV analysis is quite difficult. This is partly due to the fact that lift forces are coupled to the amplitude and frequency of vibration.

Damping computations are also complicated by the difficulty in determining where along the riser damping is present. There are regions where it is obvious that either excitation or damping must be present (e.g., near the bottom, the current may be negligible so that still water damping is most probably present), and there are also significant regions where it is unclear [Allen, 1998].

The riser structural properties determine the set of natural frequencies and mode shapes of the riser in bending. The natural frequencies are typically proportional to the tension and bending stiffness while inversely proportional to mass and length. The mode shape is affected by the variation in tension along the riser length, which is due to the submerged weight, with the node-to-node spacing being larger in high-tension regions. This means that if a negatively buoyant (heavier than water) riser has a constant VIV amplitude with depth, the highest curvature will be near the bottom of riser (because the node-to-node spacing is shorter in this area, illustrated by figure 1.2 (b)). For deepwater risers, the structural damping is usually small relative to the hydrodynamic damping and therefore does not usually significantly influence the response. Even risers known to have large structural damping, such as risers made of flexible pipe, can still experience substantial VIV despite the minimal consequences of VIV on these types of risers.

The riser cross-section is another parameter that affects the lift force, since the boundary layers are affected by even small changes in the cross section, such as the presence of marine growth. It should be noted that most practical marine risers are rough enough to cause a significant increase in the drag coefficient.

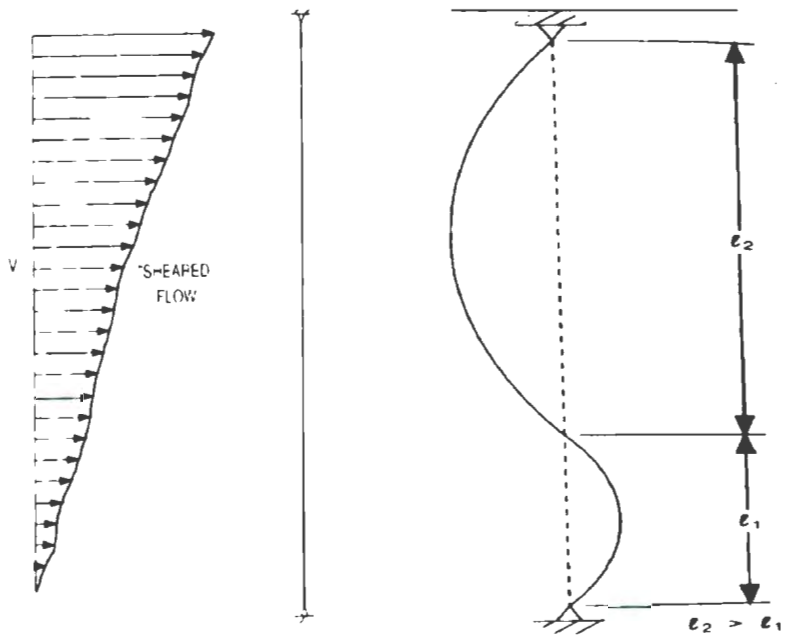

a) b)

Figure 1.2: a) Deepwater riser exposed to sheared current b) Mode shape for a riser heavier than water

The flow in the wake of a vibrating cylinder is a system that depends strongly on the frequency and amplitude of the oscillation. This flow has been the subject of many papers, far too many to cite here [refer to review articles by Sarpkaya (2004), Bearman (1984) and Williamson and Govardhan (2004)]. Despite the large volume of such experimental data, a systematic investigation that relates the variation of the hydrodynamic forces to the flow patterns in the wake is missing. Numerical investigation of the flow past an oscillating cylinder at low Reynolds number has been done by, among others, Blackburn and Henderson (1999), Anagnostopoulos (2000), Baek (2001), Blackburn (2001) and Guilmineau and Queutey (2002), but for a very limited number of frequencies and amplitudes of oscillation, not sufficient to offer a picture of the dependence of the forces on these parameters.

The fluctuating lift is dominated by the actions from the periodic phenomenon called vortex shedding, which is the principal source of cross-stream flow-induced vibration and acoustic emissions [Blake, 1986]. The fluctuating lift is mainly due to the fluctuating

pressures acting on the surface of the cylinder [Drescher, 1956; Kwon and Choi, 1996]. Except for the rearmost part of the cylinder, the pressure fluctuation energy is concentrated in a band around the mean shedding frequency f_s [Sonneville, 1976; Norberg, 1986]. The alternate periodic shedding causes pressure fluctuations at around f_s to be essentially out-of-phase between the upper and lower side of the cylinder [Gerrard, 1961; Ferguson and Parkinson, 1967], i.e., the lift fluctuation energy is concentrated in a band around f_s. The amplitudes of fluctuating drag, which are significantly smaller than the fluctuating lift [Bouak and Lemay, 1998; Posdziech and Grundmann, 2000], are dominated by fluctuating pressures that are in-phase between the upper and lower side of the cylinder, which in turn, are concentrated at very low frequencies and a band around two times f_s [Sonneville, 1976]. Mainly due to vortex shedding, (basically as an effect of frictional forces), the cylinder also experiences a fluctuating torque around its axis. Even for relatively low Reynolds numbers in the laminar shedding regime ($Re \geq 47$ to 190), the fluctuating torque appears to be of minor importance [Jordan and Fromm, 1972; Lecointe and Piquet, 1989].

The very first measurement of fluctuating lift on a circular cylinder in a continuous fluid stream was carried out by Drescher (1956), who recorded the sectional wall pressure distribution around the cylinder as a function of time in a flow of water for Re 1.1×10^5. Since this pioneering work, a vast amount of quantitative data has been reported and numerous compilation graphs on the variation of lift-related coefficients with Reynolds number have been presented, e.g. [Blevins, 1990], [Ribeiro, 1992], [West and Apelt, 1993] and [Blackburn and Melbourne, 1996]. Despite these efforts, there has been no real consensus on fluctuating forces with respect to the Reynolds number. This gap of knowledge reflects basic difficulties encountered in numerical simulations and experiments. This has created a problem in riser design and experiments.

1.3 Objectives of the thesis

During the literature review, only a very few papers were found that discuss the force coefficients for risers. Since VIV leads to alternating lift forces and drag force, understanding these forces is really important for the design and its analysis. Researchers have come to different conclusions for the magnitudes of force coefficients, depending upon their setups in the experiment and the assumptions made during the analysis. So, this creates a problem for riser designers to make a proper selection of the force coefficients magnitudes for analysis. Questions may arise, if selection of the magnitudes of force coefficients affects the structural behavior and design of the riser. This research is an effort to answer effectively whether or not force coefficients have a significant effect on the riser responses during VIV. It tries to characterize the fluid-structure phenomenon with the help of force coefficients, and reveal their effect upon the riser responses during the VIV, without carrying out a computational fluid dynamics (CFD) analysis. CFD uses numerical methods and algorithms to solve and analyze problems that involve fluid flows. The fundamental basis of any CFD problem is the Navier-Stokes equations, which define any single-phase fluid flow. The most fundamental consideration in CFD is how one treats a continuous fluid in a discretized fashion on a computer. One method is to discretize the spatial domain into small cells to form a volume mesh or grid, and then apply a suitable algorithm to solve the equations of motion (Euler equations for inviscid, and Navier-Stokes equations for viscous flow).

It is costly and often not feasible to perform a full -scale experiment on marine risers. Therefore, most researchers have put their effort into the numerical simulation to calculate the vibrational effects. Many programs have been created to simulate VIV, most use the modal analysis method where the measured vibration is separated into different frequency modes. However, there is a considerable error between the predictions of marine riser VIV fatigue damage by computer models and observed damage, by orders of magnitude [Trim, 2005]. In this work a simulation was carried out for this parametric study of VIV on a marine riser of typical configurations, subjected to uniform flow and sheared flow. The equations of the three dimensional motion of a marine riser undergoing

large elastic deformations were formulated using Kane's formalism [Raman-Nair and Baddour, 2003]. The equations were solved using a robust implementation of the Runge-Kutta method provided in MATLAB. Riser responses were measured from the simulation, which were further analyzed using the Design of Experiment methodology, which determines the significant factors to affect the riser responses. Once the significant factors were identified in affecting the riser responses, parameters were changed over an expected range to see if any rotable changes existed in the riser responses. Riser responses were measured in terms of maximum bending moment, maximum tension and tensile stress, cross-flow and in-line displacements. Ranges of selected parameters were described as low level and high level.

1.4 Layout of the thesis

The first chapter gives an introduction to the concepts and terminologies relevant to the present work. Chapter two describes the physics of vortex-induced vibration and the forces on a cylinder. Chapter three gives the description of the riser model used in the code. It also describes the methods to validate the code. Time domain analysis was adopted to address the non-linearities (because of the drag forces along the riser length) of the VIV. Chapter four describes the Design of Experiment methodology, for identifying the significant parameters affecting the riser responses. Chapter five discusses the results and discussions from the analysis, and presents the summary of riser response with the variation of the parameters within the expected ranges. Conclusions and recommendations are given in chapter six.

Chapter 2

Vortex-Induced Vibration

2. 1 Introduction

Vortex-induced vibration (VIV) of structures is of practical interest to many fields of engineering, such as heat exchanger tubes, riser tubes that carry oil from the seabed to the surface, civil engineering designs (as in bridges, chimney stacks), as well as design of marine and land vehicles.

As the fluid speed past a cylindrical section is increased, the flow changes from un-separated laminar flow to turbulent vortex flow. In a fluid current, alternating vortices will develop on the circular cylinder, at a certain frequency, called the vortex shedding frequency, which can excite the structure in one or more of its natural frequencies. When the vortices are not formed symmetrically around the body (with respect to its midplane), different lift forces develop on each side of the body, thus leading to a motion which is transverse to the flow. This motion changes the nature of the vortex formation in such a way as to lead a limited motion amplitude (differently, then from what would be expected in a typical case of resonance). Due to the 'lock-in' effect, the correlation length (may increase depending on setup) and vortex strength increases.

A non-dimensional quantity describing the flow around a smooth circular cylinder depends on the cylinder Reynolds number, defined as:

$\mathrm{Re} = \frac{D * U}{\upsilon}$, where D - diameter of the cylinder

U -velocity of the fluid

υ - kinematic viscosity

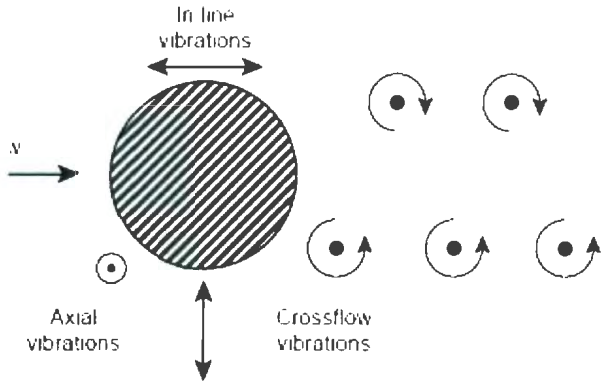

Figure 2.1: Vibrations of a cylinder submitted to vortex shedding

The flow undergoes tremendous changes as the Reynolds number increases. The flow pattern around a stationary cylinder has been investigated by several researchers [Bloor, 1964; Gerrard, 1978; Schewe, 1983; and Williamson, 1988] using flow visualization techniques. Figure 2.2 shows schematically the flow pattern for some flow regimes for smooth circular cylinders. Effects, such as the surface roughness, the cross-sectional shape, the incoming turbulence, and the shear in the incoming flow, influence the flow. For the range of the Reynolds number $40<Re<200$, the vortex street is laminar. The shedding is essentially two-dimensional, i.e. it does not vary in a span wise direction, [Williamson, 1989]. With further increase in Re, transition to turbulence occurs in the wake region (for $Re>300$). The region of transition to turbulence moves towards the cylinder as Re is increased in the range of $200<300$ [Bloor, 1964]. Bloor (1964) reports that at Re=400, the vortices, once formed, are turbulent. Gerrard (1978) and Williamson (1988) state that the two-dimensional feature of the vortex shedding becomes distinctly three-dimensional for the regimes of $Re>300$. However, except for very small Reynolds numbers ($Re\leq40$) there is one feature of the flow which is common to all the flow regimes, namely the vortex shedding. In the narrow Re band $3x10^5<3.5x10^5$ (called the critical regime) the boundary layer becomes turbulent at one side of the cylinder and laminar at the other side, which causes a non-zero mean lift on the cylinder (figure2.2). The side at which the separation is turbulent switches from one side to the other

occasionally [Schewe, 1983]. Therefore the lift changes direction as the one-sided transition to turbulence changes side, shifting from one side to the other.

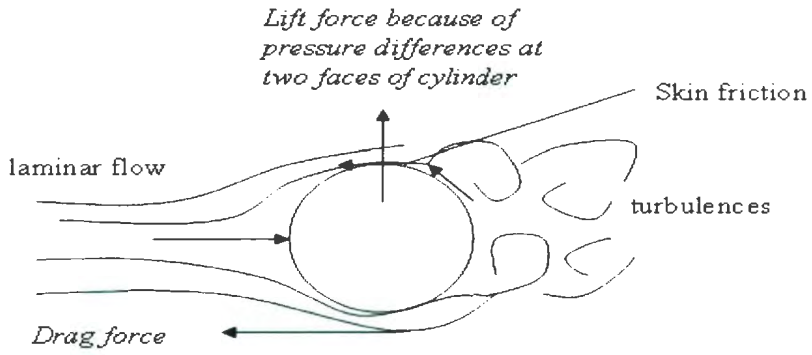

Figure 2.2: Formation of drag force and lift force on a cylinder

As a consequence of the vortex-shedding phenomenon, the pressure distribution around the cylinder undergoes a periodic change as the shedding progresses, resulting in a periodic variation in the force components on the cylinder. The magnitude and occurrence of sustained oscillations strongly depend on the lift coefficient of the stationary body.

Re<5
No separation and creeping flow

5<Re<40
A fixed pair of symmetric vortices.

40<Re<200
Laminar vortex shedding.

200<Re<300
Transition to turbulence in the wake.

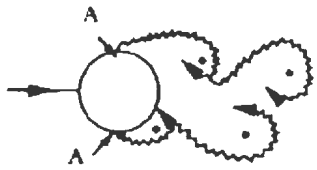

$300<Re<3x10^5$
Wake completely turbulent.
A: Laminar boundary separation.

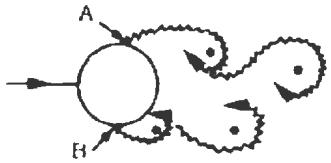

$3x10^5<Re<3.5x10^5$
B: Turbulent boundary layer separation
A: Laminar boundary layer separation

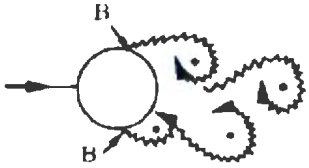

$3.5x10^5<Re<1.5<10^6$
B: Turbulent boundary layer separation; the boundary Layer partly laminar partly turbulent

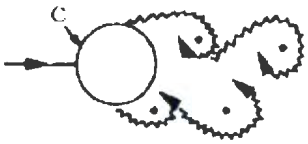

$1.5x10^6<Re<4x10^6$
C: Boundary layer completely turbulent at one side

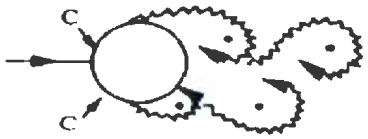

$4x10^6<Re$
C: Boundary layer completely turbulent at two sides

Figure 2.3: Regimes of flow around a smooth, circular cylinder in steady current
[based on Sumer and Fredsoe, 1979]

2.2 Forces on a cylinder in a steady current

If the structure is flexible and lightly damped internally, the resonant oscillations can be excited normal or parallel to the incident flow direction [Griffin, 1998]. A resultant unsteady fluid force, which is generated on a cylindrical structure, as a consequence of vortex shedding, described by Griffin (1980), can be divided into several components:

a) An exciting component of the lift force, by which energy is transferred to the structure

b) A reaction or damping force, which is exactly out-of-phase with the structure's velocity, and is a function of relative velocity between fluid and structure

c) An 'added mass' force, which is exactly out-of-phase with the structure's acceleration

d) A flow induced inertial force, which is exactly out-of-phase with the structure's acceleration.

These various contributions to the total force can be deduced from the total hydrodynamic force, as reported by Sarpkaya (1979), or the various components can be deduced individually as reported by Griffin (1980).

Hydrodynamic loads on a small-diameter submerged object such as a riser can be calculated using Morison's equation. Basically, if the cylinder (or a riser) is moving laterally with the velocity (v) and acceleration ($\dot{v}$), in a fluid stream that itself is moving with velocity (u) and acceleration ($\dot{u}$), then Morison's equation for the hydrodynamic force per unit length acting on the riser (or cylinder) can be written in two ways:

$$f(x) = \frac{1}{2}\rho C_D \phi (u - v)|u - v| + \rho A_c \dot{u} + (C_M - 1)\rho A_c (\dot{u} - \dot{v}) \quad \text{.....2.2.1}$$

or

$$f(x) = \frac{1}{2}\rho C_D \phi (u - v)|u - v| + C_M \rho A_c \dot{u} - (C_M - 1)\rho A_c \dot{v} \quad \text{..... .2.2.2}$$

where ρ is the fluid (mass) density, C_D is the drag coefficient, ϕ is the cylinder (or riser) diameter, C_M is the inertia coefficient, and A_c is the riser external cross-sectional area.

The first right-hand term of equations (2.2.1) and (2.2.2) represents the drag force, and the last two make up the inertia force. The term $(C_M - 1)\rho A_c$ is frequently termed the *added mass* for convenience, since it has the units of mass and the same acceleration as the riser itself. In the literature, $(C_M - 1)$ is often given the symbol C_m and is called the *added-mass coefficient.* The value of C_M is typically close to 2. Hence, C_m is typically close to 1.

The force on an element of a riser, as given by Morison's equation, can be considered to be the resultant of three dynamic pressure fields, which have to be superimposed on the static pressure field. The four pressure fields stated by Sparks (2007) can be summarized as follows:

a) The static pressure field (as has been described by Archimedes)

b) The dynamic pressure field in the fluid in the absence of a riser (represented by the middle term in equation (2.2.1)

c) The pressure field resulting from the presence of the riser and *the relative acceleration* of the flow with respect to it (the last term of equation (2.2.1)

d) The pressure field resulting from the disturbed flow relative to the riser, treated as if it was of constant velocity (the first term of equation (2.2.1).

However, Morison's equation may not be practical in use because the drag force is non-linear. When the flow is not perpendicular to the structure (riser) axis, which is the case in general, then the drag force can be evaluated in the direction of the flow and then resolved into components perpendicular and parallel to the riser axis. Also, the flow velocity can be resolved into components perpendicular and parallel to the riser axis, as an alternative solution for the evaluation of the force components.

Forces acting on the cylinder, mainly, the in-line direction (the drag force), and a non-zero force component in the transverse direction (the lift force), vary periodically with time. The drag force changes periodically over time, oscillating around the mean drag. The lift force occurs at the Strouhal frequency f_s, while the fluctuating drag force has a frequency of $2f_s$. In the case of a forced oscillation, synchronization of the two sets of forces occur when the forcing frequency, f, of the cylinder approaches the Strouhal frequency f_s, i.e. the system of cylinder and wake, oscillates at the imposed frequency f of the cylinder only, the natural Strouhal frequency is lost. This synchronization persists over a range of frequencies which may be termed the 'range of synchronization', within which the lift and drag forces suffer changes in phase and amplitude as the imposed frequency is varied [Bishop and Hassan, 1963].

2.2.1 Mean drag force

The flow around a static cylinder will exert a resultant force. There are two contributions to this force, one from the pressure and the other from the friction. For the range of Re ≥ 10^4, the contribution of the friction drag to the total drag force is less than 2-3% [Sumer, and Fredsoe, 1997]. So, the friction drag can be omitted in most of the cases, and total mean drag can be assumed to be composed of only one component, namely from the pressure drag. Therefore the mean drag force can be described as the force acting on the cylinder due to the difference in pressure between the up and the downstream sides. The inline fluid forces are considered to be the sum of an inertial force and drag force. The inertial force is due to fluid acceleration and the drag force is associated with the relative velocity. The mean drag force is a function of the Reynolds number. Figure 2.3 presents experimental data, illustrating the variation of C_D for a static cylinder with respect to the Re number.

As seen, C_D decreases monotonously until Re reaches the value of about 300. However, from this Re number onwards, C_D assumes a practically constant value, namely 1.2 throughout the sub critical Re range (300< Re<3x105). When Re attains the value of $3x10^5$, a dramatic change occurs in C_D, and the drag coefficient decreases abruptly and assumes a much lower value, about 0.25, in the neighboring Re range, the sub critical Re range. This phenomenon, namely the drastic fall in C_D is called the *drag crisis* [Sumer, and Fredsoe, 1997].

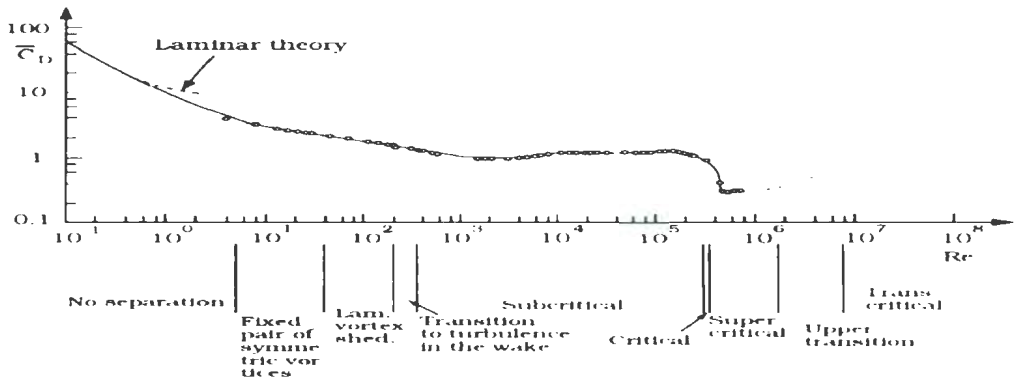

Figure 2.4: Drag coefficient for the smooth static cylinder as a function of Re number [based on Schlichting 1979]

2.2.2 Fluctuating drag force

The fluctuating drag force is an oscillatory change in the drag which occurs at a frequency of $2f_s$. The amplitude of oscillation is not a constant set of values; it varies from one period to the next.

These two forces mean and oscillating, together account for the total drag force, and can be mathematically represented in the form of:

$$F_d = \frac{1}{2}\rho U^2 A\left(C_D + C_{D_o}\sin\left(2\omega_s t + \phi\right)\right) \quad \text{.....2.2.2.1, where}$$

U = flow velocity

A = cross-sectional area of cylinder

C_D = mean drag coefficient

C_{D_o} = fluctuating drag coefficient

$\omega_s = 2\pi f_s$

ϕ is the phase angle between force coefficient and the displacement of the structure.

2.2.3 Lift force

As stated before, the transverse force, (the lift force) oscillates at the Strouhal frequency, f_s, and can be expressed as:

$$F_L = \frac{1}{2}\rho U^2 A C_L \quad \text{.....2.2.3.1, where,}$$

C_L = lift force coefficient, expressed as $C_L = C_{L_o}.\sin\left(\omega_s t\right)$, where C_{L_o} is the oscillating lift force coefficient.

Figure 2.4 shows that the amplitude of the oscillations is not constant. It varies from one period to the other.

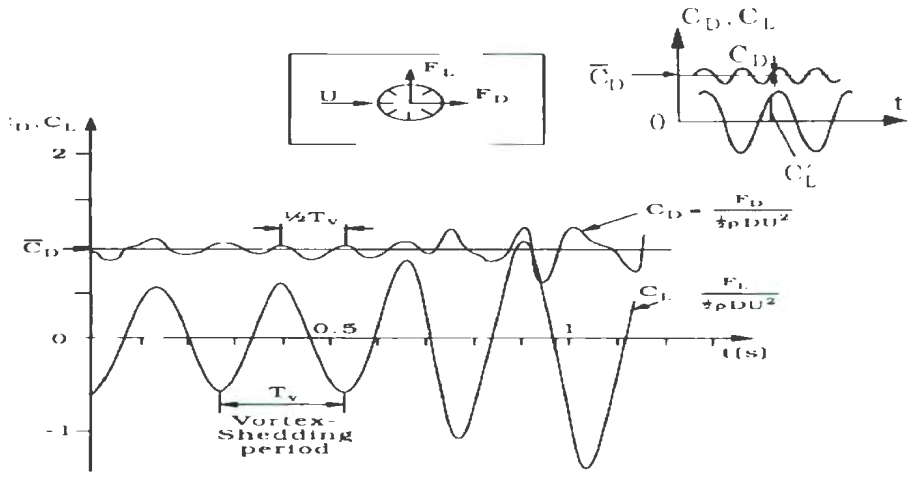

Figure 2.5: Drag and Lift forces on a cylinder

[based on Drescher, 1956]

Resulting forces (and force coefficients) during VIV are influenced by factors like the cross-section of the structure, incoming turbulence, and effect of angle of attack of flow. A non-circular cross-section may be subject to steady lift at a certain angle of attack. This is due to the asymmetry of the flow with respect to the principle axis of the cross sectional area. Schewe (1983) observed a similar kind of steady lift, even for circular cylinders in the critical flow regime, where the asymmetry occurred due to the one-sided transition to turbulence. For rectangular sections, no change in force coefficients depending on Reynolds number should be expected since the separation point is fixed at the sharp corners of the cross section. The increased level of turbulence will directly influence the boundary layer and hence its separation [Kwok, 1986]. This will obviously lead to changes in the force and therefore force coefficients.

Chapter 3

Parametric studies of VIV on a Marine riser

3.1 Marine riser

Over the last two decades, the quest for exploration and production of offshore oil has extended to deeper and more hostile water. Prime examples of such activity can be seen in the Northern North Sea and Gulf of Mexico fields [Sparks, 2007]. Floating Production Systems (FPS) offer exciting possibilities both for deep water and for marginal fields, particularly because such systems are amenable to relocation after depletion of the field.

A marine riser is a long and slender pipeline extending from a sub-sea system at the seabed to a floating vessel at the surface. It is a conductor pipe, which connects the wellhead at the seabed to a fixed (or a floating) platform, or a vessel. It may be categorized mainly as either a production riser or a drilling riser. A riser that is used to transport the crude oil from floating platforms is termed a production riser. They were first used in the 1970s with architecture inspired by that of top-tensioned drilling risers. Since then, they have taken many other forms, including bundled risers, flexible risers, top-tensioned risers (TTRs), steel catenary risers (SCRs) and hybrid risers, which are a combination of steel and flexible risers. The drilling riser of today is a low-pressure riser, open to atmospheric pressure at the top end. Drilling risers are made up of a number of riser joints, for the circulation of drilling fluids [Guesnon and Laval, 2000]. The top end of the riser is connected to the floating vessel through guides and tension regulators, to allow some freedom in axial and rotational movements, but it is constrained in lateral directions. This will restrict the top end of the riser to follow the lateral motions of the vessel. At the bottom end, the production/sales riser is connected to the blowout preventer (BOP) or to a pipeline through a flexible joint, which has mechanical design constraints/operational limits on the permissible angular motions. Drilling mud and cuttings from the borehole are returned to the surface through the riser. A BOP placed at

the seafloor between the wellhead and the riser provides protection against over pressured formations and sudden release of gas.

The primary design considerations of risers are governed by such factors as the operational limits of the riser at the surface and seabed, bending stresses and axial tension. Since the bending stiffness of the riser is small, large displacements are possible due to the wave and current loads. This gives rise to geometric nonlinearities associated with large displacements and those due to displacement dependent loadings such as drag loading arising from relative velocity effects. A non-linear time domain analysis is therefore considered necessary for a more accurate assessment of the dynamic behavior of the risers [Huse, 1996].

The initial tension in the riser has a significant influence on the dynamics of the riser and its performance. The top tension is typically 20% greater than that required to support the weight of the riser. In many cases, wall thickness and mass distribution of the riser varies along its length. In some cases, additional buoyancy is also provided at various locations along the length of the riser to maintain positive tension at the bottom flex-joint and to reduce instability (buckling) of the riser. Constant axial force is applied to the top of the riser system by means of hydraulic cylinders at the platform. If buoyancy elements are not used, the axial tension will decrease with the depth, resulting in significant bending of the riser near the bottom. The static bending moment will be developed by the steady drag on the riser itself, and by platform offsets typically caused by winds and currents.

A variety of problems are encountered in riser designs that arise mainly from structural dynamics, non-linear effects, and mechanical constraints. These may be listed as follows [Allen, 1998]:

a) Imposed motion at the top end
b) Top end boundary conditions
c) Variations in the top end tension
d) Wave loading considerations
e) Effect of current profile

f) Relative velocity effect on drag loading

g) Large displacement effects on loading and stiffness

h) Bottom end fixity conditions

Observations of marine riser response show current-induced vortex-induced vibrations (VIV) to be a widely occurring phenomenon, with a potential to cause costly and environmentally damaging fatigue failures. Figure 3.1 shows a catenary riser suspended from FPSO which touches the sea bed. The contact zone of the riser with sea bed is termed the touchdown point (TDP).

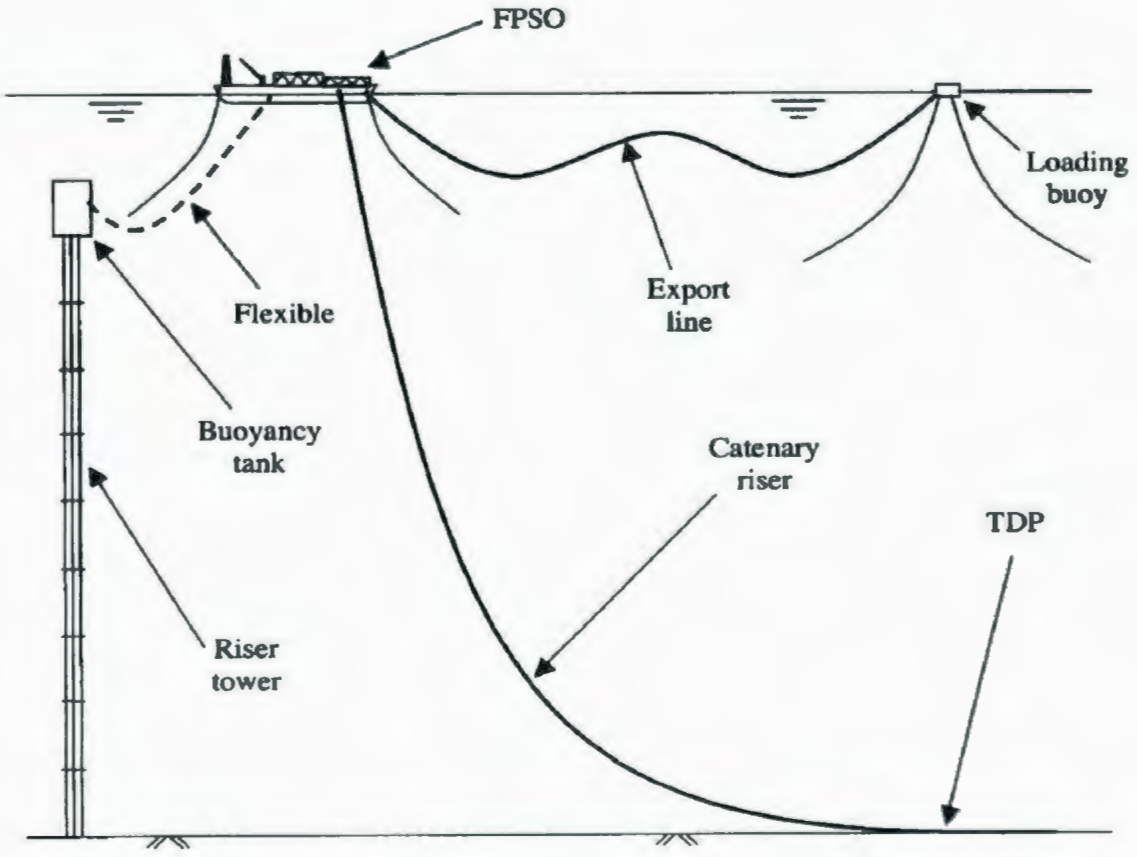

Figure 3.1: Riser towers, catenary risers, and mid-depth export lines

In the deep water of the Gulf of Mexico, West Africa and Brazil, for example, where oil and gas exploration and production continue apace, VIV may make the largest

contribution to overall riser fatigue damage [Kozicz and Newman, 2005]. Wave and vessel motion-related damage may remain at roughly the same level or even diminish as water depth increases, but currents can act over the full depth of the water column, which tends to make VIV more important in deeper water.

3.2 Method of analysis

Riser analysis has become a major interest and has drawn considerable attention, partly due to the fact that the riser is and will continue to be an important link between the floating platform and the sub-sea bore hole, and partly because the analysis itself is challenging. The analysis requires the consideration of the wave, and current forces, due to most severe as well as nominal sea states, water depth, the rig motion, and suitably defined boundary conditions [Sarpkaya, 1981].

The riser analysis may be static or dynamic. The static analysis is more concerned with the maximum riser response in a vertical plane and does not take into consideration the time-varying effects of waves, vessel motion and the inertia of the system. Various static methods adopted are: finite difference formulations [Bathe, 1974 and NESC, 1966], finite element formulations [Gosse, 1969], direct integration using a fourth order Runge-Kutta method [Burke, 1973], and assumed deflection shapes of an elastic catenary [Jones, 1975] or power series [Fischer and Ludwig, 1966].

The dynamic analysis considers the relative velocity and acceleration between the fluid and the riser, and yields a time history of the responses. Sarpkaya (1995) has outlined three methods for dynamic response analysis: deterministic time-history analysis, a steady state or a frequency-domain analysis, and a non-deterministic random vibration analysis.

A majority of the published work is based on simplified frequency domain analysis methods and some literature addresses time domain analysis methods with varying degree of sophistication. In evaluating the dynamic response of marine risers, it is

sometimes considered more appropriate to carry out the analysis in the time domain rather than in frequency domain. However, at the early stages of design, time domain analysis may prove very expensive. In a time domain analysis, the equations of motion are solved by time step integration starting from a set of initial conditions. Therefore, rounding-off errors and numerical accuracy take special significance for non-linear problems because of possible divergent solutions. Time domain analysis is quite flexible and can accommodate variations in the riser dimensions, buoyancy, boundary conditions and external time-varying loads and/or motions.

Frequency domain analysis method is well suited for computing the steady state response transfer functions of linear problems. Since the principle of superposition is implied in this method, any non-linearities (such as material, geometric nonlinearity due to large deflections), displacement dependent loading, need to be linearised. In this, the geometric nonlinearities are ignored, and the loads and stiffness of un-displaced position or in some cases, the static offset position are evaluated. The advantages of the frequency domain analysis are that one can directly apply a frequency-domain definition of the environment or ship motion to the riser and generate within a relatively short computer run, a response spectrum suitable for subsequent fatigue life estimation [Sarpkaya, 1995]. In a time domain analysis, these non- linearities can be built into the formulation.

It is costly and often not feasible to perform an experiment at the full scale on marine risers. Therefore, researchers have put their efforts into numerical simulations to calculate the vibrational effects. Many programs have been created to simulate the VIV, most use the modal analysis method, where the measured vibration is separated into different frequency modes. Of these methods, only a few are commercially available to the riser designer, including the DnV Rules and the analysis programs SHEAR7 and VIVA, both developed at MIT, ORCAFLEX, and PIPEFLOW. However, there is considerable error between the predictions of marine riser VIV fatigue damage by computer models and observed damage, by orders of magnitude [Trim, 2005]. In a numerical method, the VIV problem is solved by CFD or structural dynamics based approaches. In the former approach, an interaction between structure and fluid is analyzed by directly solving the

Navier–Stokes equations [Hong et al. 2002]. In the latter approach, VIV is solved using experimental hydrodynamic coefficients [Vandiver, and Li 1997; Grant et al. 2000].

Raman-Nair and Baddour (2003) had developed a program that simulates riser dynamics, based on a time domain analysis. The riser is simulated using lumped masses connected by springs that model the riser's properties such as bending and extensional stiffness. A lumped-mass formulation allows the flexibility of dealing with varying material properties and fluid loading along the riser's length. The number of the lumped masses can be changed, depending on the accuracy of the results required. The description of the riser model is given in the following section.

3.3 Description of the model

The riser is modeled as a hollow circular section divided into n segments S_k ($k=1...n$,) by points P_0, $P_1...Pn$, (Figure 3.2). In addition to gravity and other applied loads, the riser is subjected to hydrodynamic forces due to the ambient fluid as well as forces due to an internal flow [Raman-Nair and Baddour, 2003]. Surface waves are described by Stoke's second order wave theory. The effect of internal flow is included in the model. The detailed algorithm is presented in the paper by Raman-Nair and Baddour (2003) and the equations are solved using a robust implementation of the Runge-Kutta method provided in MATLAB. Fluid structure coupling is achieved by the application of the hydrodynamic loads via Morison's equation and added-mass coefficients are set using the instantaneous relative velocities and acceleration between the fluid field and the riser segments. The deformations are necessarily large, but still elastic (i.e. non-plastic) and the lumped mass model has been applied, using the methods of multi body dynamics and Kane's formalism to determine the motions and resulting internal forces. As reported by Banerjee (1997), this approach is computationally more efficient than using non-linear finite element codes.

The following assumptions have been made:

1) Primary deformations are due to the longitudinal and flexural vibrations

2) No model has been introduced for shear or torsional deformations.

The mass of each segment is lumped into halves at the ends, except for the segment S_1, the entire mass of which is lumped at P_1. Segment S_k has unstretched length l_k, material area of cross section A_k (not including the internal flow area), second moment of area about the neutral axis I_k, and mass per unit length ρ_k. Beam extension and compression is modeled by linear springs as shown in the figure below.

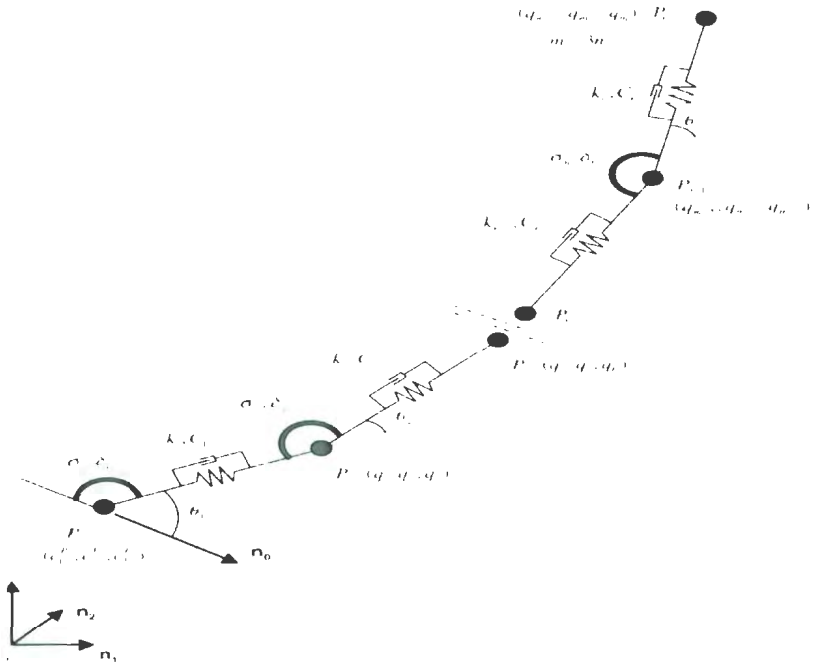

Figure 3.2: Riser Model used in the simulation

[Raman-Nair and Baddour, 2003]

The damping coefficient C_j may be determined experimentally or estimated as $C_j = \zeta \times 2 \times \sqrt{(k_j \times \text{segment mass})}$, where ζ is the damping ratio which lies between 0 and 1. The spring stiffness σ_j ($j = 2 \ldots n$) is chosen as described by [Huston, 1990], using a linear beam theory. For identical segments of length l and flexural rigidity EI, these values are found as $\sigma_j = \frac{EI}{l}$, ($j = 2 \ldots n$). The stiffness σ depends on the prescribed support

condition at point P_0. For a pinned support, $\sigma_1 = 0$. If the beam is cantilevered at P_0, σ_1 is determined as described by Banerjee (1997), as defined below for the case of identical segments.

$$\sigma_1 = \frac{6nEI}{(3n-1)l} \quad \text{.....3.3.1}$$

The validity of this use of linear beam theory for modeling the large deflection behavior of beams has been demonstrated by Banerjee (1997). The origin of inertial coordinates is an arbitrary point O on the seabed and the inertial frame is denoted by N with unit vectors n_1, n_2, n_3. The time dependent location of point P_0 is specified as:

$OP_0 = c_1^{P_0}(t)n_1 + c_2^{P_0}(t)n_2 + c_3^{P_0}(t)n_3$ .....3.3.2, where

$c_i^{P_0}(t)$ $(i = 1, 2, 3)$ are known functions of time t. The system has 3n degrees of freedom.

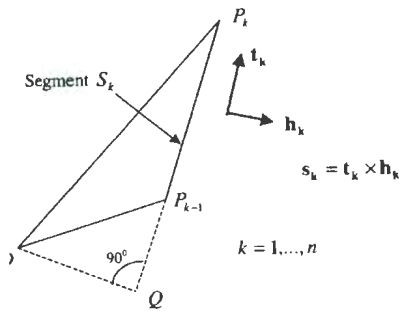

Figure 3.3: Unit vectors for beam segments

The following parameters have been included in the code.

1) Kinematics of the different points on the riser
2) Inertial forces
3) Gravity, buoyancy and touchdown of the riser portion
4) Internal forces due to extension and bending
5) Viscous drag on the riser
6) Hydrodynamic pressure forces (added mass effects)
7) Vortex-induced lift forces
8) Structural damping
9) Forces due to internal fluid flow inside the riser

10) Possible external loads

11) Touchdown

The algorithms used to get the outcomes were applied for this work to measure the different responses of a riser, modeled by the code.

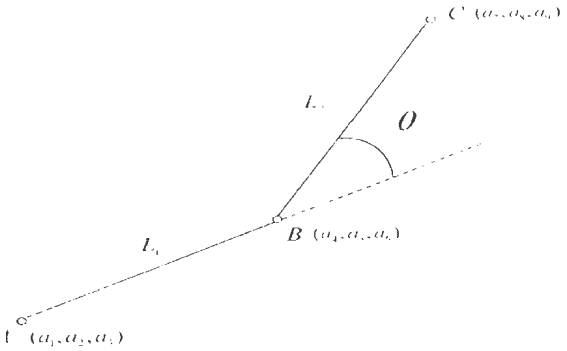

Figure 3.4: Evaluation of angle between two segments of length L_1 and L_2

If internal fluid is flowing uniformly inside the riser, then the rate of momentum entering and leaving the riser should be incorporated. The code accounts for the internal fluid flow, which in turn, addressed the internal pressure inside the riser. Only a linear pressure variation was considered during this study. Figure 3.5 shows the riser model with the internal flow.

Although full-scale data provide completely comprehensive phenomena of marine structures, it is very expensive to acquire such data and usually the result is affected by many kinds of external turbulence such as currents, vortex, waves and wind, and it is therefore difficult to interpret it.

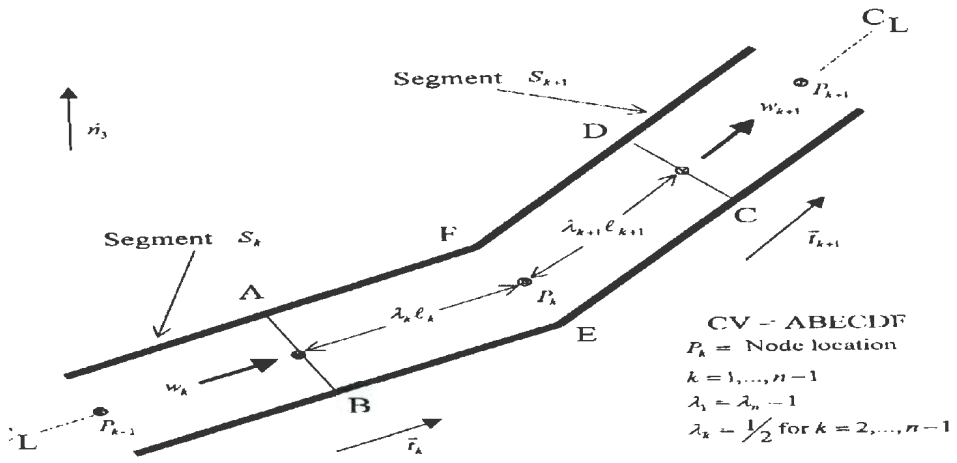

Figure 3.5: Internal flow configuration and control volume

The code by Raman-Nair and Baddour (2003) was used to make a parametric study on VIV on a typical configuration of marine riser. There was a necessity for the validation of the code to use this code as a benchmark for the further study. So, this work started in two stages: 1) Validation of the code and

2) A Parametric Study

3.4 Validation of the code

Two sources were chosen for the validation of the code, 1) analytical proof and 2) experimental proof. Known results were more difficult to locate as tests which could be simulated as the code was unable in accounting all the parameters and setups in the experiments and analysis. However, the code was able to develop a certain parameters of the proofs like 1) Elastic Catenary and 2) MARINTEK experiment. Details of these proofs are described in the following sections.

3.4.1 Elastic catenary mooring proof

This proof calculates the deformed shape of a uniform elastic cable supported by horizontal and vertical forces, when it is suspended at the two points as shown in the

figure 3.6. The two ends of the cable are pinned, and supported by two forces H and V. Total deformed length of a cable is L, and the arc length from A to a general point P (x, z) is p (deformed shape). When the cable is un-stretched, the arc length is 's' from A to P.

This catenary proof states that with the given values of H and V, a catenary profile can be determined, which in turn, calculates the value of 'a' and 'b'. For the known values of 'a' and 'b', the horizontal and vertical forces H and V can be determined for the given elastic catenary profile. So, a profile can be developed either for the known values of supporting forces H and V, for which 'a' and 'b', can be evaluated, or vice-versa.

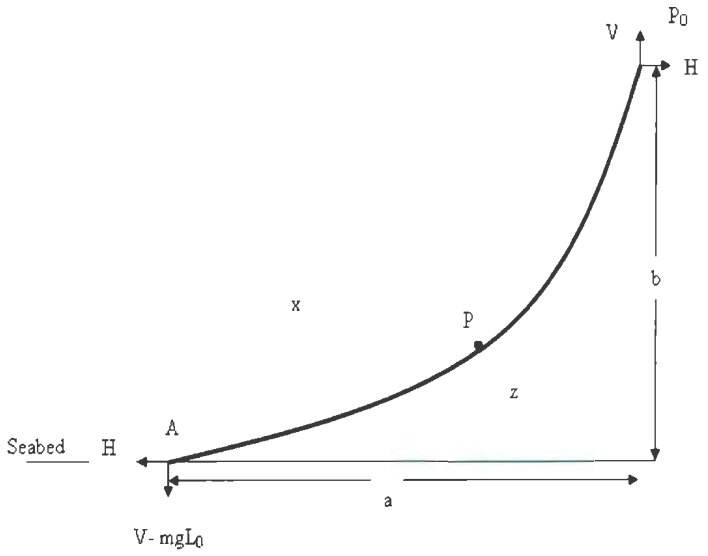

Figure 3.6: Deformed elastic catenary profile

The relationships between the supporting forces and cable dimensions, a and b can be expressed by the following equations [Irvine, 1981].

$$x(s) = \frac{Hs}{EA_o} + \frac{H}{mg}\left\{\sinh^{-1}\left(\frac{V - mgL_o + mgs}{H}\right) - \sinh^{-1}\left(\frac{V - mgL_o}{H}\right)\right\} \quad \text{.....3.4.1.1}$$

$$z(s) = \frac{s}{EA_o}\left(V - mgL_o + \frac{1}{2}mgs\right) + \frac{H}{mg}\left\{1 + \left\{V - mgL_o + mgs\right\}^2\right\}^{\frac{1}{2}} - \left\{1 + \left(\frac{V - mgL_o}{H}\right)^2\right\}^{\frac{1}{2}}\Bigg\}$$

.....3.4.1.2

where, H is the horizontal force, V is the vertical force, m is the mass of the cable, g is the acceleration due to gravity, L_0 is the unstretched length of the cable, E is the elastic modulus of elasticity , and A_o is the cross sectional area.

In the same way, 'a' and 'b' can be expressed in terms of the forces H and V.

$$a = \frac{HL_o}{EA_o} + \frac{H}{mg}\left\{\sinh^{-1}\left(\frac{V}{H}\right) - \sinh^{-1}\left(\frac{V - mgL_o}{H}\right)\right\}$$

.....3.4.1.3

$$b = \frac{L_o}{EA_o}\left\{V - \frac{1}{2}mgL_o\right\} + \frac{H}{mg}\left\{\left(1 + \frac{V^2}{H^2}\right)^{\frac{1}{2}} - \left\{1 + \frac{\{V - mgL_o\}}{H}\right\}^2\right\}^{\frac{1}{2}}$$

.....3.4.1.4

A code was developed in MATLAB, to develop a catenary profile, using the above stated equations. The code was used in the preliminary steps of setting up the riser parameters. The results show that the present formulation converges from non-equilibrium initial conditions to known analytic solutions at steady state. The damping mechanisms for the riser are fluid drag, and structural damping in both extensional and flexural modes. With the values of 'a' and 'b' (values are arbitrary), a catenary profile (with and without bending stiffness i.e. σ_k =0 for k =$1,...n$) was set up with the two ends defined by P_0 and P_n, and the reaction forces measured by H and V were calculated. For the vice-versa case of the forces and dimensions (a and b), the code was able to produce the same catenary profile. After, the code was used in developing a riser profile with the following properties. (The line properties are not intended to be realistic).

Riser properties:

Length of the riser = 3000m

Outside diameter of the riser =0.5m

Inside diameter = 0.4m

Material Density = 7995 kg/m^3 (Steel)

Modulus of Elasticity=2x10^{11} N/m^2

For the defined value of a=1950m and b=2100m, the magnitude of the horizontal and vertical forces, H and V were found, as calculated using the above listed equations.

H= 4.5601x10^6 N

V= 1.1182x10^7 N

Figure 3.7 shows the riser profile created using the code. The riser base P_0 was located at the point (0, 0, 0) in inertial coordinates (meters). The motion of the top end and P_n was specified about a mean position (1950, 0, 2100). Once the riser profile was set up with both ends pinned, simulation was carried out for 1000 seconds. All simulations were performed with non-equilibrium initial conditions. A uniform current velocity of 0.5 m/sec was set for this simulation. The riser, after the simulation, attained a steady-state profile, which coincided with the catenary profile as shown in figure 3.8. For both the cases, with and without bending stiffness, the riser profile matched the elastic catenary profile after the simulation. This shows that bending effects are not significant for the static equilibrium of a long riser (3000 meter long) in this case.

Furthermore, for estimated values of H and V from the equations, tension at the top-end of the riser can be calculated analytically as a resultant of these two forces, simply by the relation, $T = \sqrt{H^2 + V^2}$, which for this case is equal to 1.2025x10^7 N.

After the simulation, the tension was measured at the top-end of the riser, and was found to be 1.2076x10^7 N. So, there was a close agreement (0.042% error) between the values of tension obtained from the analytical calculations and the simulation.

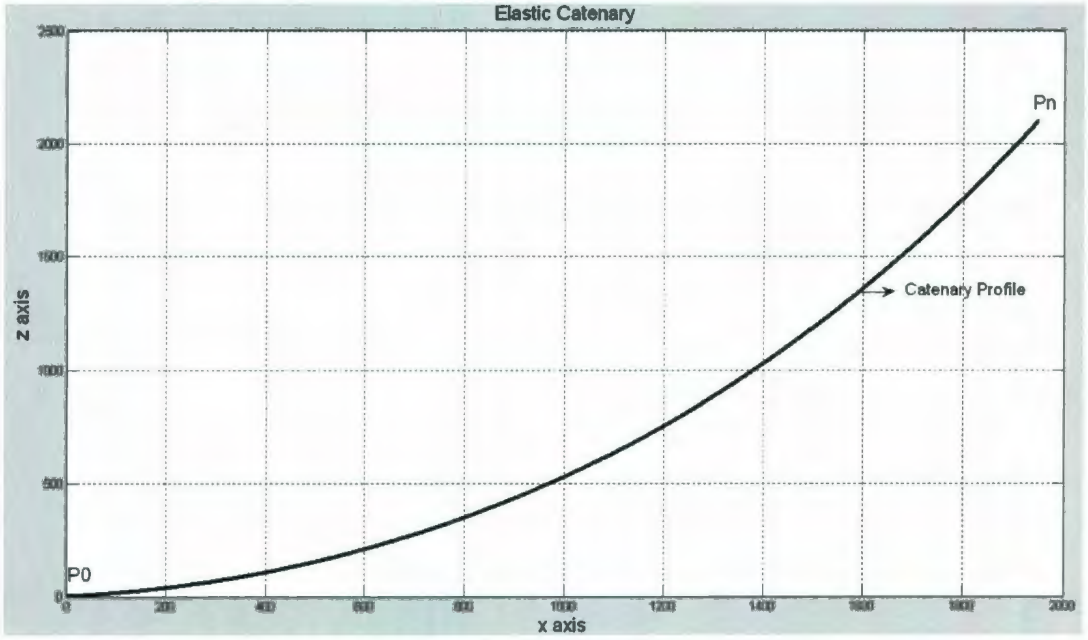

Figure 3.7: Catenary profile of a riser for a=1950m and b=2100m (x-z plane) (from the analytical solution)

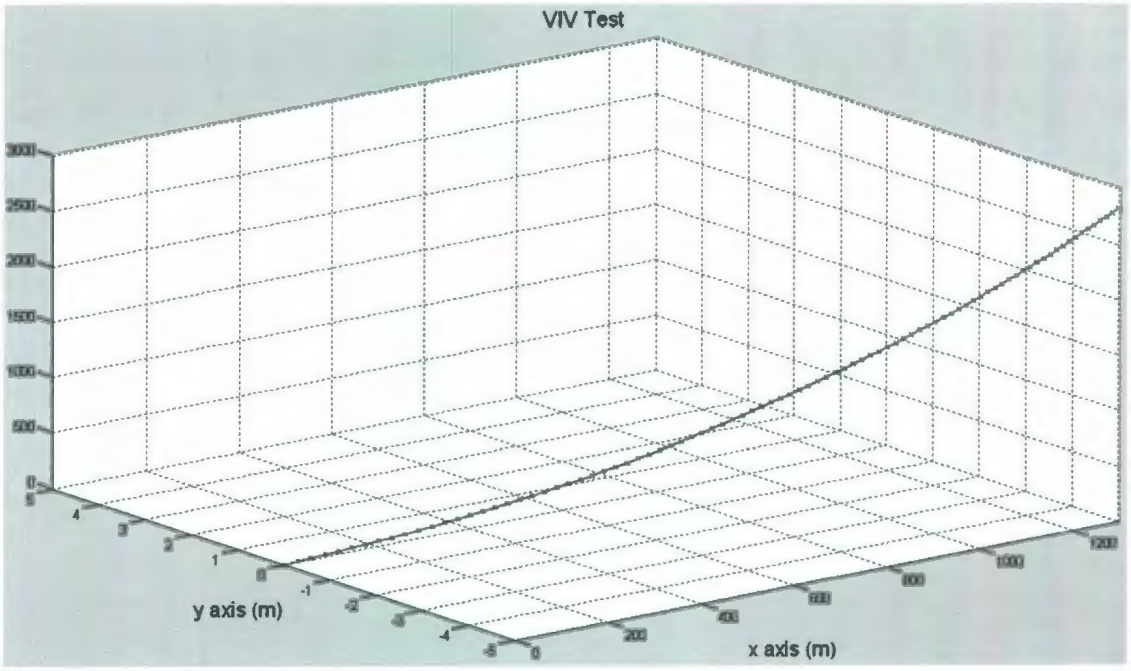

Figure 3.8: (a) Animated riser profile after the simulation

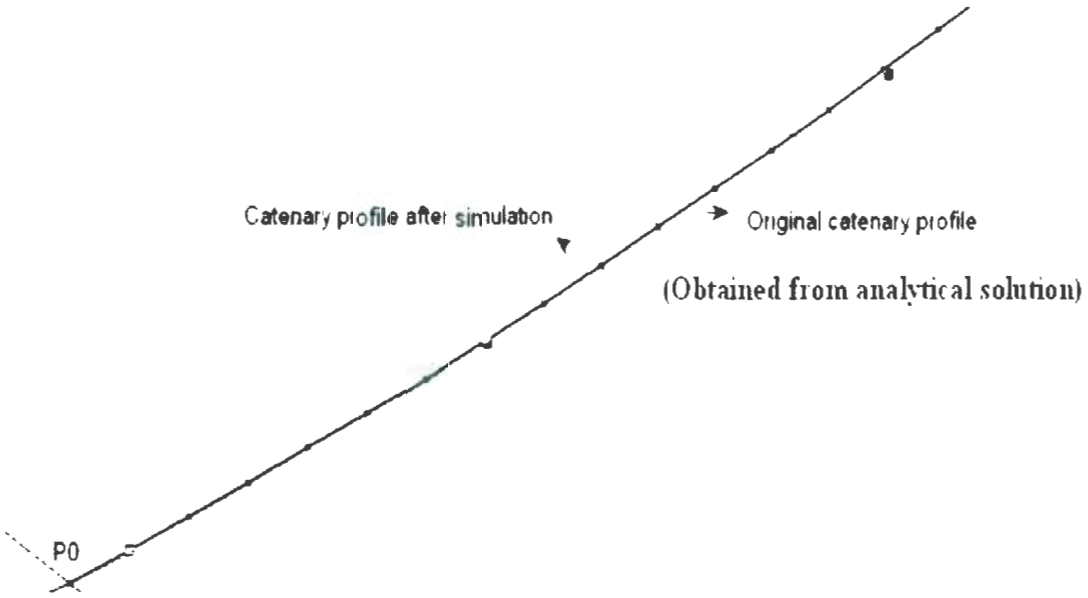

(b) Magnified portion to show the catenary profile before and after the animation

Hence, there was a considerable agreement between the code with the developed elastic catenary proof .

3.4.2 Experimental proof

The Norwegian Deepwater Programme (NDP), a group of oilfield licenses in Norway, commissioned experiments on riser models over a range of scales and current conditions in order to improve the ability to predict VIV. An experiment was conducted at Marintek's Ocean Basin in Trondheim, on a riser model, with length to diameter ratio of 1400. The riser was set up in a horizontal position in a flow tank and the current velocity was set to be 0.5 m/s. The experiments were performed in a tow tank that provided well-controlled flow conditions. In all cases, a model riser made of 27 mm fiberglass pipe was towed in a tank. Testing was also done with various straked configurations by adding sleeves to the riser. The riser was pinned at the ends, and either towed by the two ends to simulate uniform current or towed in a circle from one end to simulate sheared current

conditions as illustrated in figure 3.9. Uniform current was simulated by towing the rig in one direction using the crane. Linearly sheared current was simulated by fixing one end of the riser and using the crane and gondola in tandem to transverse a circular arc.

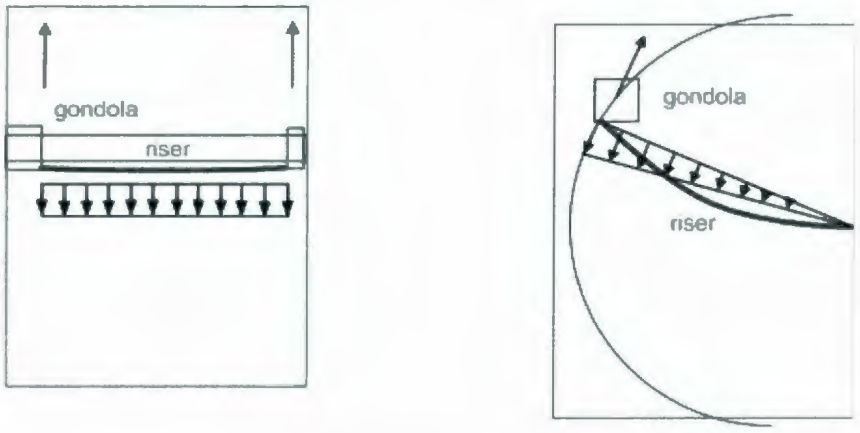

Figure 3.9: Tow tank configurations to simulate uniform currents (left) and sheared currents (right)

Figure 3.10: Riser position in the experiment [Marintek, 2005]

The code was used in setting the riser in a horizontal position as shown by setting two ends P_0 and P_n, both pinned, at the coordinates (0,0,0) and (38,0,0) respectively. The riser was divided into 10 lumped masses for the measurement of riser displacements along different segments.

○ = *lumped mass*

Figure 3.11: Schematic riser configuration adopted in the simulation code

The material properties used in the experiment are listed below:

Material of the riser: *Reinforced Fiberglass*
Length of the riser: *38 m*
Outer diameter of the riser: *0.027m*
Inner diameter of the riser: *0.024m*
Current velocity: *0.5 m/s*
Current profile: *Linear and shear*
Mass ratio: *1.6*
Young's Modulus of elasticity: $36.2x10^9\ N/m^2$

The experimental results show that for a bare riser, cross-flow displacement is higher than in-line displacement for all the set of velocities. There were less parameters listed in the experiment by Trim (2005) which this code can account for such as the riser position, current velocity, dimensions of the riser. The code was able to produce the riser profile with most of the listed properties in the experiment. However, there was no indication of the force coefficients in the experiment for which the measured displacements could be measured for different force magnitudes.

The code accounts for the drag (both the mean and the oscillating) and lift coefficients, which is based on the ranges of Reynolds number. So, magnitude of 1.2 and 0.2, for $Re>3x10^5$ were used for mean and oscillating drag force coefficients in addition to the value of 0.2 for lift coefficient. Then the cross flow oscillations were measured. With these values of force coefficients, the cross flow oscillations ranged from around $\frac{1}{3}$ to $\frac{1}{4}$ of the diameter. While in the experiment, the range was from about $\frac{1}{2}$ to 1 diameter of the riser. So, to see if the range could be made closer, the lift coefficient was increased to 0.4 with the hope that cross flow oscillation would increase. Also, there was no indication of the material density in the experiment. The riser was made of reinforced fiberglass, and density of 1800 kg/m^3 was adopted after the series of trials to mimic the report's findings of displacements. Later, it was found that the measurements were close to that of the experiment.

The following is the cross flow oscillation measured from the simulation between 35 and 40 seconds, for the material properties listed above.

Table 3.1: Cross-flow displacement at lumped masses for simply supported riser

Mass Number	1	2	2	4	5	6	7	8	9
Amplitude(m)	0.0137	0.0156	0.0192	0.023	0.0243	0.023	0.0191	0.0155	0.014

These magnitudes of the cross flow oscillations from the simulations, as seen vary from ½ to 1 diameter of the riser (Riser Diameter = 0.027m). The riser set up in the code resembles a simply supported beam pinned at both ends, with uniformly distributed load. The maximum deflection would be at the mid span of the beam when is subjected to uniform load. As can be seen from table 3.1, lumped mass 5, which represents the mid segment of the riser, experienced the highest displacement. Both the cross flow displacements and in-line displacements were obtained from the simulation at the lumped masses to find the frequency relationship. Vandiver (1981) reported the relationship between the in-line and cross flow oscillation of the riser VIV. He came up with a conclusion from his experimental work of the flexible cylinders tested at Castine, Maine in 1981 that at 'lock in' the in-line response is at twice the frequency of the transverse motion. Also, the in-line motion may have two-modes; the dominant one has a frequency twice that of transverse frequency and the smaller response component has the same frequency as of the cross flow oscillation.

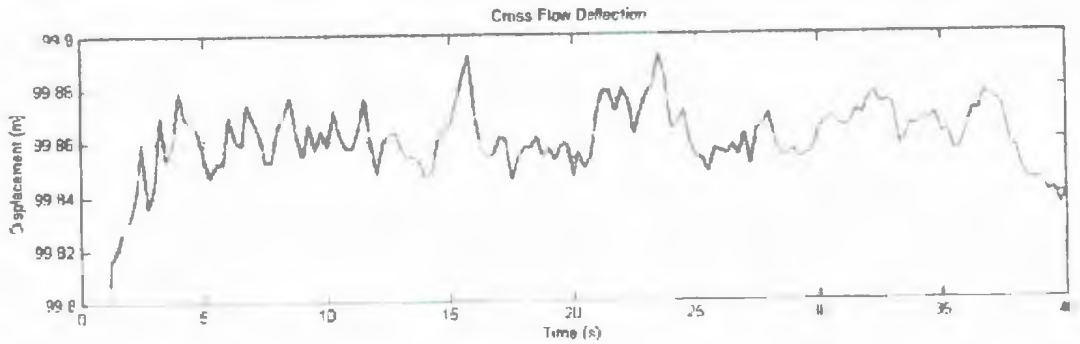

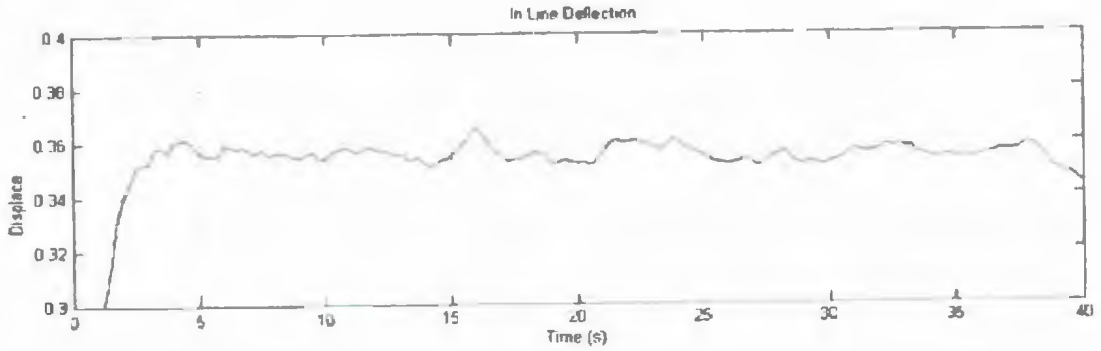

Figure 3.12: Cross flow and In-line oscillations obtained from simulation for a riser of 38m long for comparisons with Marintek experiment

The in-line oscillations were obtained from the simulation at the same lumped masses and tried to establish the relationship between the frequencies between in-line and cross flow displacements (figure 3.12).

Figure 3.13 shows the in-line and cross flow oscillations at the lumped mass 5 obtained from the simulation, which shows the frequencies of both oscillations to be almost of same magnitude. Vandiver's (1981) findings showed that in line deflection amplitude is half that of the cross flow deflection amplitude but occurs at twice the frequency. This is a surprising outcome because the formula used in the marine riser program for lift and drag differs by this ratio while modeling this frequency relationship. However, this frequency relationship will be examined more for the long riser during the parametric case study.

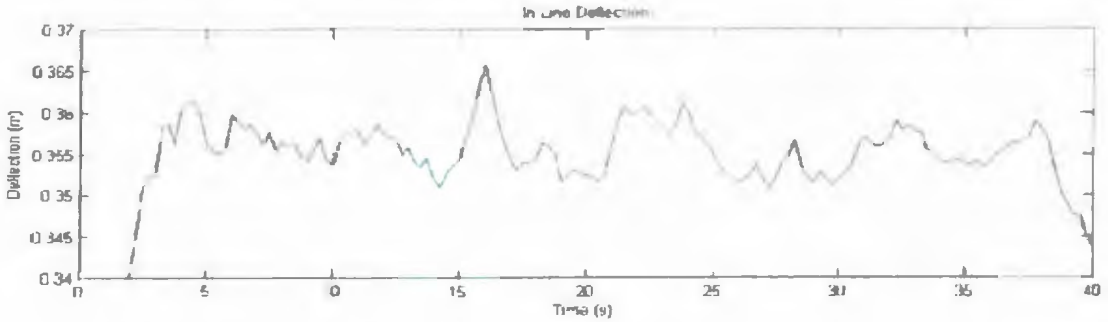

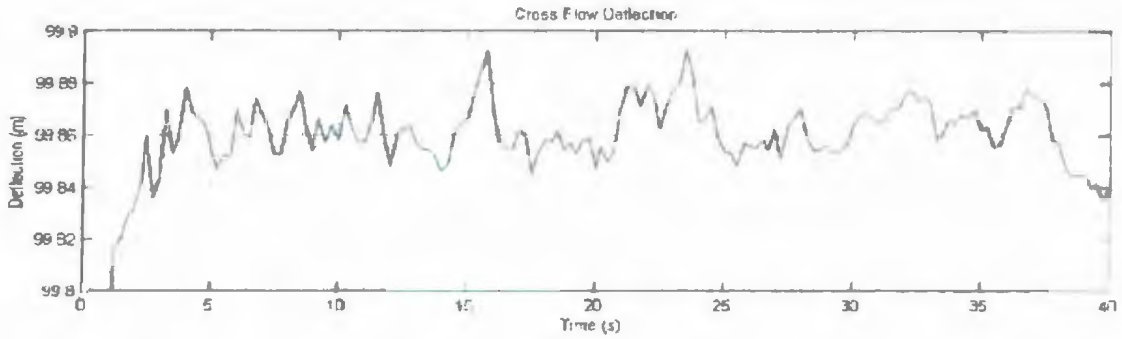

Figure 3.13: Comparison of frequencies for the cross flow and in-line deflections

In these tests, there were many obstacles that had to be overcome in simulating these tests. Sometimes, the correct setup could not be modeled by the program, due to assumptions made when developing the proofs and some parameters had to be changed. This caused a disagreement between the computer generated results (from the simulation) and the formulated ones (algorithms and assumptions used in the code).

The ability for the program to simulate a real experiment and produce comparable results is a very encouraging finding, but it is difficult to find tests that clearly state their setup parameters and/or results clearly. It is recommended setting up own tests to compare the riser program against. This way the testing parameters are known and specific properties can be changed.

Furthermore, Raman-Nair, and Baddour (2003) validated the code by considering the problem of determining the large deflection profile of a cantilever beam under a vertical load at the free end. The catenary profile of the riser was compared between the equilibrium profile determined from the solution of Bishop, and Drucker (1945) and the steady-state profile obtained from the numerical simulation at the end of a 100 seconds run.

3.5 Parametric studies of VIV on Marine Risers

The overall goal of a VIV analysis effort is to develop a general VIV analysis procedure capable of representing the wide range of vibration behavior associated with long flexible cylinders in a current. No single test can provide measurements and data for all the parameters involved in VIV. Most of the tests provide data for a few parameters (Strouhal number and lift coefficient are the most common) disregarding the effect of others. Selection, integration and interpretation of test data are critical to model VIV of marine risers. Vandiver (1992), carried out parametric studies to explain the reason for varying of flow-induced vibration of long cylinders from single mode lock-in to broad-band random vibration. He found the parameters such as mass ratio, reduced damping, and also fractional variation in the flow velocity affect the responses of the riser subjected to the sheared flow. As suggested by Vandiver, (1992), 'lock-in', usually results the largest amplitudes of vibration and the largest mean drag coefficients, and, are therefore considered in most riser designs, to be the worst case. Also, he found out that when 'lock-in' is likely to occur, mass ratio has a strong effect on determining the range of reduced velocity over which lock-in can occur. If this range is narrow, then lock-in may occur for narrow bands of flow velocity. This work by Vandiver (1992) was able to reveal the parameters which have greatest influence over the occurrence of the lock-in for flexible cylinders with large L/D and provided case studies. Another study was carried out by Willden, and Graham, (2003), on a flexible pipe with the length to diameter ratio of 1544 and Re= 2.84×10^5, for the case study of effect of mass ratio upon the responses of the vibrational behavior of a pipe. The mass ratio was varied between 1.0 and 3.0. Despite the inflow current being uniform, the pipe was observed to vibrate multi-modally and all excited modes vibrated at the same Strouhal frequency. The fluid, via its added mass was found to be able to excite modes whose natural frequencies differed from the excitation frequency. This ability was observed to decrease with increasing mass ratio.

Despite the large volume of experimental data, a systematic investigation that relates the variation of the hydrodynamic forces to the flow patterns in the wake is missing. Numerical investigation of the flow past an oscillating cylinder at low Reynolds number

has been done by, among others, Blackburn and Henderson (1999), Anagnostopoulos (2000), Baek (2001), Blackburn (2001) and Guilmineau and Queutey (2002), but for a very limited number of frequencies and amplitudes of oscillation, not sufficient to offer a picture of the dependence of the forces on these parameters.

Researchers have put effort in to finding the force coefficients of a circular cylinder. However, there has been no close agreement among the values of force coefficients found by different researchers, which in turn, causes confusions for riser designers in selecting the proper force coefficient magnitudes for analysis. This creates the need for a parametric study of force coefficients on riser responses in determining, if a wide selection of force coefficients affects the riser responses.

The code was used in this work for a parametric study of force coefficients (primarily) and other factors such as internal fluid flow, on a long and flexible riser. The study proceeded first, by identifying the important parameters that affect the riser responses, and then by studying the variation of riser responses with the expected ranges of significant parameters.

As stated in the previous chapter, drag and lift force can be written as:

$$F_d = \frac{1}{2}\rho U^2 A(C_D + C_{Do}\sin(2\omega st + \phi)) \quad \text{.....3.5.1}$$

$$F_L = \frac{1}{2}\rho U^2 A C_L \quad \text{.....3.5.2}$$

And the dimensionless coefficients can be stated as:

$$C_D = C_{Dmean} + C_{Do}\sin\left(2\omega_s + t\right) \quad \text{.....3.5.3}$$

$$C_L = C_{Lo}\sin\left(\omega_s + t\right) \quad \text{.....3.5.4}$$

The following responses of a riser were considered.

1) Maximum Bending Moment
2) Maximum Tension
3) Maximum Tensile Stress
4) Cross flow Displacement

5) In-line Displacement

Only the maximum responses were measured at different lumped masses on a riser from the simulation. For most of the cases, the bottom-end mass and top-end mass were chosen along with the middle lumped mass.

After identifying the parameters to be considered, a certain profile of riser was chosen on which the parametric studies could be carried out. As steel catenary risers are widely used in almost every new deepwater field development, a steel catenary riser was taken as a typical riser configuration for this study.

3.5.1 Steel catenary risers

Steel catenary risers (SCRs) have been associated with floating platforms since the mid-1990s and were first used as export risers for the Auger TLP [Phifer et.al, 1994]. Generally, a catenary is in fact a precise mathematical curve, but the term is used loosely in the offshore industry to refer to a catenary riser that approximates to that mathematical curve. Their use has given a new dimension to oil exploration and transportation in water depths where other riser concepts could not tolerate the environmental loads or would have become very costly [Sparks, 2007]. SCR designs are very sensitive to floating support platform or vessel motion characteristics to which they are typically attached. In addition to pipe stresses, the main design issue for the SCR concept is fatigue related.

SCRs are horizontal at the lower end (figure 3.14) and generally within 20^0 of the vertical at the top end. Hence, their total profile and curvature cannot be even remotely analyzed using small angle deflection theory. They can be analyzed by defining local axes, for a number of sections for which the angles do not evolve by more than $10^{0,}$ which is the limit normally accepted for small-angle deflection theory.

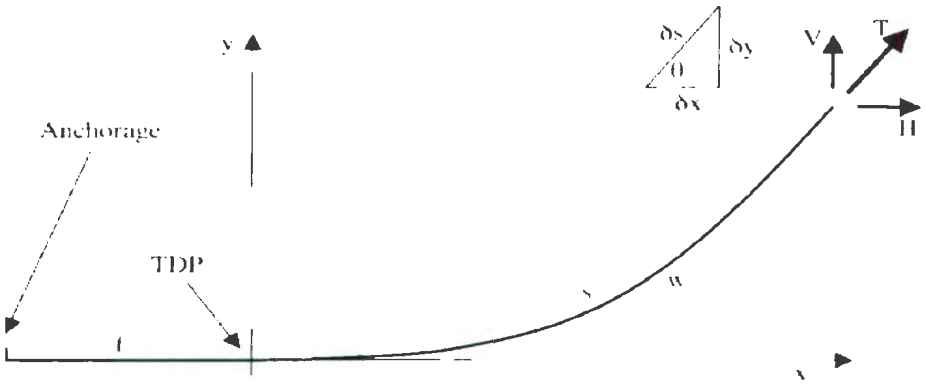

Figure 3.14: Catenary riser

The basic differential equation governing curvature and deflection of a tensioned beam (with uniform bending stiffness) subject to large deflections as has been described by Sparks (2007) is as follows:

$$EI\frac{d^3\theta}{ds^3} - T\frac{d\theta}{ds} + w\cos\theta + f(s) = 0 \quad \text{.....3.5.1.1}$$

where $w\cos\theta$ and $f(s)$ are the respective components of the self weight and the in-plane current load, acting perpendicular to the catenary axis. T is the tension. The above equation can be expressed in terms of the curvature, which can be expressed as $1/R = \frac{d\theta}{ds}$.

so
$$EI\frac{d^3\theta}{ds^3} - T\frac{d\theta}{ds} + w\cos\theta + f(s) \quad \text{.....3.5.1.2}$$

$$EI\frac{d^2}{ds^2}\left(\frac{1}{R}\right) - T\left(\frac{1}{R}\right) + w\cos\theta + f(s) = 0 \quad \text{.....3.5.1.3}$$

For a cable catenary in zero current, since the bending stiffness and current load will be zero [Sparks, 2007], the following equation results.

$$\frac{1}{R} = \frac{wH}{T^2} \quad \text{.....3.5.1.4}$$

Curvature $\left(\frac{1}{R}\right)$ is maximum at the TDP (touchdown point), where it is equal to w/H.

This is obvious since the part of the catenary adjacent to the TDP can be treated as a horizontal cable subject to vertical load w and axial tension H. The above equation can be used to estimate the shift of the TDP resulting from the riser top-end movements, which may be large.

Floating platforms can be subject to large static lateral displacements as a result of wind, current, and any other loads. When these displacements are in the plane of an SCR, they may result in large changes in the position of the TDP.

Any change in the horizontal projection will cause a change in the top tension. Also, the riser experiences the stretch due to changes in factors like temperature, pressure and internal fluid density. The stretch may be small for SCRs made from steel, but could be more significant for more elastic materials.

Moreover, the structural response of a catenary riser also depends on the structural properties like bending stiffness, boundary conditions (pinned support or free cantilever support), and density of the material. The behavior of beams (with EI) and cables (*EI* being zero) depends upon the bending stiffness. The beam curvature is very close to cable curvature (for which EI is neglected) everywhere except for zones close to the supports. The extent of those zones depends on the flexibility factor *kL*, which in turn depends on bending stiffness [$k = \sqrt{\frac{T}{EI}}$, L is the length of the beam, T is the magnitude of tension, and EI is the bending stiffness]. For the case of catenary risers, the same relationship exists. The influence of bending stiffness on the TDP position, top tension, TDP shear force, and the soil interaction has been of great interest to riser designers and analysts. Results of static simulations made using computer programs have shown that bending stiffness has little effect on catenary curvature except for zones close to the TDP and top-end [Sparks, 2007]. Curvature is greater for stiff catenaries than for cable catenaries; the greater the stiffness, the greater will be the curvature.

At the TDP, due to the presence of the sea floor, the displacement of the riser is reduced during VIV as the relative thickness of the incoming boundary layer profile along the seafloor bottom can also have significant effect on the response of the riser. As explained by Schulz and Kallinderis (1998), the boundary layer profile alone can change whether a riser experiences 'lock-in' or not.

Owing to the importance of steel catenary riser in the industry, for this work a steel catenary riser was chosen, with the two ends pinned, and with the material properties as listed below.

3.5.2 Properties of a Typical Riser used for the simulation

1) Length of riser: 3000m (un-stretched)
2) Outer diameter: 0.5m
3) Inner diameter: 0.4m
4) Number of lumped masses: 100
5) Material density: 7995 kg/m^3 (Steel)
6) Density of sea water: 1025 kg/m^3
7) Modulus of Elasticity: 2x10^{11} N/m^2
8) Earth stiffness coefficient: 10000 N/m
9) Internal fluid flow: 0.02m^3/sec, {at the typical production rate of approximately 10,000 barrels per day}.
10) Density of the internal fluid: 800 kg/m^3
11) Internal pressure in the riser segment: 10000psi, where 1psi=6897 N/m^2
12) Strouhal Number: 0.2
13) Damping ratio: 0.4

The analysis involved two cases:

1) Parametric study of force coefficients. The force coefficients chosen were:

i. Mean drag coefficient
ii. Oscillating drag coefficient
iii. Lift coefficient (oscillating)

2) Parametric study of force coefficients along with internal fluid flow and riser top-end movement. Parameters varied were:

i. Mean drag coefficient
ii. Oscillating drag coefficient
iii. Lift coefficient
iv. Internal fluid carried by the riser (this gives riser to internal pressure)
v. Position of the top end of the riser.

For a parametric study with the force coefficients only, the riser was subjected to a uniform flow, whereas for the later case, the riser was subjected to a sheared flow. For both cases, the current was set to be in an oblique direction to the riser segments as shown.

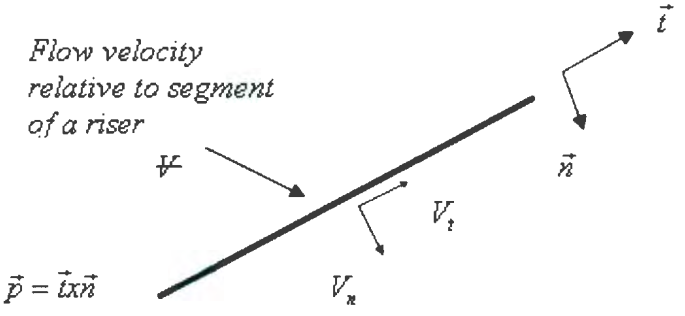

$\vec{n}$ *defined in plane of segment and flow vector*

Figure 3.15: Schematic representation of the current on a segment of a riser

Figure 3.15 shows a schematic representation of the current acting on a riser. The current velocity was resolved into the tangential and normal components (V_t and V_n). Even though the code accounts for three-dimensional vibrational effects, only two-dimensional effects were considered for this analysis. Current velocity was resolved into three

components along x,y, and z coordinate axes. This study takes current velocity in the x-direction, so the displacement occurring in the x-direction refers to the in-line displacement, whereas the oscillations along the y-coordinate reflect the cross-flow displacement. For this case, the drag forces act in two directions, namely the tangential and normal drag forces. They can be expressed as:

$$F_{drag\ T} = \frac{1}{2}\rho_f\ A_T\ C_{DT}\ |\vec{v}.\vec{t}|\ (|\vec{v}.\vec{t}|)\ \vec{t} \quad \text{.....3.5.2.1}$$

$$F_{drag\ N} = \frac{1}{2}\rho_f\ A_N\ C_{DN}\ |\vec{v}.\vec{n}|\ (|\vec{v}.\vec{n}|)\ \vec{n} \quad \text{.....3.5.2.2}$$

$$F_{lift} = \frac{1}{2}\rho_f A_N C_L |\vec{v}.\vec{n}|^2\ \vec{p} \quad \text{.....3.5.2.3}$$

Generally, the tangential drag force is small compared to the normal drag force. The tangential drag force was not studied in this study. A constant value of 0.2 was used; and no variation was carried out in the tangential drag.

After the riser properties and boundary conditions were set up, simulations were carried out to measure the riser responses. For responses like tension, tensile stress and bending moment, their peak values were considered during the analysis. The maximum bending moment, maximum tension, and maximum tensile stress reflects to their peak positive values. The riser displacements were measured in terms of cross-flow and in-line amplitude.

The following figure 3.16 shows the time series of bending moment measured at lumped mass 99. This lumped mass represents the top portion of the riser. Even though the magnitude of bending moment is higher at the beginning, the peak value around 900-1000 seconds was measured as the maximum (positive) bending moment. In this case, maximum bending moment is 4.209×10^4 Nm.

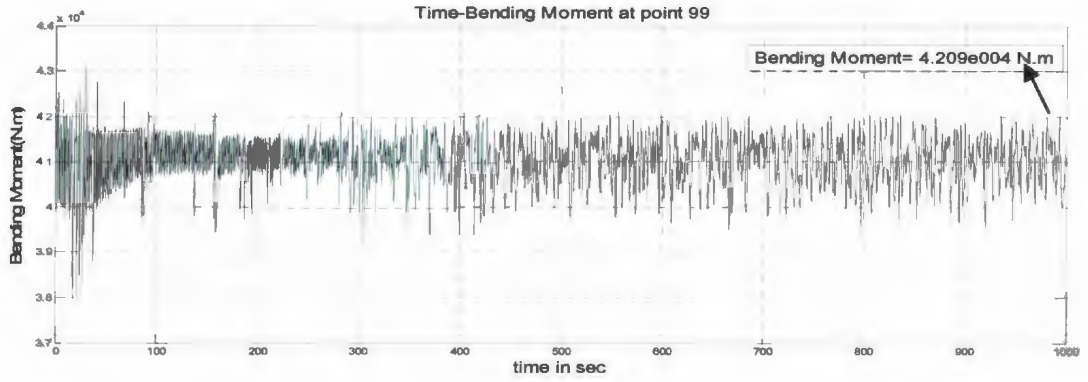

Figure 3.16: Time-Maximum Bending Moment at lumped mass 99

Figure 3.17, shows the cross-flow and in-line displacement of lumped mass 99, after the simulation, where the riser was subjected to uniform flow. As can be seen, the in-line displacement occurs at around at two times the frequency of the cross flow displacement.

Frequency=0.2-0.65 Hz

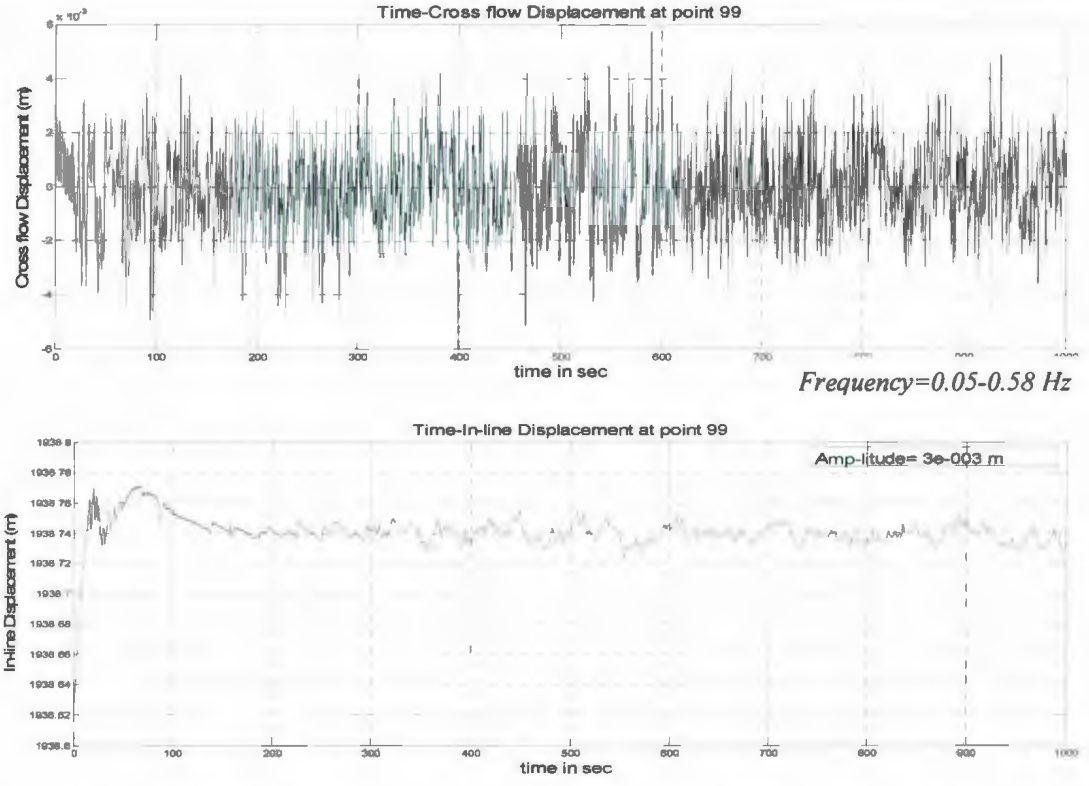

Figure 3.17: Cross flow and In-line displacement at lumped mass 99

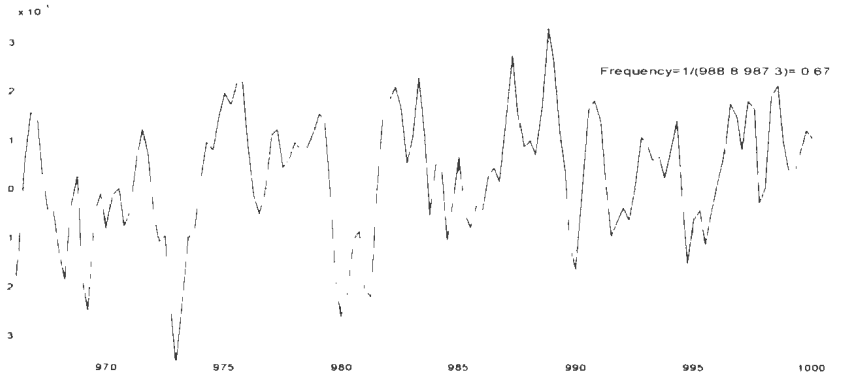

(a) Cross-flow amplitude frequency at lumped mass 99

amplitude= (a-b)/2

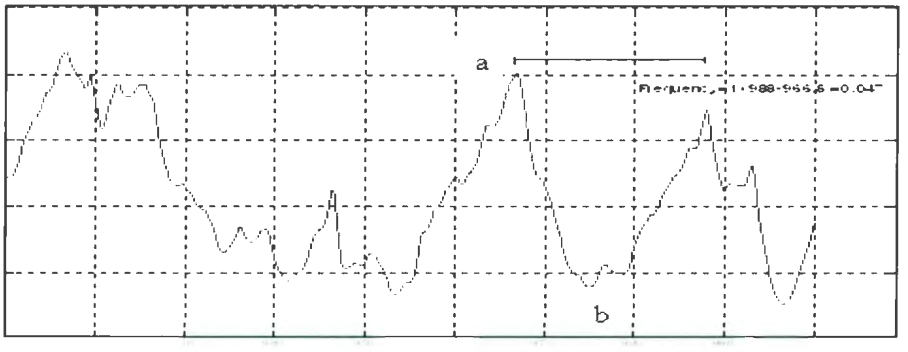

(b) In-line amplitude frequency at lumped mass 99

Figure 3.18: Frequencies comparison of displacement amplitudes at lumped mass 99

Figure 3.18 (a) and (b) show the (magnified portion for 900-1000 secs from figure 3.17) cross-flow and in-line displacement with same scale factor for *x* axis at lumped mass 99 showing the frequencies at which they occur. Amplitudes of the displacements were measured by taking the difference between two antinodes and dividing by two as shown in figure 3.18. As seen, cross flow displacement occurs at a frequency of 0.67 while in-line displacement occurs at a frequency of 0.047. In general, cross-flow displacement occurs at a frequency of around 1.5 times that of in-line displacement (figure 3.17, refer frequency ranges). So, the frequency relationship between the cross-flow and in-line displacement is also valid for a long riser.

3.5.3 Current profile

VIV is more sensitive to the current profile then to any other parameter [Allen, 1998], so, modeling the current velocity was an important part of this study. For risers of short spans, the current magnitude determines whether or not VIV will occur, and determines whether the response is in-line or transverse or both. While for the deepwater risers, a very low current will produce some VIV due to the low natural frequency of the risers in bending. The variation of the current along the riser span determines which modes will be present in the response [Allen, 1998].

If strength or direction of current, or both, vary along the riser length, the current is called a sheared current. Shear currents can be separated into two-dimensional and three-dimensional shear currents; and two-dimensional sheared currents also have various patterns. These patterns include positive shear currents, negative shear currents and block currents as illustrated in figure 3.19. In this work, a block shear current was modeled. Only current in the *x*-direction was considered for the analysis in this study. However, the code can account for a three-dimensional current. The current magnitude was defined as: vfluid (*t*,*X*), where *t* denotes time, and *X* denotes the positions (*x*-*y*-and *z*). The current in the *x*-direction can be expressed as V_x=az+b, where a and b are arbitrary depending on water depth z, measured from seabed.

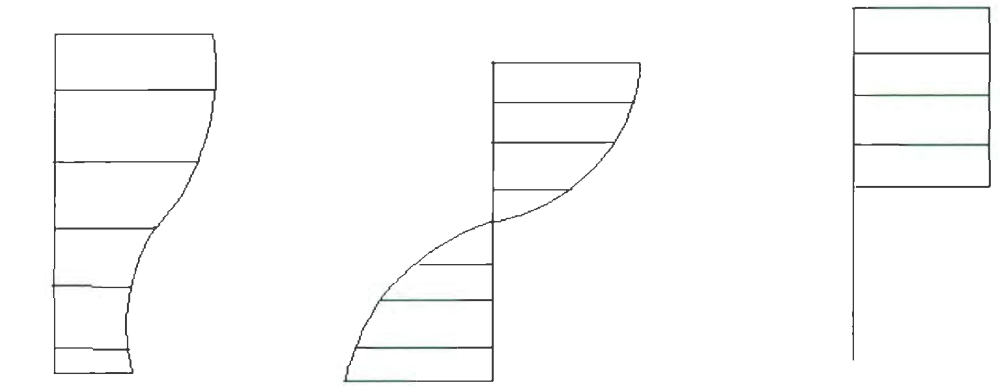

Figure 3.19: Shear current category

The current magnitude was varied with water depth as shown in the figure 3.20.

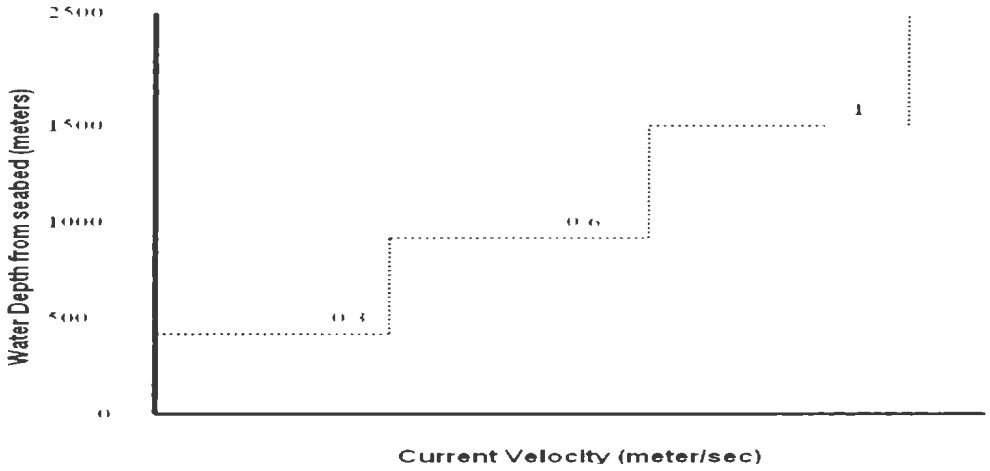

Figure 3.20: Current profile for sheared flow

After the identification of the parameters to be analyzed, and the responses of the riser to be looked upon, a parametric study was carried out which involved the measurement of the riser responses for the changes in the magnitudes of the parameters. Each response had to be measured for changes in the magnitude of each parameter. For example, keeping the drag force coefficients at a constant value, the lift force coefficient was changed and the responses were measured to find the parametric relationship of responses with the lift force coefficient. This can be a good way to understand the behavior of riser responses with changes of certain parameters keeping other parameters unchanged. However, there may be cases where increasing/decreasing a certain parameter causes the riser responses to change to a certain extent with the changes in other parameters. This means that there may be a better approach to understand the riser responses variations with changes in different combinations of variations in the parameters concerned. The Design of Experiment (DOE) is a statistical method where a parametric study can be done by varying the selected parameters at two levels (three levels are for Response Surface methodology). This gives the combinations of variations of parameters in the form of main parameter variations and interaction of parameters variations. The parameters for this study therefore, were chosen at two levels, levels being named as high

and low level. Force coefficients were chosen as low level and high level, considering average low and high ranges for a circular cylinder based on Reynolds number dependency. Effects of internal fluid flow were studied by varying the discharge from no flow to a certain flow within the pipe, which in turn, gives pressure variation. Only linear variations were considered. Riser top-end, P_n was moved to a certain position away from its original position to study the riser top end movement on riser responses.

Chapter 4

Design of Experiment

4.1 Introduction

Design of Experiment (DOE) is a systematic approach to the investigation of a system or process. A series of structured tests are designed, in which planned changes are made to the input variables of a process or system. The effects of these changes on a pre-defined output are then assessed. DOE is important as a formal way of maximizing information gained through an experiment or analysis [Montgomery, 2005]. It has more to offer than 'one change at a time' experimental methods, because it allows a judgment on the significance to the output of input variables acting alone, as well input variables acting in combination with one another.

'One change at a time' testing always carries the risk that the experimenter may find one input variable to have a significant effect on the response (output) while failing to discover that changing another variable may alter the effect of the first (i.e. some kind of dependency or interaction). This is because the temptation is to stop the test when this first significant effect has been found. In order to reveal an interaction or dependency, 'one change at a time' testing relies on the experimenter in the appropriate direction. The OFAT (one factor at a time) method was once considered as the standard, systematic, and accepted method of scientific experimentation. Both of these methods have been shown to be inefficient and in fact, can be disastrous [Lye, 2002, and Montgomery, 2005]. However, DOE plans for all possible dependencies in the first place, and then prescribes exactly what data are needed to assess them i.e. whether input variables change the response on their own, when combined, or not at all.

DOE is a methodology for systematically applying statistics to the experimentation. DOE aids in developing a mathematical model that predicts how input variables interact to create output responses in a process or system. It can be used to find answers in situations such as "what is the main contributing factor to a problem?", "how well does the

system/process perform in the presence of noise?", "what is the best configuration of factor values to minimize variation in a response?" In general, these questions are given labels as particular types of study.

4.2 Principles of DOE

Following are the principles of DOE as outlined by Easton and Coll (1997).

1) Replication:- Replication refers to running each combination of factor levels in the design more than once. This will allow estimating the so-called *pure error* in the analysis or experiment. When replicating the design, one can compute the variability of measurements within each unique combination of factor levels. This variability will give an indication of the random error in the measurements (e.g. due to uncontrolled factors, unreliability of the measuring instruments, etc), because the replicated observations are taken under identical conditions (settings of factor levels). Such an estimate of the pure error can be used to evaluate the size and statistical significance of the variability that can be attributed to the manipulated factors.

2) Randomization:- Randomization is the process by which experimental units (the basic objects upon which the study or experiment is carried out) are allocated to treatments; that is, by a random process and not by any subjective and hence possibly biased approach. The treatments should be allocated to units in such a way that each treatment is equally likely to be applied to each unit. Randomization is preferred since alternatives may lead to biased results. The main point is that Randomization tends to produce groups for study that are comparable in unknown as well as known factors likely to influence the outcome, apart from the actual treatment under study.

3) Blocking:- It is a technique dealing with nuisance factors. A nuisance factor is a factor that probably has some effect on the response, but it is of no interest to the experimenter. However, the variability it transmits to the response needs to be

minimized. Blocking is an arrangement of experimental units into groups (blocks) that are similar to one another. Blocking reduces known but irrelevant sources of variation between units and thus allows greater precision in the estimation of the source of variation under study.

However, in this analysis, two principles, namely the replication and the randomization, were not followed as simulation on a computer yields no difference in replicating the treatments of the factors. However, blocking was undertaken for the sheared flow case. For the case where the riser was subject to a sheared flow, five factors were considered. Each factor was selected at two levels, defined by high level and low level (high level corresponds to their maximum value and low level corresponds to their low value) which gave total of 32 runs for the simulations. One simulation normally took 10-12 hours depending on the computer processor. So, to reduce the time, only half factorial simulation was carried out for this case and full factorial for the case of study of force coefficients only.

4.3 2^k Factorial design

This is the design in an experiment or an analysis, where the factors are taken at two levels and designated as 2^k, where 2 denotes the level and 'k' denotes the number of factors. Two levels of the factors may be arbitrarily called 'high' and 'low', denoted as '+' and '-' respectively. So, 2^3 design in DOE means three factors with two levels. For the parametric study with force coefficients taken into consideration, three factors were chosen and represented symbolically as shown in table 4.1:

Table 4.1: Factor levels for uniform flow

Factors	Coded factors	High Value (+1)	Low value (-1)
Mean Drag Coefficient	A	1	0.2
Amplt. of Drag Coefficient	B	0.5	0.2
Amplt. of Lift Coefficient	C	0.3	0.05

Force coefficients were chosen for the Re > $3x10^5$, i.e. the sub critical Re range as shown in the figure 2.3.A 2^3 simulation means there were altogether 8 treatments of the factors, which included the main factors and their interactions. A, B, and C are called the main factors and are represented by a capital letter, while ab, ac, bc and abc are the interactions of the factors, represented by the lower case.

Hence, the simulation was run 8 times with the combination of the factors and the responses were measured for each treatment. This is called 'Full Factorial Design', where all the possible combinations of the factors were run.

Designs with the factors set at two levels implicitly assume that the effect of the factors on the dependent variable of interest is linear. It is impossible to test whether or not there is a non-linear (e.g. quadratic) component in the relationship between factors and a dependent variable, if the factor is evaluated only at high and low levels. So, to check the linearity, all of the factors were run at their mid point with the regular treatment. So, there were 9 combinations of factors (this includes main factors and the interaction of main factors), for which the simulation was run. The responses were measured for all the simulations.

Design of Experiment, version 7.1 (www.statcase.com), was used to carry out the parametric studies. Since the riser was modeled by 100 lumped masses, each mass may respond in a different way to the responses, so analyzing all the masses was not feasible. Hence, the bottom most and the top most and the middle masses were chosen for most of the responses of a riser. The bottom most portion of the riser, represented by mass 1 (and also mass 10), refer to the portion of the riser that touches the seabed, and lumped masses such as 99 and 50 represent the riser portion which is almost vertical and above the seabed.

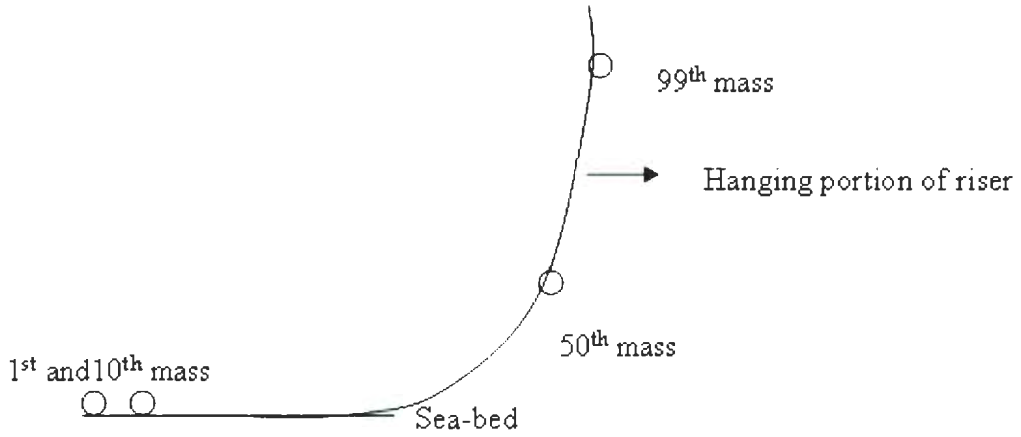

Figure 4.1: Position of lumped masses on the riser

4.4 Analysis of main factors and their interactions

4.4.1 Maximum bending moment at lumped mass 1

Table 4.2: Contribution of factors on maximum bending moment at mass 1

Term	Stdized Effects	Sum of Squares	% Contribution
Intercept			
A-Mean Drag Coeff.	-18932.50	7.169E+008	99.32
B-Amplt. of Drag Coeff.	-1382.50	3.823E+006	0.53
C-Amplt. of Lift Coeff.	367.50	2.701E+005	0.037
AB	-467.50	4.371E+005	0.061
AC	-317.50	2.016E+005	0.028
BC	-67.50	9112.50	1.262E-003
ABC	-82.50	13612.50	1.886E-003
Curvature	-1.270E+005	1.731E+005	0.024
Lenth's ME	1792.73		
Lenth's SME	4290.35		

Table 4.2 lists all the estimable effects for the coded levels of the factors. As can be seen, factor A (i.e mean drag coefficient) contributes around 99.32% of the effect on the bending moment at the lowest end of the riser. Following A, factor B, holds the next significance. This table gives a glimpse of the factors to be considered significant. However, all the factors should be decided significant or not, depending on their p-value, which can be obtained from ANOVA (analysis of variance). Factors that are considered

important from this table are included in the model and analyzed further to check if the model itself is significant with the factors included. So, factors A and B are considered as significant factors as their contribution percentage is higher and included in the model. Also, the curvature is included, though its contribution is only 0.024%. Curvature, here defines whether responses are linearly or non-linearly related to the parameters. To check curvature, it is included in the model, which further from ANOVA decides the linearity of responses with parameters depending on its p-value. It should be noted that the curvature as given by ANOVA is for the model but there may be case when the quadratic relationships may exist among the considered factors. Significant factors are denoted by by 'M', while un-chosen effects are labeled 'e' for error. These effects would be incorporated in the residual used to test the model in the subsequent ANOVA. The software also reports the Length's margin of error (ME) and simultaneous margin of error. It is recommended against these because Length's method doesn't pick effects in a consistently good manner. The SME criterion is more conservative and won't pick as many effects as the ME. It may work for larger sets of data. So, selection of the factors can be drawn based on a Half Normal plot (refer to design expert manual for details).

Factors, which are far away from the straight line in the plot, are considered to be the most significant that affect the response.

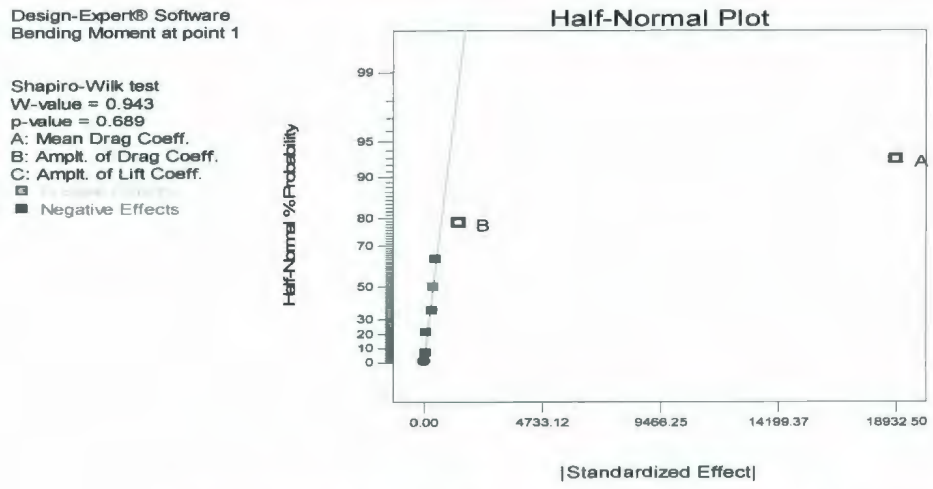

Figure 4.4.1: Half Normal plot of factors for max. BM at mass 1

As shown in the plot 4.4.1, factor A is the furthest point from the straight line indicating a highly significant factor. Next to A is B, which is far away from the straight line showing its significance in affecting the bending moment at lowest point of the riser. Other main factors and the interaction of the factors along the straight line are used as an error in ANOVA. The Half Normal plot and % contribution table give the approximate figures of the significant factors, which further, will be proved from ANOVA, depending on p-value. Generally, curvature is marked as significant in the % contribution table, which is further analyzed in ANOVA to check if it is significant or not based on its p-value.

After identifying the significant factors, analysis of variance (ANOVA) was carried out to check whether the model was significant with the factors included. The analysis of variance can generally be used to confirm the magnitude and direction of the factor effects to determine which variables are likely to be important.

4.4.1.1 Analysis of variance (ANOVA)

In ANOVA, focus should be given to the p-values of the factors included in the model and the p-value of the model itself to decide if the model with the factors included based on a Half Normal plot, are statistically significant or not. The p-value of the curvature here will determine if responses are linearly or non-linearly varied with the parameters concerned.

ANOVA (figure 4.4.2) shows the model with factors A and B is significant as the p-value is less than 0.05, and also each factors, A and B are significant as their p-values are less than 0.05. The p-value of the curvature in this case in not significant, which shows the bending moment at lumped mass 1 varies linearly with the factors A and B. Other terms in ANOVA such as sum of squares, and degrees of freedom are the statistical terminologies in determining the p-values manually. In the 2^3 design with n replicates, the sum of squares for any effect is given as:

$$SS = \frac{(Contrast)^2}{8n}$$, where $Contrast$ gives the total effect of factors.

For example, contrast of factor A can be defined as: $Contrast_A$ = ab+a-b-(1)

where, a, b denotes the main factor effects (a- a is at high level and b at low level) and ab denotes the effect of interaction of factors a and b (both at high levels), (1) denotes both factors at low levels.

Now, it is necessary to check the residual analysis to check the validity of the assumptions of ANOVA.

Use your mouse to right click in individual cells for definitions.

Response 1 Bending Moment at point 1

ANOVA for selected factorial model

Analysis of variance table [Partial sum of squares - Type III]

Source	Sum of Squares	df	Mean Square	F Value	p-value Prob > F	
Model	7.207E+008	2	3.604E+008	1934.12	< 0.0001	significant
A-Mean Drag	*7.169E+008*	*1*	*7.169E+008*	*3847.72*	*< 0.0001*	
B-Ampli. of D	*3.823E+006*	*1*	*3.823E+006*	*20.52*	*0.0062*	
Curvature	1.731E+005	1	1.731E+005	0.93	0.3794	not significant
Residual	9.316E+005	5	1.863E+005			
Cor Total	7.218E+008	8				

The Model F-value of 1934.12 implies the model is significant. There is only a 0.01% chance that a "Model F-value this large could occur due to noise.

Values of "Prob > F" less than 0.0500 indicate model terms are significant.
In this case A, B are significant model terms.
Values greater than 0.1000 indicate the model terms are not significant.

Figure 4.4.2: ANOVA for the bending moment at lumped mass 1

4.4.1.2 Residual Analysis

.

1) **Normal Plot of Residuals:** A check of the normality assumption can be made by constructing a normal probability plot of the residuals. This is a plot of studentized residuals, number of standard deviations of the actual values from their respective predicted values. It is simply a graph of the cumulative distribution of the residuals. Ideally, this will be a straight line indicating no abnormalities. In this case, the

residuals are along the straight line (figure 4.4.3) showing that the residuals follow the normal distribution.

2) **Residuals vs. Predicted**: If the model is correct and if the assumptions are satisfied, the residuals should be structureless, in particular, they should be unrelated to any other variable including the responses. A simple check is to plot the residuals versus the predicted values. A defect that occasionally shows up on this plot is non-constant variance. Sometimes the variance of the observations increases as the magnitude of the observation increases. If this were the case, the residuals would get larger and the plot of residuals would be like an outward-opening funnel or megaphone. The size of the studentized residual should be independent of its predicted value. In other words, the spread of the studentized residuals should be approximately the same across all levels of the predicted values. In this case (figure 4.4.4), points are scattered between the upper and lower margin, which shows the assumption of constant variance is valid.

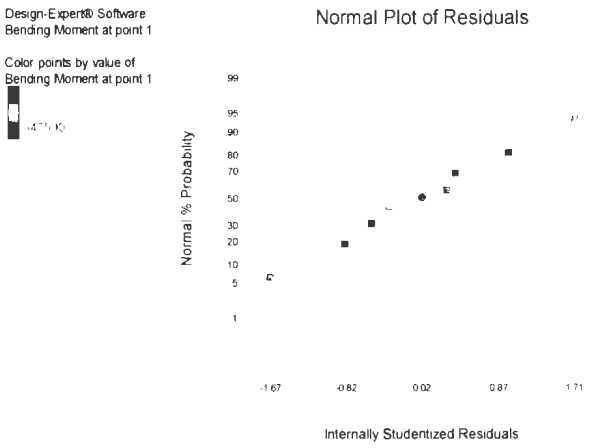

Figure 4.4.3: Normal Plot of Residuals

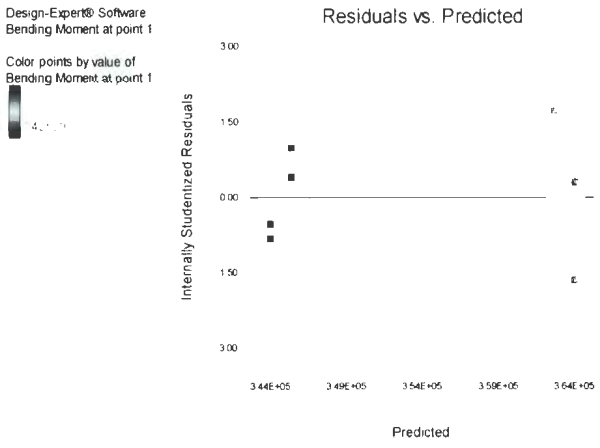

Figure 4.4.4: Residual Vs. Predicted

3) **Box-Cox plot**: This diagnostic plot is to calculate the best power law transformation analytically. The text on the left side gives the recommended transformation, in this

case it is 'None'. The vertical line on 1 in figure 4.4.5 shows the current transformation, which is the power applied to the response values. Since there is no transformation of data done in this case, a value of 1 is identified. If the designer or the experimenter knows the relationship between the variance of the observations, and the mean, they can use this information to guide them in selecting the form of transformation. In some cases, all the observed values should be transformed to the recommended form, for better ANOVA and statistical checks.

4) **Residuals vs Run**: Plotting the residuals in time order of the data collection is helpful in detecting correlation between the residuals. A tendency to have runs of positive and negative residuals indicates positive correlation. This would imply that the independence assumption on the errors has been violated. This plot 4.4.6 shows all the points inside the margin line. If there were any outliers, then it shows some measured magnitudes of the responses far away from the others for the different combinations. In this case, there is no such response value, figure 4.4.6

After the residual checks and confirmation of all statistical assumptions, the relationship between the significant factors and bending moment at lumped mass 1 was investigated. As found, only the drag coefficients affect the maximum bending moment whereas the lift force coefficient, statistically does not affect the bending moment.

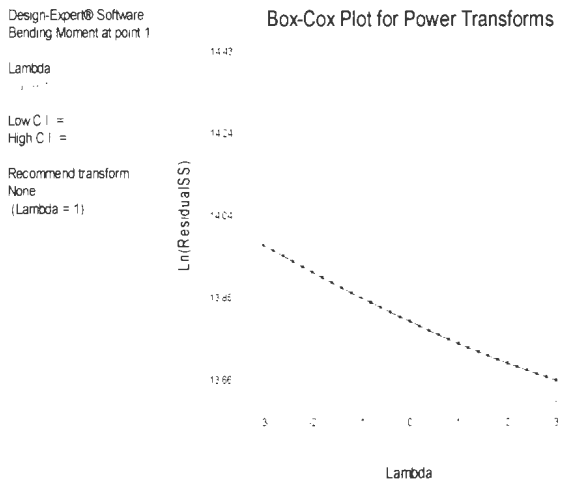

Figure 4.4.5: Box-Cox plot

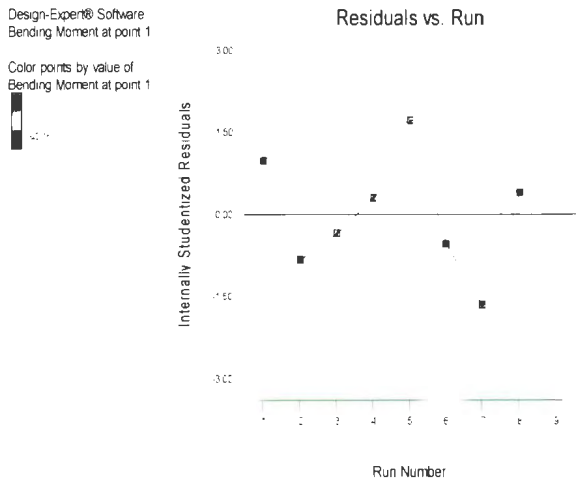

Figure 4.4.6: Residuals vs. Run

4.4.1.3 Examine the main effects

1) Influence of mean drag coefficient

Figure 4.4.7 is a plot obtained after ANOVA, and residual checks, which shows the direction of Bending Moment with the changes of the magnitude of Mean Drag Coefficient. It shows the maximum bending moment at the touchdown zone of the riser, represented by lumped mass 1, decreases sharply with the increment of the mean drag force coefficient. The text on the left side of the plot shows the magnitude of other factors, for which the bending moment is varied with the variation of drag force coefficient.

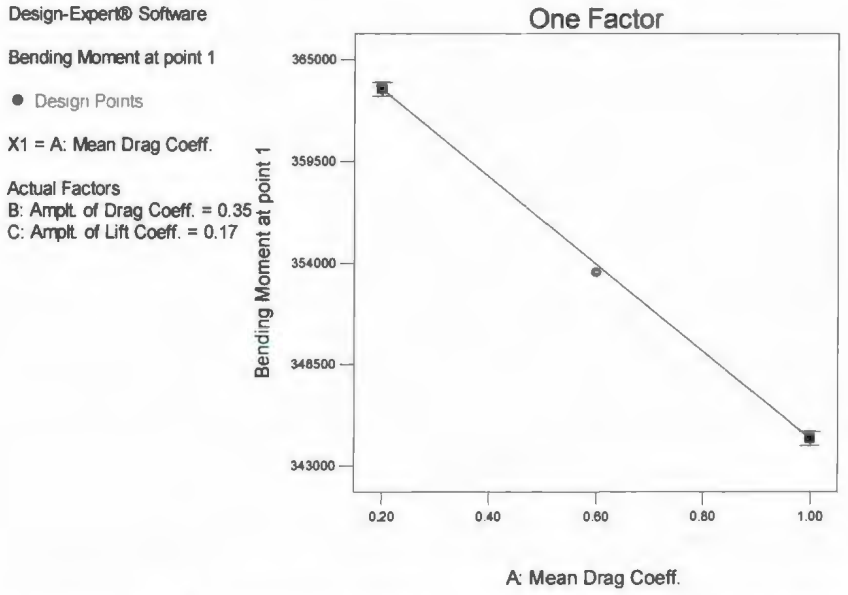

Figure 4.4.7: Influence of Mean Drag Coefficient on max. BM at lumped mass 1

2) Influence of amplitude of drag coefficient

Next in importance to the mean drag coefficient is the oscillating drag coefficient in affecting the maximum bending moment at the touchdown zone of the riser. The plot 4.4.8 shows the nature of bending moment with the variation of oscillating drag. The rate of change in bending moment due to oscillating drag is lower than that of the mean drag.

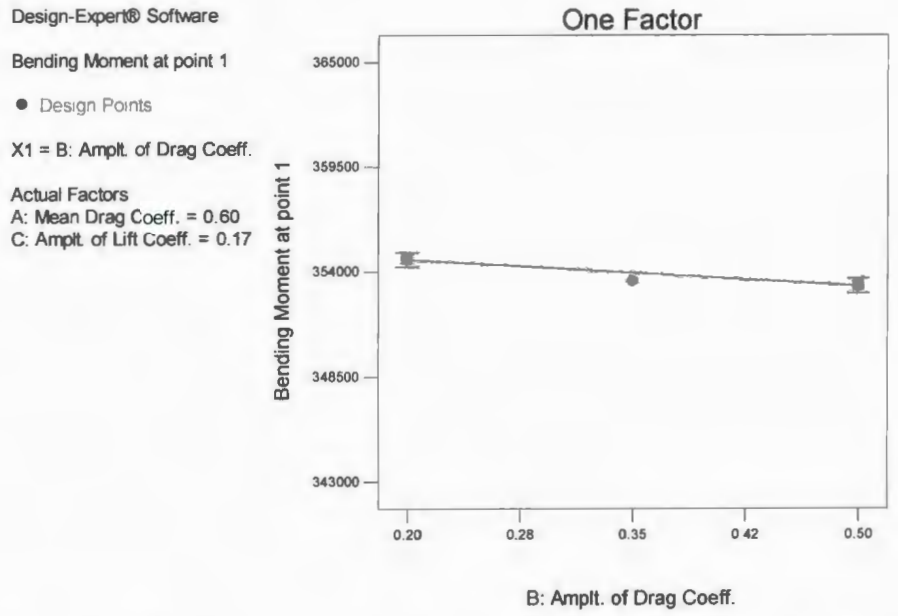

Figure 4.4.8: Influence of Amplitude of Drag Coefficient on max. BM at lumped mass 1

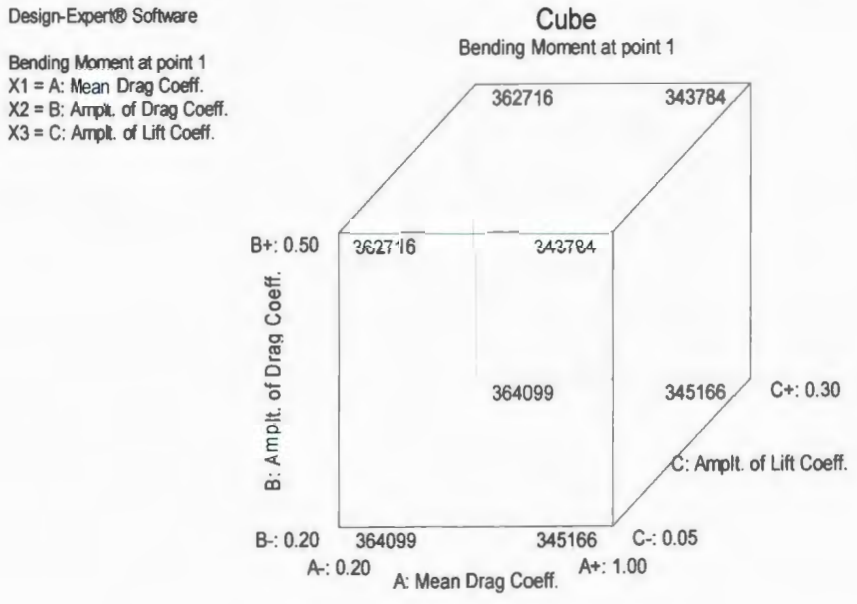

Figure 4.4.9: Cubical plot for max. BM at lumped mass1

Figure 4.4.9 shows the maximum bending moment at lumped mass 1 with all the force coefficients. As can be seen, with the increment of drag force coefficient from low level to high level, maximum bending moment decreases from 364099 Nm to 345166 Nm.

Also, increasing the oscillating drag from its low to high level, maximum bending moment at the touchdown zone of the riser reduces to 362716 Nm from 364099 Nm. Maximum bending moment doesn't change with the change in levels of lift force coefficient. The maximum bending moment is developed for the combinations of lowest levels of drag force coefficients as seen at the left corner of the plot.

A linear mathematical model can be developed with the help of ANOVA. For the case of curvature being significant, the Response Surface methodology can fit a second order equation. Bending moment at the lowest point, i.e. at mass 1, can mathematically be represented as given by ANOVA in the form of:

*Bending Moment at point 1 = 3.69789*10^5-23695.875*Mean Drag Coeff.-4691.6667 * Amplitude of Mean Drag Coeff.*

To check the accuracy of the mathematical model developed from ANOVA, bending moment was measured at the lumped mass 1 from the simulation for the values of mean drag coefficient of 0.6, oscillating drag of 0.35 and lift coefficient of 0.17, which gave the magnitude of 3.532×10^5 Nm. For the same values of force coefficients, the bending moment from the developed mathematical model gives the bending moment as 3.53×10^5 Nm. It shows the mathematical model developed from the ANOVA shows the permissible agreement with the values from the simulation. An error of 0.20% between the values may be due to the lift force coefficient. The lift force coefficient is omitted in the equation while it was included during simulation.

The same procedure was followed for the rest of the responses.

4.5 Blocking and confounding

For the second parametric study, where the current was varied with the water depth, five factors were taken into consideration. In addition to the force coefficients, internal flow was chosen, which considers the discharge ranging from 0 m^3/sec (no flow) to 0.02 m^3/sec. Because of the internal fluid flow, pressure is induced within the walls of the

riser. Only the linear variation of internal pressure has been considered within the riser segments. Effects of the internal flow were incorporated in the code to account for the changes in the discharge within the riser. Change in the levels of internal flow discharge in this study was accounted for by changing the pressure variation within the riser.

Table 4.3: Factors for the case of sheared flow

Factors	Coded factors	High Value (+1)	Low value (-1)
Mean Drag Coefficient	A	1	0.2
Oscillating Drag Coefficient	B	0.5	0.2
Lift Coefficient	C	0.3	0.05
Internal fluid discharge	D	0.02 m^3/sec	0
Position of the top point Pn	E	50 m	0

Another factor E, represents the change in the position of the top-end of the riser with respect to its original position, which may occur during the riser launching, positioning and production. The top end point P_n was fixed to a position of 50 m away from its original position, which is coded as a high value in the analysis, 0 m represents the original position of the top end. The movement was in the right direction to its original position as shown in the figure 4.5.1.

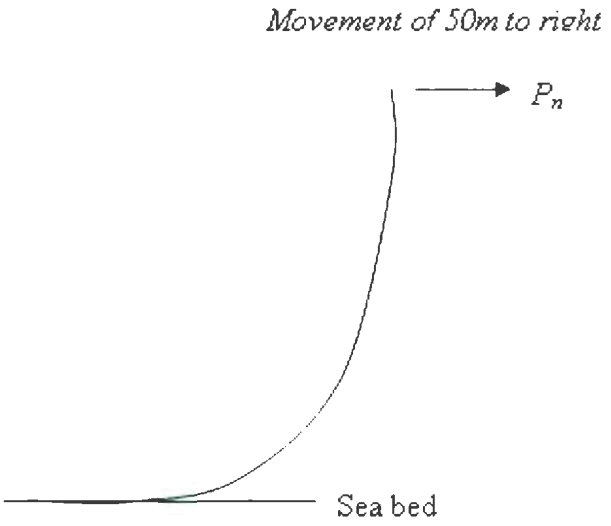

Figure 4.5.1: Movement of top-end of riser towards the right from its original position

Therefore, this analysis involves two levels, and can be represented as 2^5 (32 treatments for the simulation). Running 32 simulations was time consuming as one simulation takes about 10-11 hours depending on the computer processor. However, the statistical information can even be derived without running 32 simulations, which can be achieved through the process called blocking and confounding, where only certain and appropriate treatments are run at the expense of losing other interaction effects. The treatment of factors and their interactions are divided into blocks after the contrast is defined. Only a certain block is selected for the analysis through which statistical information can be determined. In this case, 2^{5-1} fractional factorial design was adopted, where one interaction of factors of higher order would be neglected. This means, out of 32 simulations, only half simulations would be run. In 2^{5-1} design, 1 represents the number of confounded effects, and is assumed to confound the higher order interaction of the factors. In this case, interaction ABCDE was confounded.

So, I=ABCDE, is a defining contrast. Running half of the full factorial designs lead to the development of two blocks, the first block is called the 'Primary block' which includes all the factors at low levels, denoted by '1'.

In blocking, the main effects get aliased with the interaction of the main factors. The alias structure may be found by multiplying each effect column by the defining relation.

Table 4.4: Treatment of factors divided into two blocks

Primary Block	Block 2
l	a
ab	b
ac	c
bc	abc
ad	d
bd	abd
cd	acd
abcd	bcd
ae	e
be	abe
ce	ace
abce	bce
de	ade
abde	bde
acde	cde
bcde	abcde

So, in this case, factor A will be aliased with BCDE.

[A]= BCDE

[B]= ACDE

[C]= ABDE

[AB]= CDE

[BC]= ADE

[AC]= BDE

In the analysis which involves confounding, attention should be paid in making decisions regarding the aliased terms. For example, if the main factor (which is aliased with other main factors or interactions) affects significantly the responses, it should not necessarily

be concluded that the main factor is the only factor to affect that response. Since the effects are aliased, further analysis has to be carried out, called the 'Fold Over Design', which de-aliases the terms, and the effects of the main factors can be investigated. In this analysis, no main effect or two-factor interaction was aliased with any other main effect or two-factor interaction, but two-factor interactions are aliased with three-factor interactions. This sort of design is called the 'Resolution V Design'. In some cases, no main effects are aliased with any other main effect, but main effects are aliased with two-factor interactions and two-factor interactions may be aliased with each other. This is called "Resolution III Design', represented as 2^{3-1}. Another design represented as 2^{4-1}, is called Resolution IV Design, in which no main effect is aliased with any other main effect or with any two-factor interaction, but two-factor interactions are aliased with other.

Defining the confounding effect (and arranging the treatment of factors as shown in table 4.4) and aliasing terms, a block was chosen to carry out the simulation. Primary block treatment was considered for the simulation, so with eight treatments of the factors as shown above, the simulation was run for 1000 seconds and the various responses were measured. Block 2 would have been taken for the simulation for the case of de-aliasing terms. However, there was no need of de-aliasing the terms in this study. To check the linear relationship among factors and the effects, a simulation was run with the mid value for all the factors. The main difference between running the simulation for full factorial and half factorial is the introduction of aliased terms with the main factors.

After getting all the response magnitudes, the same procedure was followed to find the parametric relationships. To show the difference between the full factorial and the fractional factorial design, analysis for bending moment at point 1 has been discussed, which shows how the main factors were aliased with the other factors interactions of higher orders.

4.5.1 Maximum bending moment at lumped mass 1

Table 4.5 lists the percentage contribution of factors in affecting the maximum bending moment at the touchdown zone. In this case, the maximum bending moment is highly affected by the lateral drift of the riser top-end. It contributes about 99.13% in affecting the maximum bending moment, followed by the mean drag and internal fluid pressure. Among the force coefficients, the mean drag force coefficient has the highest influence on bending moment. Since, the riser top-end movement has 99.13% influence, the force coefficients contribution in this case seems to be negligible. However, among the force coefficients, the same relationship exists for the case of maximum bending moment at the touchdown zone irrespective of the flow type (uniform or shear). Factors holding a higher percentage of the total contribution were included in the model, and they are represented by 'M'. Other terms like C, AB, AC, which are represented by 'e' are the residual terms or the error terms. The terms such as ABC, ABD, represented by '~' are the aliased terms, as defined earlier. So, it should not be necessarily assumed that a contribution by factor 'A' is just a sole contribution, as its structure exists in the form of [A] = BCDE. So the contribution could be from BCDE. But in this case, terms B and C are almost negligible, and their combined effects are negligible. So, it is reasonable to conclude that this highest significance is due to factor A primarily. The same results were derived from the Half-Normal plot (figure 4.5.2). Factors such as E lie furthest from the straight line, showing its highest significance for the response of bending moment, followed by other factors such as A and D. The rest of the blocks along the straight line are the errors, which were not included in the model for ANOVA.

Table 4.5: Contribution of factors on bending moment at mass 1 for shear flow

Term	Stdized Effects	Sum of Squares	% Contribution
Intercept			
A-Mean Drag Coeff.	-4875.00	9.506E+007	0.59
B-Amplt. od Drag Coeff.	-550.00	1.210E+006	7.525E-003
C-Amplt. of Lift Coeff.	-200.00	1.600E+005	9.951E-004
D-Inside Fluid	3000.00	3.600E+007	0.22
E-Sway at the top	-63125.00	1.594E+010	99.13
AB	-425.00	7.225E+005	4.493E-003
AC	-475.00	9.025E+005	5.613E-003
AD	-275.00	3.025E+005	1.881E-003
AE	400.00	6.400E+005	3.980E-003
BC	-350.00	4.900E+005	3.047E-003
BD	-300.00	3.600E+005	2.239E-003
BE	275.00	3.025E+005	1.881E-003
CD	-350.00	4.900E+005	3.047E-003
CE	225.00	2.025E+005	1.259E-003
DE	775.00	2.402E+006	0.015
ABC		Aliased	
ABD		Aliased	
ABE		Aliased	
ACD		Aliased	
ACE		Aliased	
ADE		Aliased	
BCD		Aliased	
BCE		Aliased	
BDE		Aliased	
CDE		Aliased	
ABCD		Aliased	
ABCE		Aliased	
ABDE		Aliased	
ACDE		Aliased	
BCDE		Aliased	
ABCDE		Aliased	
Curvature	4.106E+005	9.888E+005	6.150E-003
Lenth's ME	1349.56		

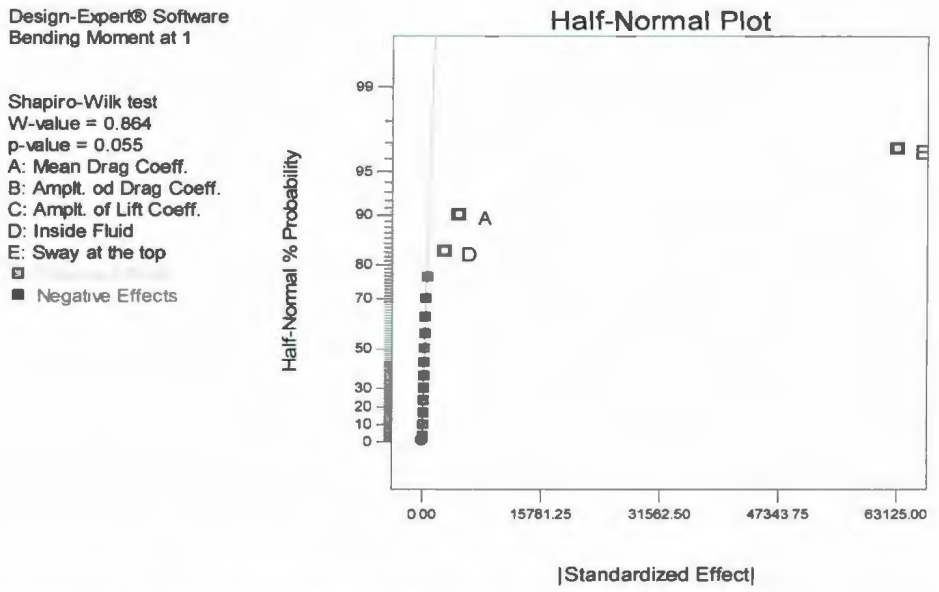

Figure 4.5.2: Half Normal plot for max. BM at lumped mass 1

After identifying the significant factors to be included into the model, an ANOVA was carried out to check whether the model was significant with the terms included, followed by the residual checks. Further, each factor and interaction term was diagnosed to check its relationship with the responses.

The curvature for the model was found insignificant for the case of bending moment, in-line amplitude, whereas, curvature for the model was found significant for the case of maximum tension, maximum tensile stress and the cross flow displacement. So, there was a linear parametric relationship of factors with the responses for the case of bending moment and in-line amplitude. To develop a mathematical model for the case, when curvature is significant, all the treatments of factors have to be run at three levels, and then using the 'Response Surface Methodology', quadratic equations are be fit to the model. In this study, understanding parametric relationships among the parameters and responses was of major concern, so no simulations were carried out at three levels. Also there was no need to carry out the 'fold over design' to de-alias the terms. Otherwise, complete or semi-fold-over design should be carried out to de-alias the terms.

The results obtained from DOE are presented and discussed in the next chapter in detail.

Chapter 5

Results and Discussion

5.1 Analysis for the force coefficients

Full factorial simulation was carried out for the parametric study of force coefficients upon the riser responses, where the riser was subjected to a uniform current velocity of 0.5m/s at a Reynolds number>$3x10^5$. Different lumped masses were chosen along the riser length to check the variation of effects on the riser responses on different segments. After running the simulation for the described treatment of the parameters for the same time period, responses like Maximum Bending Moment, Maximum Tension, Maximum Tensile Stress, Cross Flow, and In-line Amplitude were measured. Then statistical analysis was carried out using the Design Expert 7.1 software. The following parametric relationships were obtained after the proper statistical checks.

5.1.1 Maximum bending moment

i. At the lowest point of the riser (touchdown zone), represented by the lumped mass 1, maximum bending moment is affected significantly only by the drag force coefficients, the mean and the oscillating drag. The mean drag force coefficient affects the maximum bending moment at a higher rate than the oscillating drag (figure 5.1.1). With a positive increment of the mean and oscillating drag, the maximum bending moment decreases.

ii. At the top-most point of the riser, represented by the lumped mass 99, the mean drag and the oscillating drag coefficient affect the bending moment. With the increment of drag force coefficient, the bending moment increases sharply, and moderately increases with the increment of oscillating drag force coefficient. Figure 5.1.2 shows the variation of bending moment at the lumped mass 99 where drag force coefficient affects the bending moment highly than the oscillating drag coefficient.

iii. At the 10th lumped mass, the drag force coefficient follows the same effect as for the lumped mass 1. Drag force coefficient decreases the response.

iv. At the 50th lumped mass, the drag force coefficients increase the bending moment.

The variation of the bending moment with the force coefficients was linear, as shown in figure 5.1.1 and 5.1.2.

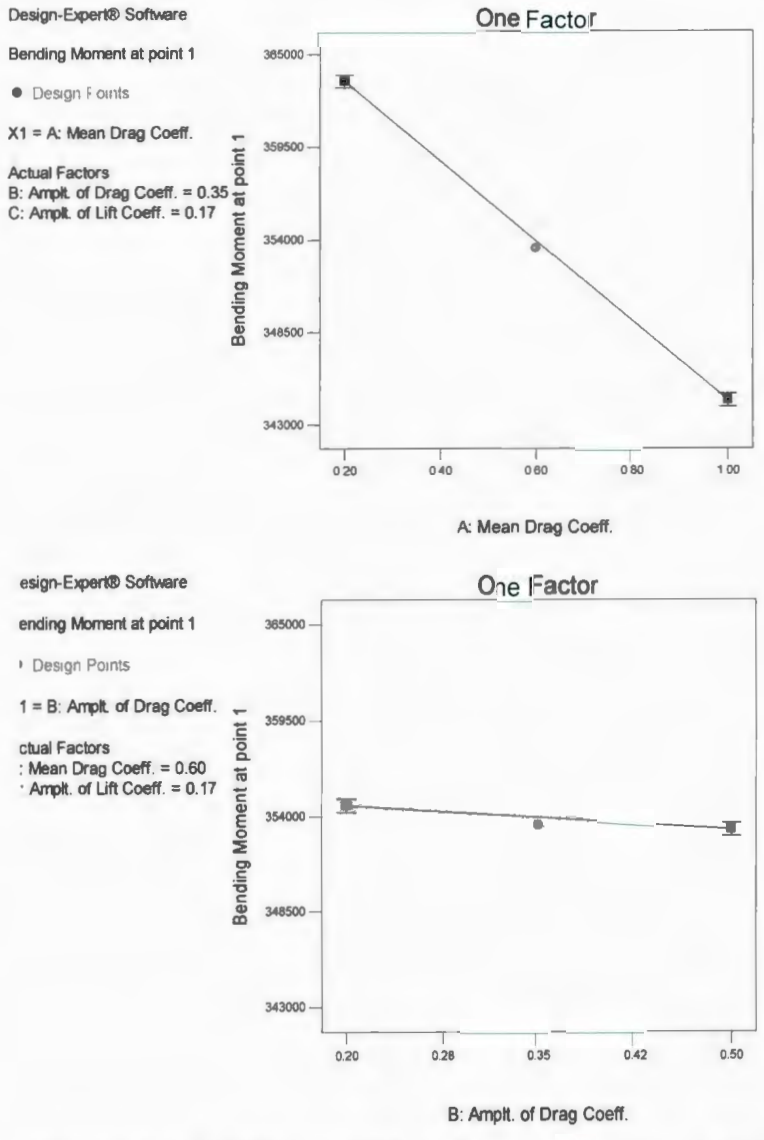

Figure 5.1.1: Influence of drag force coefficients on max. B.M at lumped mass 1

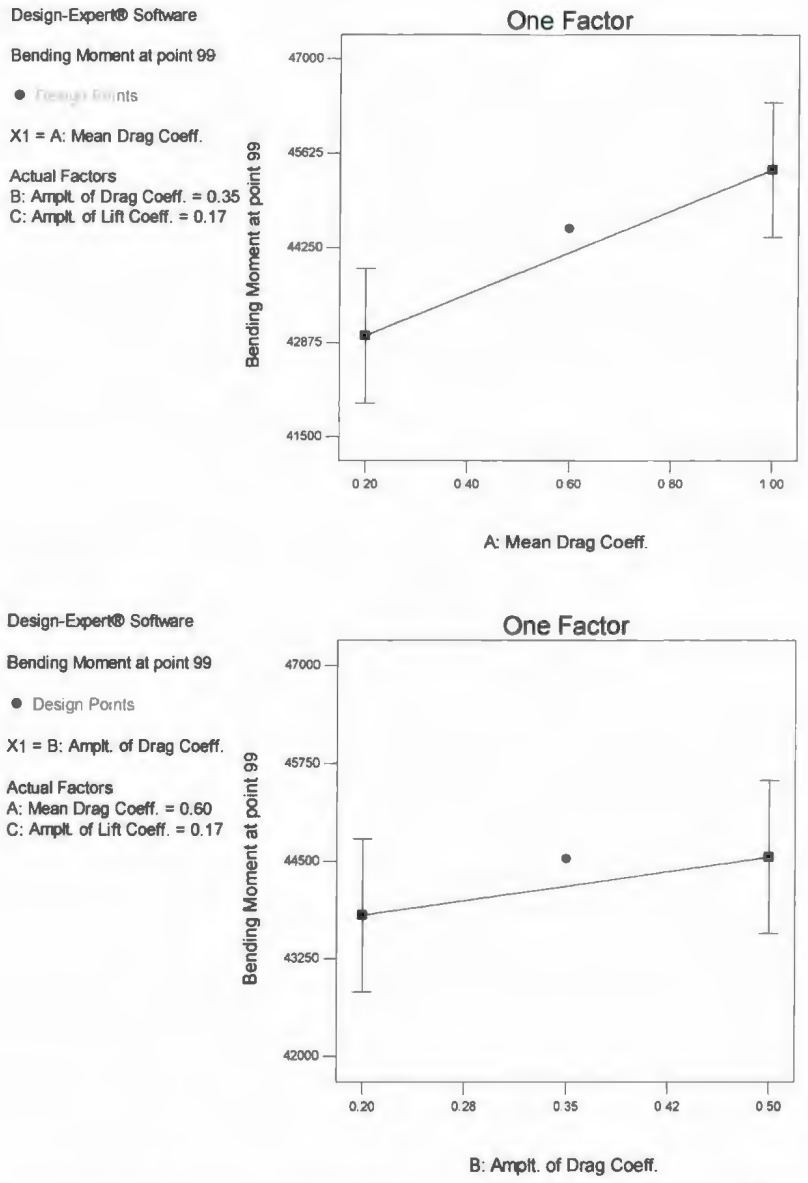

Figure 5.1.2: Influence of drag force coefficients on max. BM at lumped mass 99

Therefore, it shows that drag force coefficients affect the maximum bending moment of the riser, while lift force coefficient does not contribute a significant effect to bending moment. However, the drag force shows the contrasting effect on different segments of the riser. Bending moment is reduced with the increment of the drag forces on the portion of riser which is in contact with the seabed (represented by lumped mass 1 and 10),

whereas the drag forces increase the bending moment on the riser above the seabed (lumped mass 50 and 99). This is because of the geometry of the riser. Riser segments, represented by lumped masses 1 and 10, lie on a seabed, where the riser geometry is curved, and the increased drag forces reduce the bending moment. Whereas, the riser portions, above the seabed, are straight and hanging (because of weight of the lumped masses), and the increased drag forces (with time) increase the bending moment.

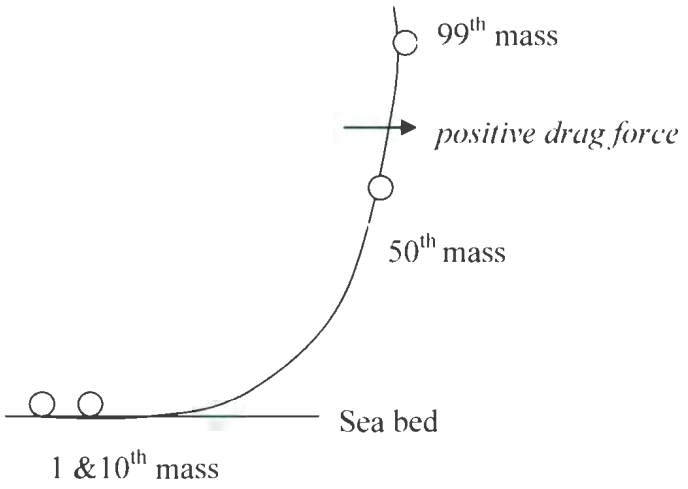

Figure 5.1.3: Position of lumped masses on a riser

Maximum bending moment at the riser portions on the seabed initially is higher than that of the portions above the seabed. The increment of the drag force tends to straighten the riser portions in touchdown zone, and decreases the maximum bending moment. While for the portions above the seabed, the drag force increases the maximum bending moment. However, maximum bending moment at touchdown zone is comparatively higher than that of hanging portion. The following figures show the maximum bending moment developed at lumped masses 1and 99, which show the comparative magnitude of bending moments. Bending moment at the transient state (which is higher) is reduced with the increased drag force. For example, as shown in figure 5.1.4 and 5.1.5, bending moment at lumped mass 1 is reduced to 3.636×10^5 Nm from 3.98×10^5Nm. However, the

bending moment at touchdown zone is comparatively higher than of the hanging portions.

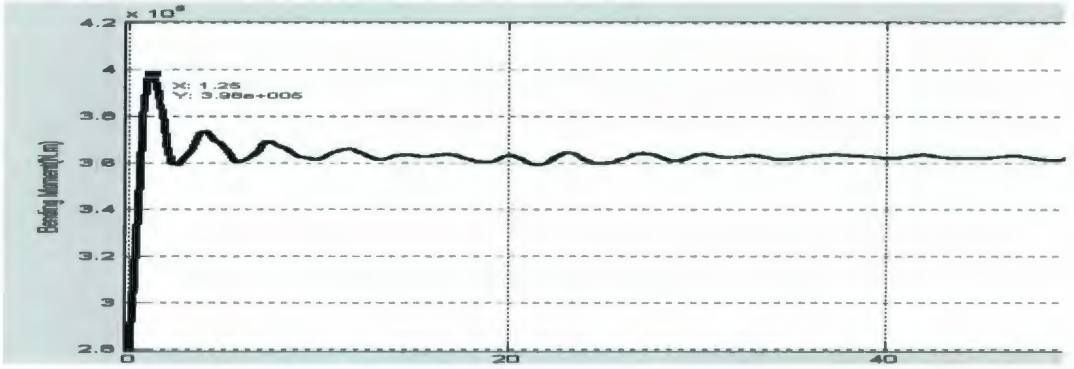

Figure 5.1.4: Initial Maximum Bending Moment at lumped mass 1

(B.M. =3.98x10^{5}Nm)

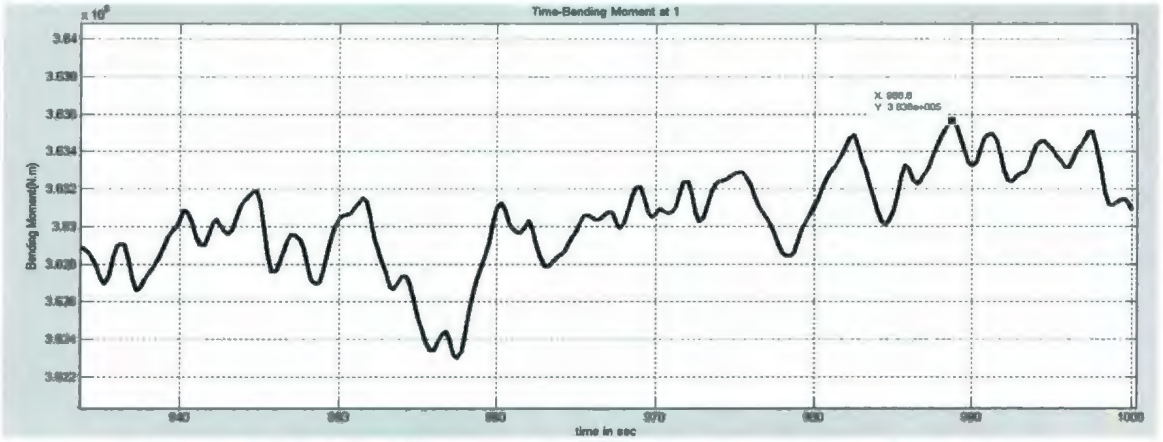

Figure 5.1.5: Final Maximum Bending Moment at lumped mass 1

(B.M. =3.636x10^5 Nm)

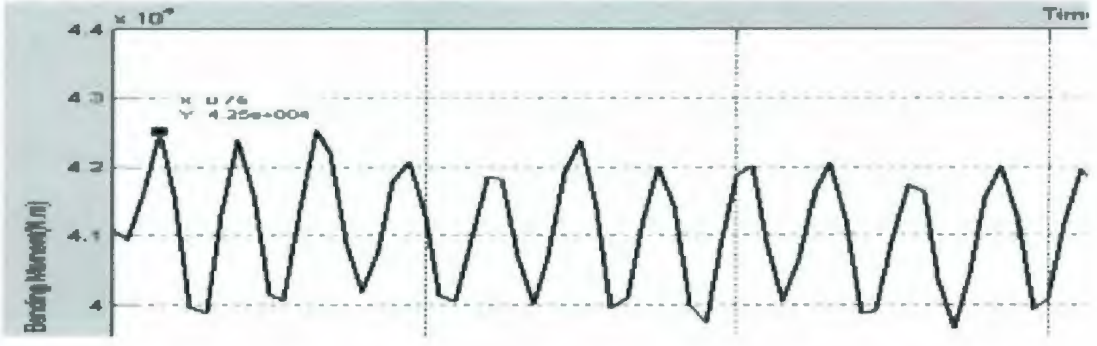

Figure 5.1.6: Initial Maximum Bending Moment at lumped mass 99

(B.M. =4.25x10^4 Nm)

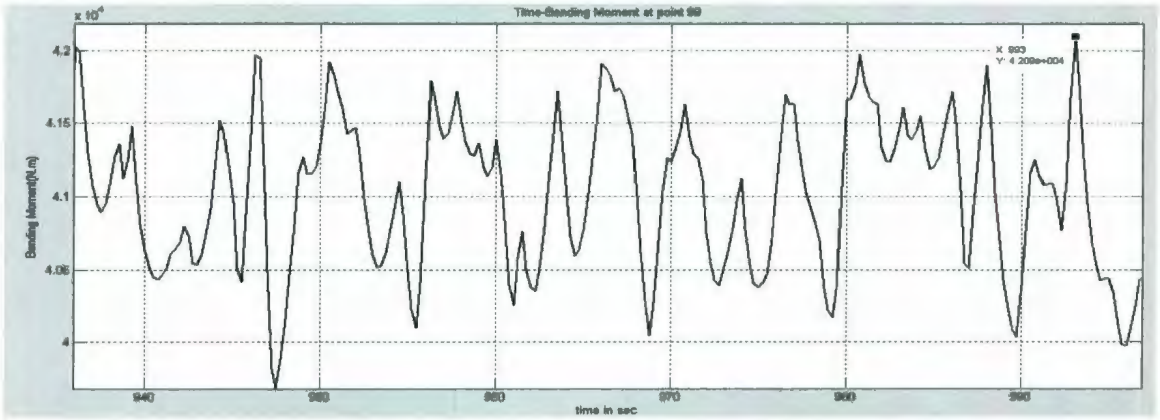

Figure 5.1.7: Final Maximum Bending Moment at lumped mass 99 (B.M=4.209x10^4 Nm)

5.1.2 Maximum tension

Only the drag force coefficients affect the maximum tension on the riser segments, while, the lift force coefficient has no significant contribution. Mean drag increases the tension at a higher rate than the oscillating drag. It was found that irrespective of the riser portion either lying on seabed or hanging, the drag force increases the tension on the riser. A linear relationship exists between the tension and the drag coefficients for all the masses. Figure 5.1.8 shows the variation of maximum tension at the lumped mass 100. As seen, maximum tension increases when the mean drag force coefficient increases from 0.2 to 1. Mean drag being higher than the oscillating drag, increases the tension on riser segments at a higher rate than the oscillating drag. Also, for lumped mass 50, the same relationship exists. Increased drag force increases the tension on riser segments. Figure 5.1.9 shows the increment of tension when drag forces are changed from low level to high level. The variation of tension was linear with the drag forces. The lift force doesn't influence the tension significantly.

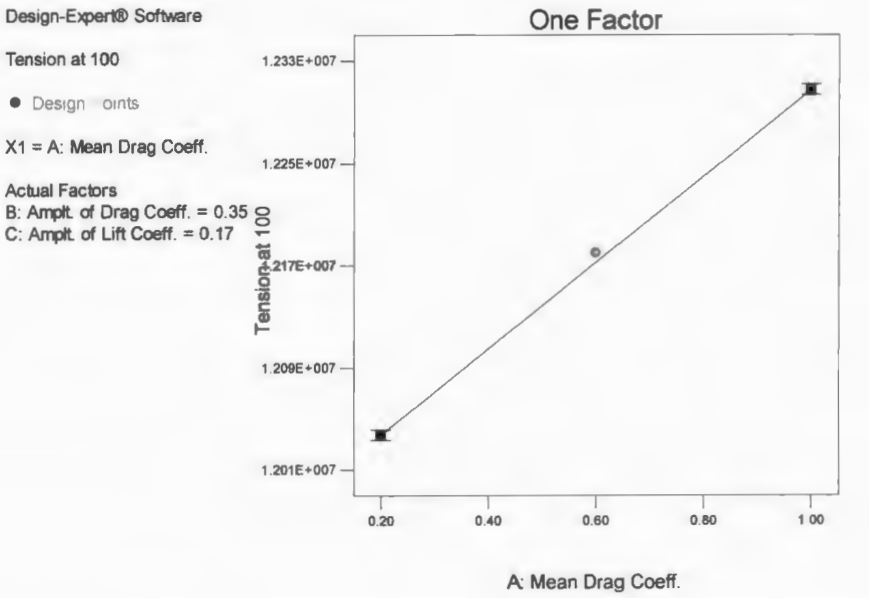

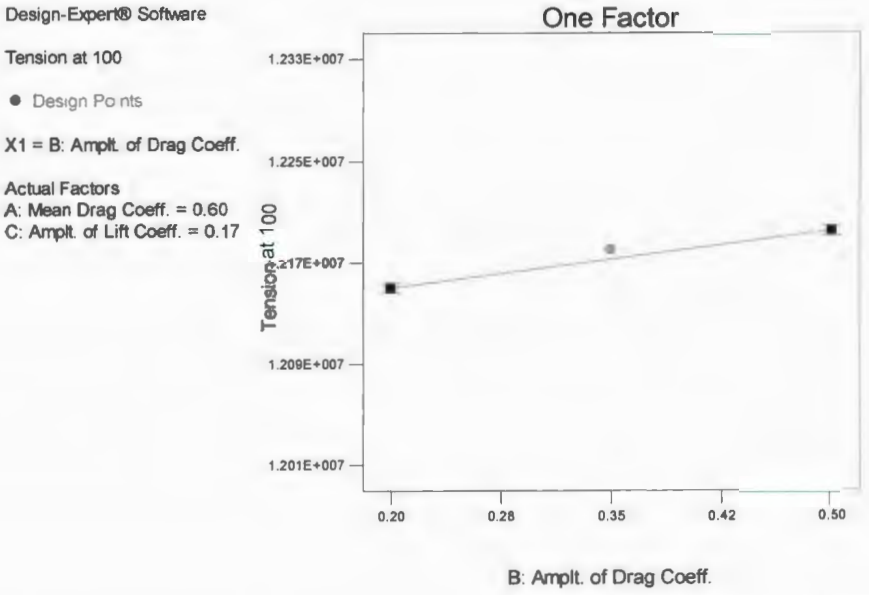

Figure 5.1.8: Influence of drag force coefficient on max. tension at lumped mass 100

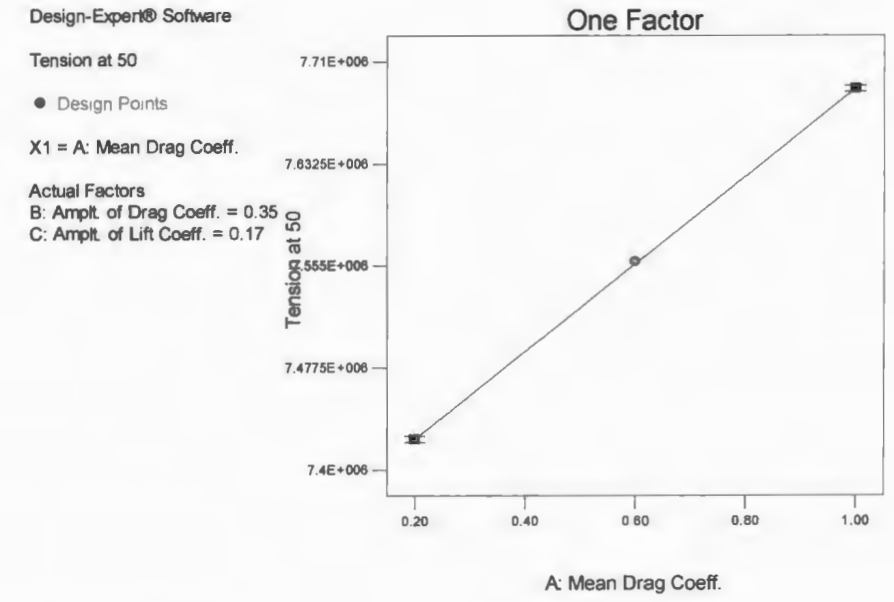

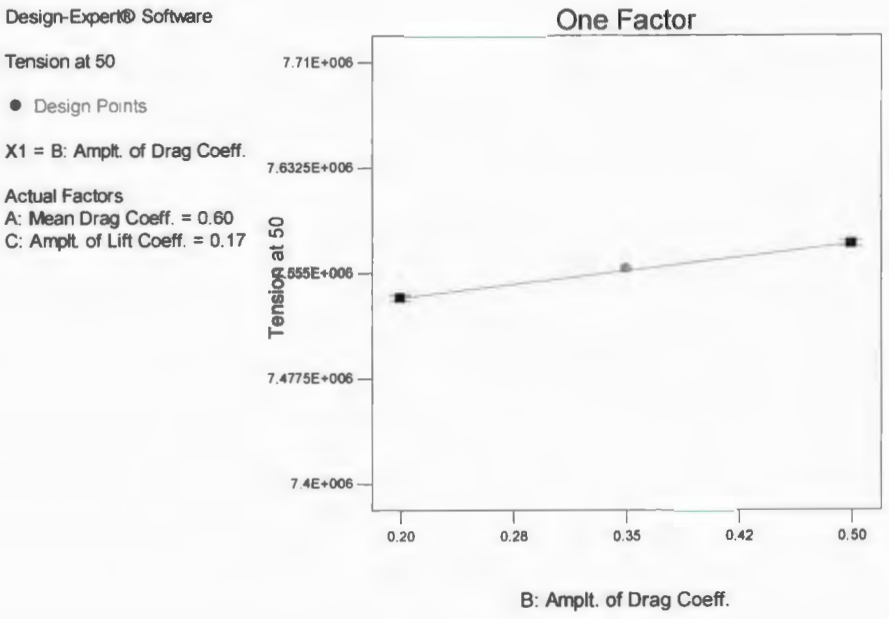

Figure 5.1.9: Influence of drag force coefficient on max. tension at lumped mass 50

5.1.3 Maximum tensile stress

The maximum tensile stress on the riser segments is affected by the drag force coefficients. The lift force coefficient has a negligible effect. Mean drag coefficient increases the tensile stress highly, whereas the oscillating drag has a moderate effect. The same linear relationship exists for all the masses. Since both the end points of the riser are pinned, drag tends to straighten the riser, which in turn increases the maximum tensile stress on riser segments.

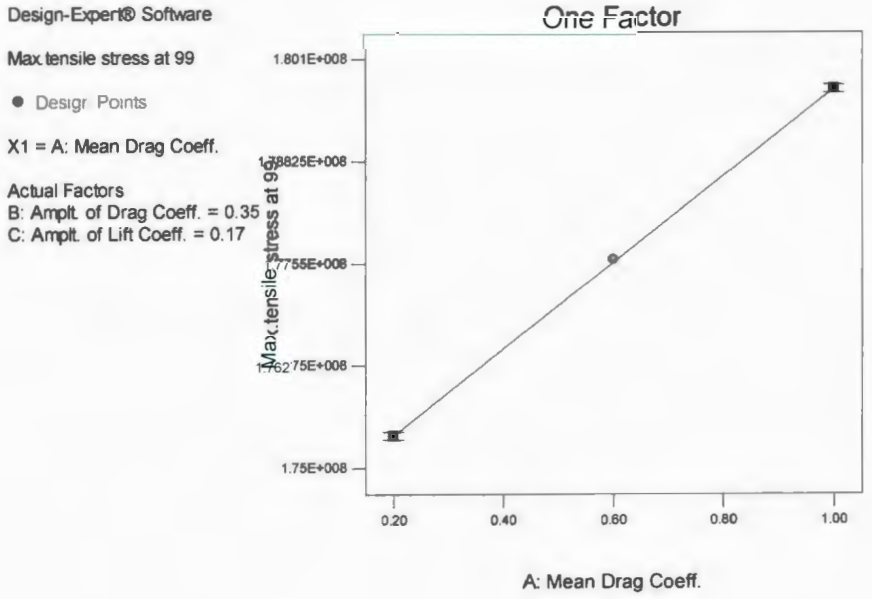

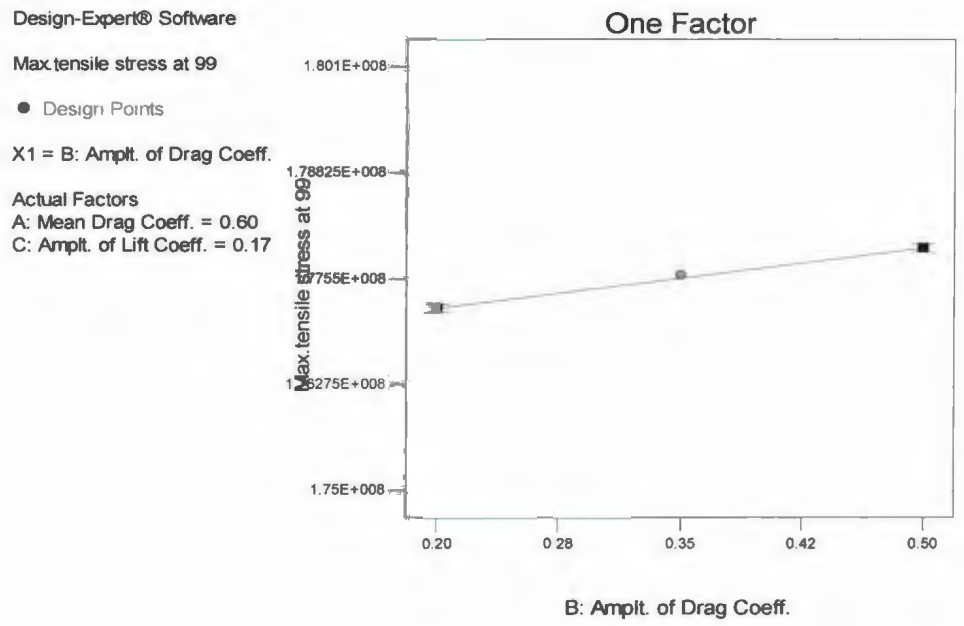

Figure 5.1.10: Influence of drag force coefficient on max. tensile stress at lumped mass 99

In general, it is seen that the riser positions affect the variation of bending moment with the variation of drag force coefficients. However, other responses like maximum tension and tensile stress are unaffected by the riser geometry. Drag force increases the maximum tension and tensile stress along the riser length as the riser is pinned at both ends. Bending moment is highest at the lowest end of the riser, which decreases on riser segments away from the bottom end. While, tension and tensile stress is higher on riser segments on and near to the top-end of the riser. Positive drag force tends to straighten the riser portion on the sea bed, which decreases the maximum bending moment on it, while drag increases its maximum tension and tensile stress. Drag force on the riser segments above the seabed in increases the maximum tension and tensile stress.

5.1.4 Cross flow displacement

The cross flow displacement is affected mostly by the lift force coefficient, and partly by the drag force coefficient. With the increment of lift force, the cross flow amplitude

increases linearly for the lowest and top-most point on the riser (figure 5.1.12). An increase in mean drag reduces the cross flow displacement (figure 5.1.13). This relationship exists for the lumped mass 5 and 99. The mean drag coefficient increases the tension and tensile stress which may reduce the oscillations of the riser segments in the cross-flow direction. Fluctuation of the drag force may be expected to increase the cross-flow oscillations, but as the mean drag force is higher than oscillating, suppresses the influence of the oscillating drag. This was found to statistically significant. Displacement in this study was measured in terms of its amplitude.

There was no significant effect of oscillating drag on the cross flow displacement.

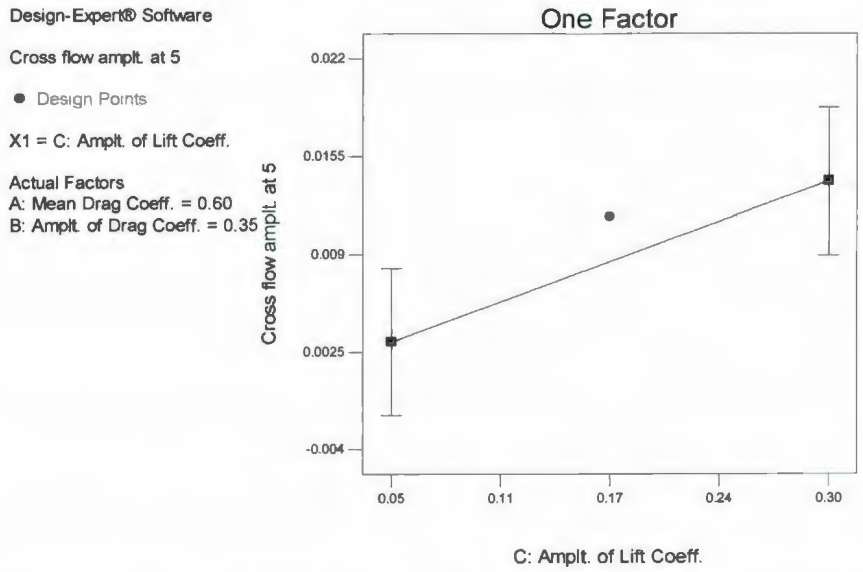

Figure 5.1.11: Influence of lift force coefficient on cross-flow amplitude at lumped mass 5

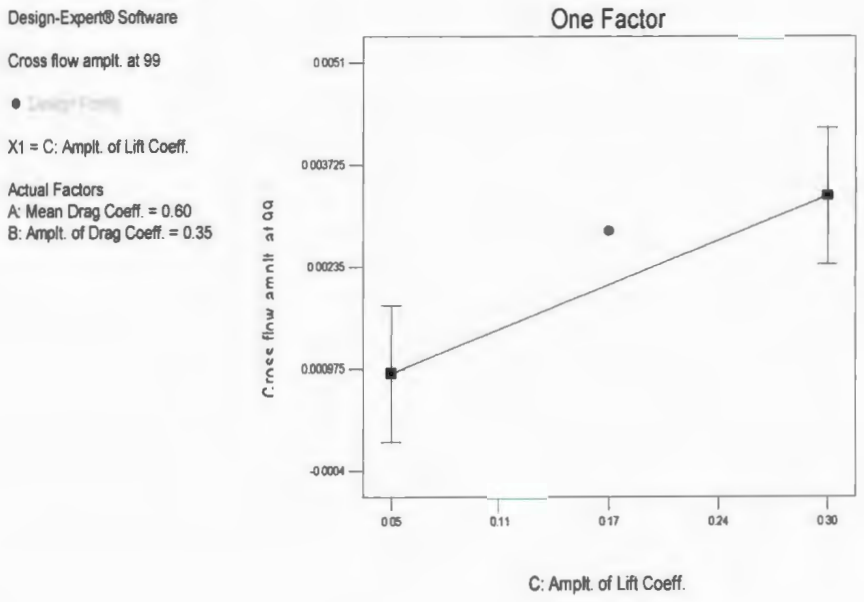

Figure 5.1.12: Effect of lift force coefficient on cross flow amplitude at lumped mass 99

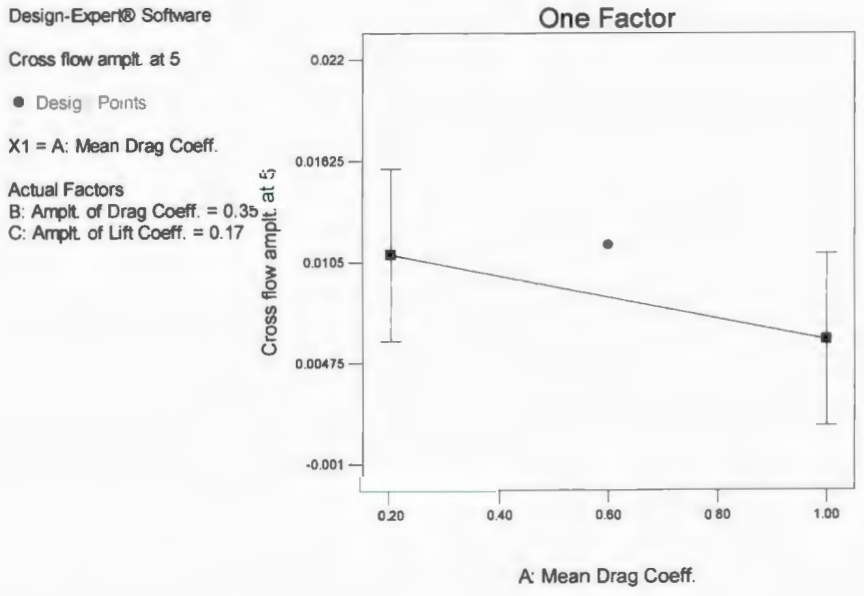

Figure 5.1.13: Effect of mean drag coefficient on cross-flow displacement at lumped mass 5

5.1.5 In-line displacement

The in-line displacement, measured by its amplitude on different riser segments show different responses to the variations of force coefficients, depending on the riser position.

i. At lumped mass 5 (at the touchdown zone), the lift force coefficient increases the in-line displacement as does the drag force coefficient. The lift force coefficient influence is the main effect for the in-line displacement. The interaction between the mean drag and oscillating drag affects the in-line displacement (figure 5.1.15). For a low level of the oscillating drag, the in-line displacement increases with the increment of the mean drag force as shown in figure 5.1.14. While, for a higher level of oscillating drag, the in-line displacement decreases with the increment of the mean drag. The triangular block in the figure represents the higher level of oscillating drag, while the rectangular block represents the oscillating drag at low level for which in-line displacement increases with mean drag (figure 5.1.15). This could be because the mean drag force coefficient acts as opposing force enough to reduce the in-line displacement for negative drag amplitude. For the positive side of the oscillating drag, the mean drag force coefficient may not be high enough to overcome the resistive force for which oscillating drag increases the in-line displacement.

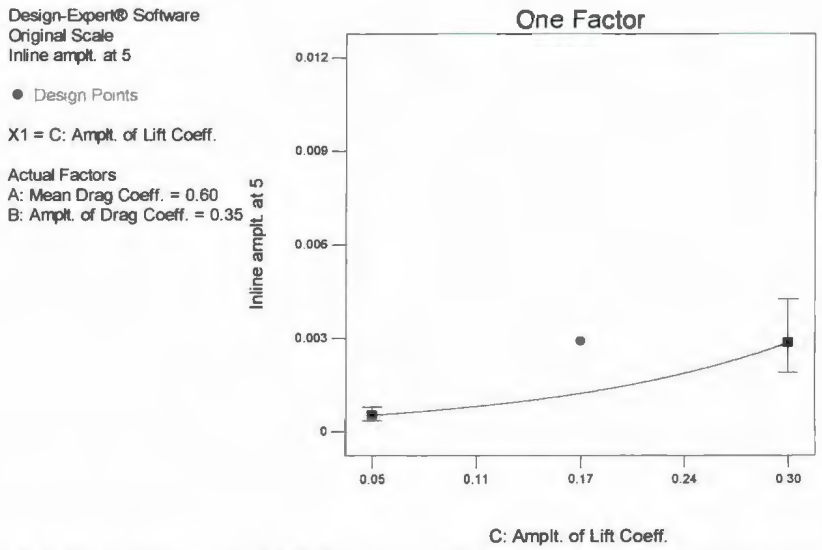

Figure 5.1.14: Influence of lift force coefficient on in-line displacement at lumped mass 5

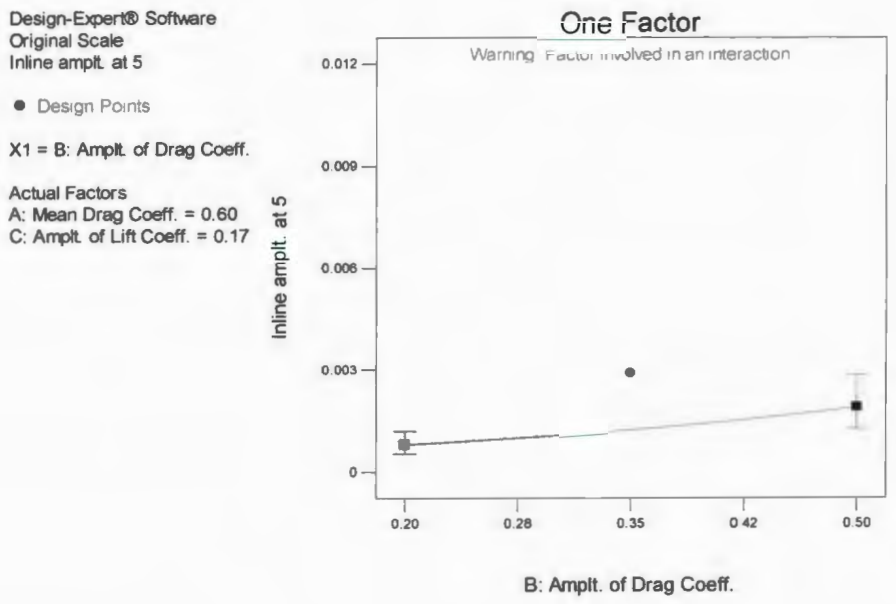

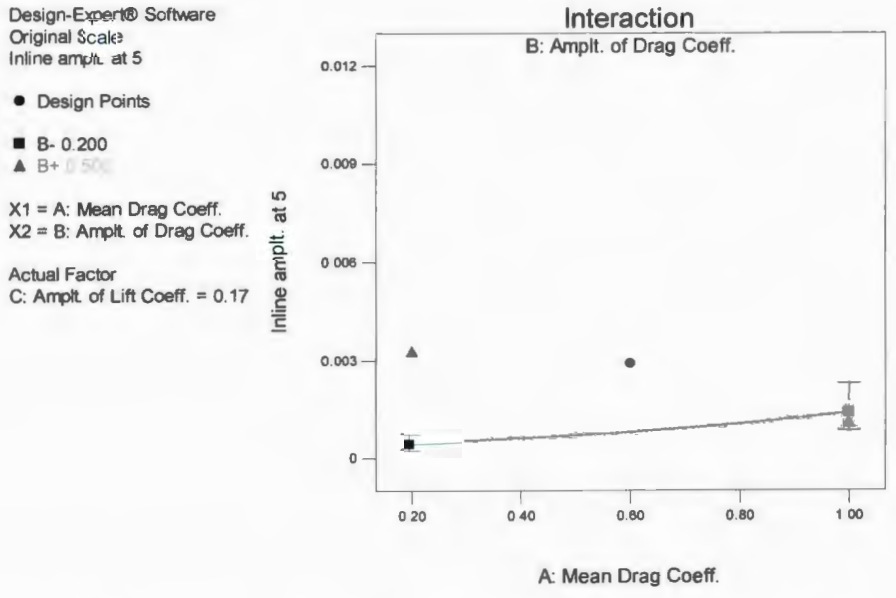

Figure 5.1.15: Influence of drag coefficients on in-line displacement at lumped mass 5

In the figure 5.1.15, a warning stating *factor involved in an interaction* can be seen, where the in-line displacement seems to be varying with the increment of oscillating drag level. This means oscillating drag affects the in-line displacement at mass 5 depending on the level of mean drag coefficient, so the analysis of oscillating drag should be done

along with the mean drag at the same time. Since, mean drag force affects the response in conjunction with oscillating drag, analysis of the response using only that plot would not be appropriate as in-line displacement may increase/decrease with change in oscillating drag force for non-constant mean drag.

ii. The in-line displacement at the point 50 is affected by the mean drag coefficient and the combination of oscillating drag and lift force coefficient. Mean drag alone reduces the in-line displacement as shown in figure 5.1.16. This could be because drag force for this portion (above the sea bed and vertical) tends to increase the maximum tension and tensile stress, which opposes the riser displacement both in in-line and cross flow displacements. While, for the riser portion on the seabed (lumped mass 5), the mean drag force tends to straighten the riser, and positive and negative amplitudes of oscillating drag suppress the influence of the mean drag in affecting in-line displacement depending upon the levels of oscillating drag as for lumped mass 50. The combined effect of oscillating drag and lift force behaves in two ways. For a low level of the lift force coefficient, the oscillating drag increases the response while at a high level of the lift force coefficient, response increases with an increment of oscillating drag as shown in figure 5.1.17.

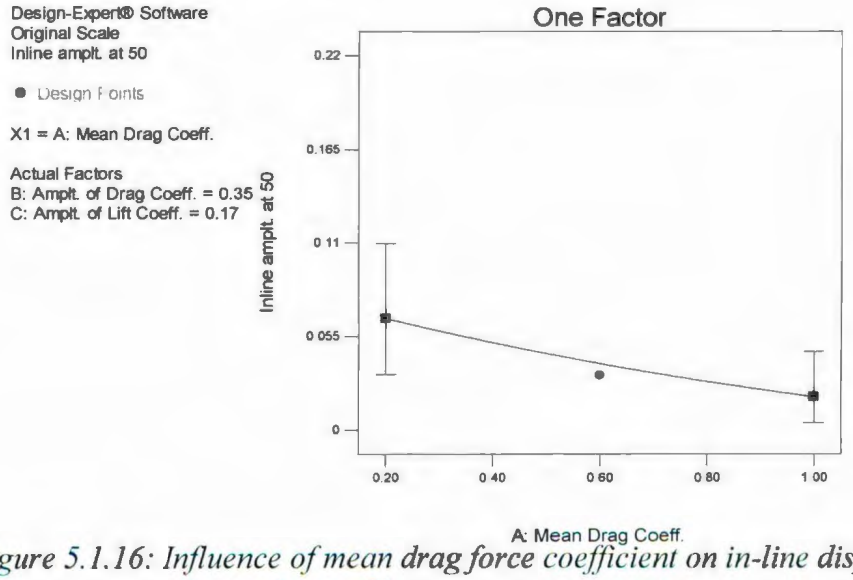

Figure 5.1.16: Influence of mean drag force coefficient on in-line displacement at lumped mass 50

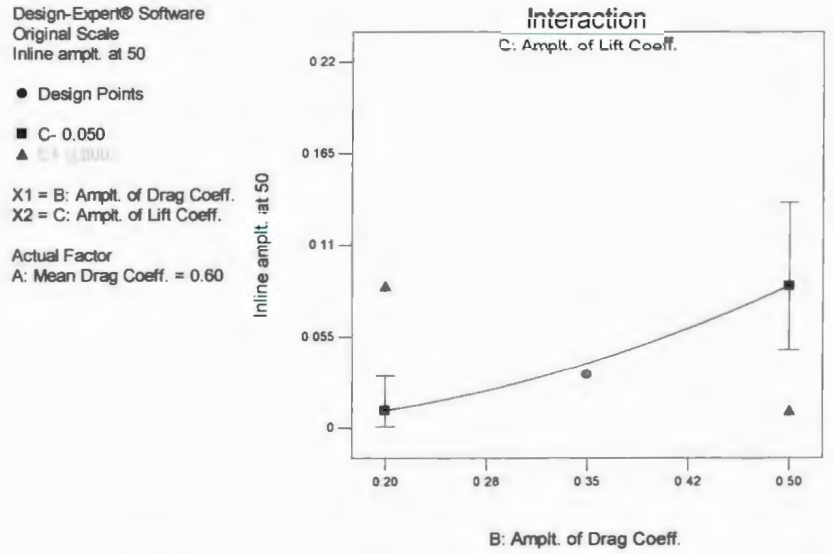

Figure 5.1.17: Influence of oscillating drag and lift force coefficient on in-line displacement at lumped mass 50

iii. At the top-end of the riser, i.e., mass 99, the combined effect of two factors, mean drag and lift force coefficient affects the in-line displacement. For a high level of lift force coefficient, mean drag increases the in-line displacement, while decreases the in-line displacement at the low level of lift force coefficient (figure 5.1.18).

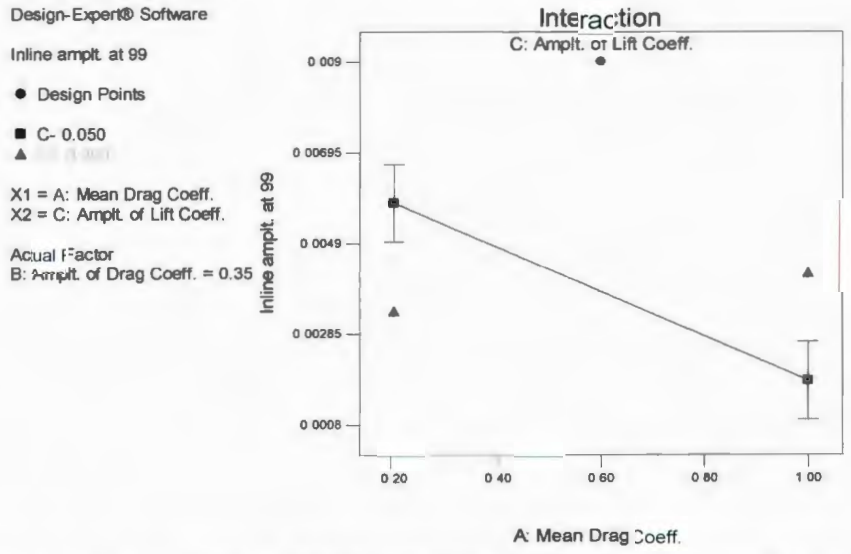

Figure 5.1.18: Influence of mean drag and lift force coefficient on in-line displacement at lumped mass 99

5.2 Analysis for sheared flow:

For the riser subjected to a sheared current flow, half factorial design was carried out. Along with the force coefficients, factors like internal pressure variation (because of internal fluid flow), and change in the position of the top-end of the riser were included. Higher order interaction of the main factors was confounded, where the main factors were aliased with other interaction of the main factors. The following parametric relationships were obtained after the proper statistical checks.

5.2.1 Maximum bending moment

Maximum bending Moment at the lowest end of the riser, i.e. the lumped mass 1, is mostly affected by the movement of the top end from the original position of the riser (towards the right from original position), followed by the mean drag and internal flow. The influence of the lift force and the oscillating drag force coefficients are almost negligible. When the riser top-end is moved away from its original position, the bending moment on riser segments decreased remarkably as shown in figure 5.2.1. Moving the riser top-end stretches length of the riser, and bending moment is decreased. The same parametric relationship exists for all considered lumped masses irrespective of their position on the riser.

Increasing internal fluid flow, which causes an increment of the pressure variation in the riser segments, has a positive effect on bending moment, i.e. increases the bending moment with the increment of pressure variation. However the increment is at a moderate level as shown in the figure 5.2.2. Internal pressure variation within the riser walls tends to straighten the bent portion of the riser, hence reduces the bending moment.

Among the force coefficients, the mean drag force coefficient was found to be significant. Depending on the riser positions, bending moment increases or decreases with the variations of drag force coefficients. Figure 5.2.3 shows the variation of bending moment with mean drag force coefficient at lumped mass 99. It shows the bending moment increases with the increased drag force. Hence, it can be concluded that

irrespective of the type of flow (uniform or shear), drag forces influence the bending moment depending on the riser positions.

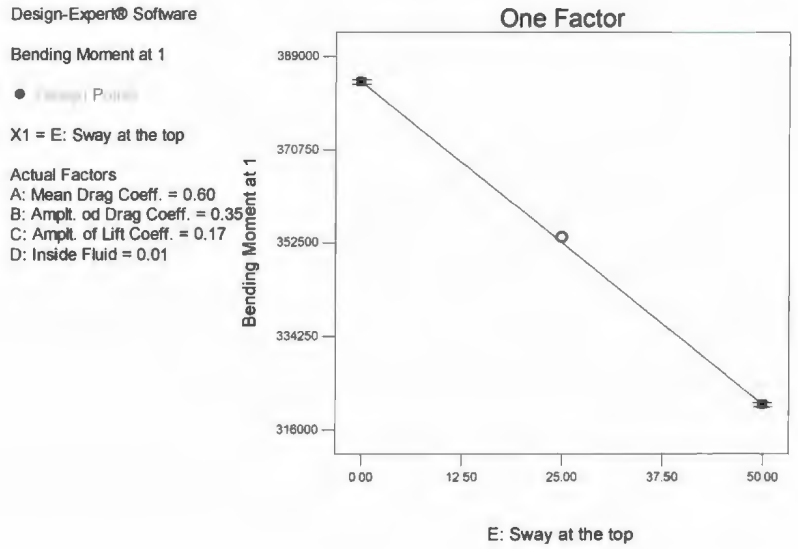

Figure 5.2.1: Influence of change in position of top-end of riser on max. BM

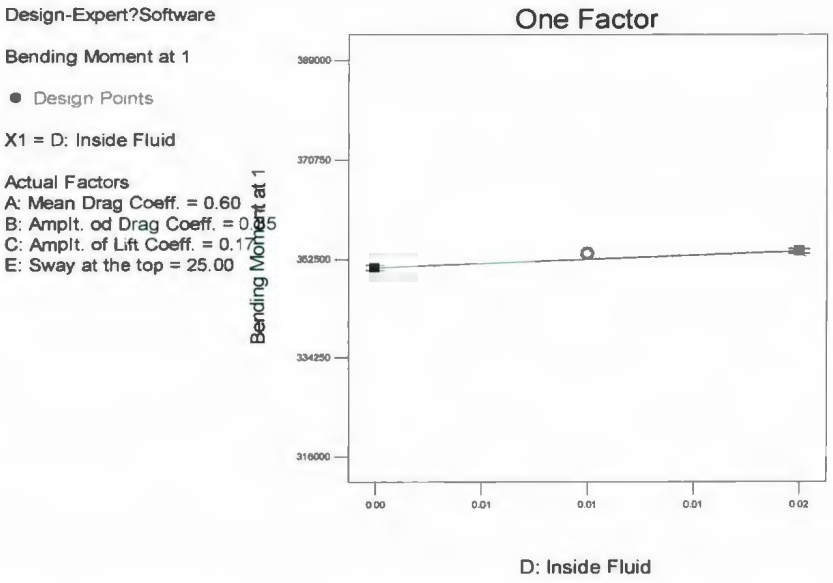

Figure 5.2.2: Influence of internal flow on max. BM at lumped mass 1

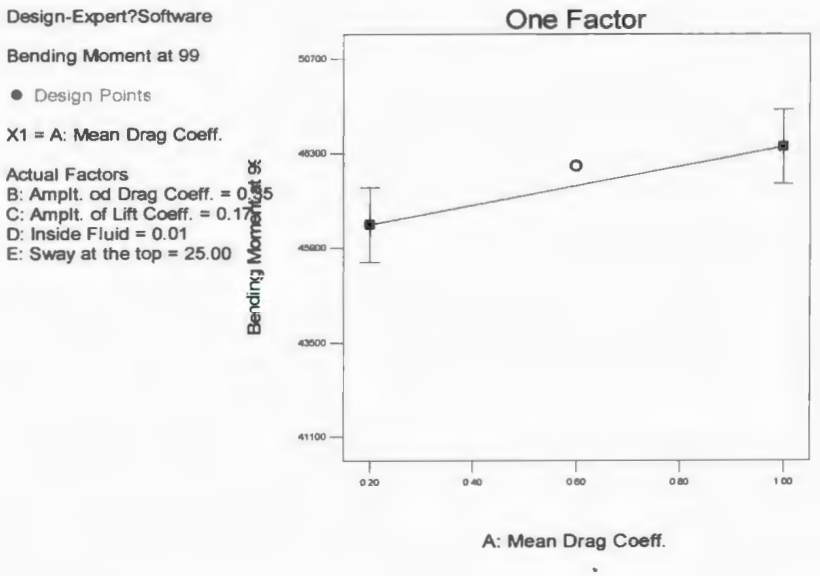

Figure 5.2.3: Influence of mean drag force coefficient on max. BM at lumped mass 99

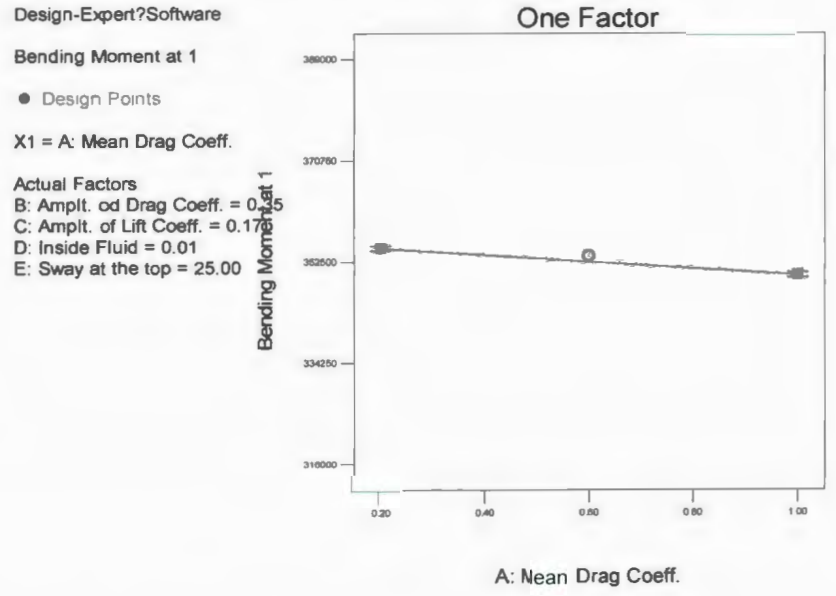

Figure 5.2.4: Influence of mean drag force coefficient on max. BM at lumped mass 1

5.2.2 Maximum Tension

Maximum Tension on a riser is affected by the pressure variation due to internal fluid flow (figure 5.2.5), followed by the riser movement at the top-end. Among the force coefficients, only the mean drag force increases the maximum tension. Unlike for other cases, the curvature was found significant for this response because of the direction of current along the riser length.

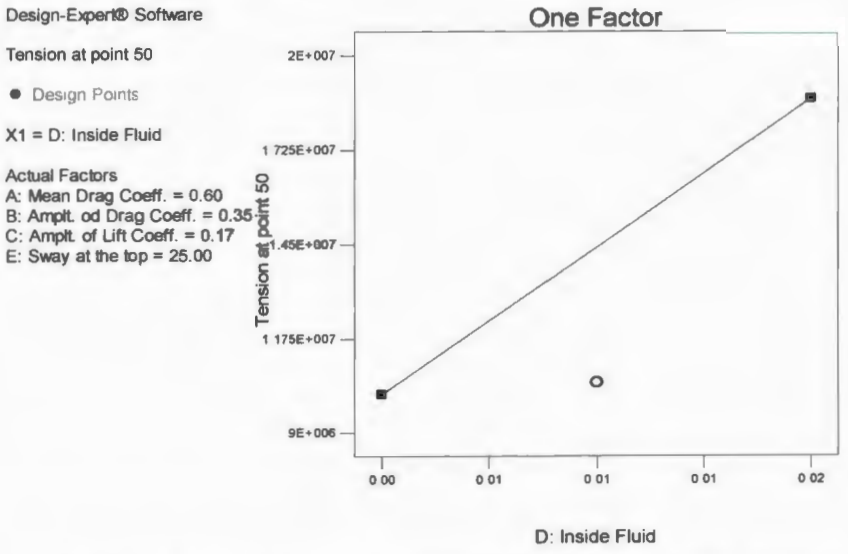

Figure 5.2.5: Influence of internal fluid flow on max. tension 50 at lumped mass

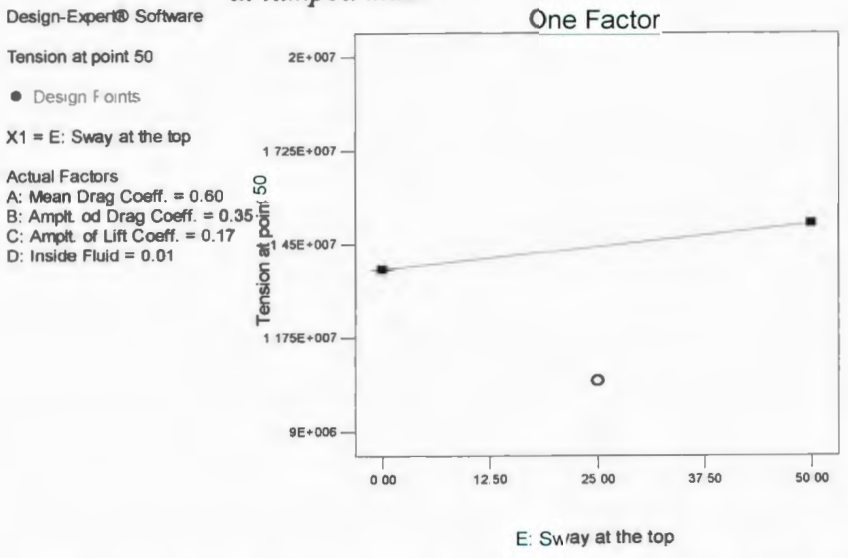

Figure 5.2.6: Influence of riser top-end movement on max. tension at lumped mass 50

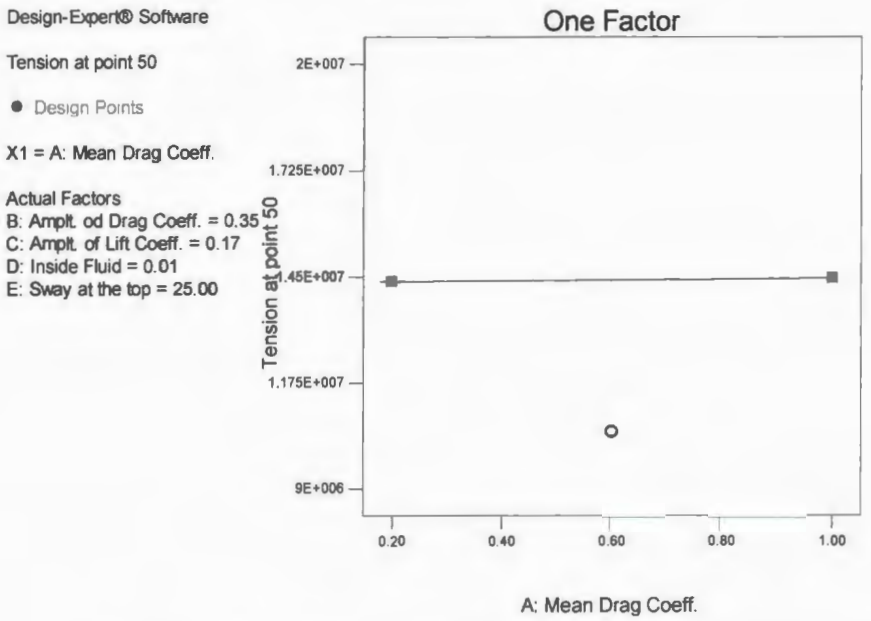

Figure 5.2.7: Influence of mean drag coefficient on max. tension at lumped mass 50

The same parametric relationships exist for the maximum tension with the factors considered irrespective of the position along the riser. Increasing the internal fluid within the riser induces an internal pressure, which in turn, increases the tension on riser segments. Moving the riser top-end away from its original position stretches the riser length, and will give rise to increased tension.

5.2.3 Maximum tensile stress

i. Tensile Stress on a riser segments is greatly affected by the internal fluid flow (figure 5.2.8).The movement of the riser top-end also increases the tensile stress as shown in figure 5.2.9, but this is not as high as the internal fluid flow.

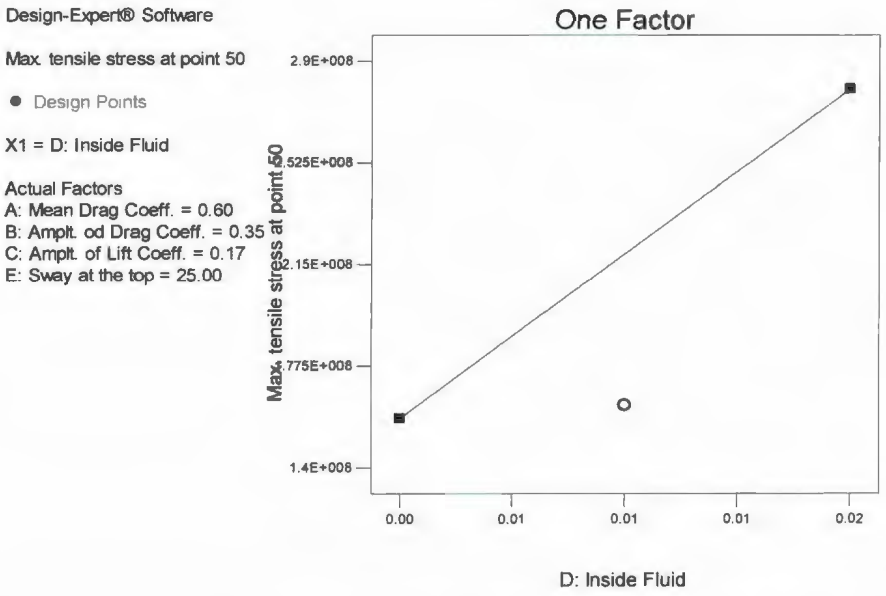

Figure 5.2.8: Influence of internal fluid flow on max. tensile stress at lumped mass 50

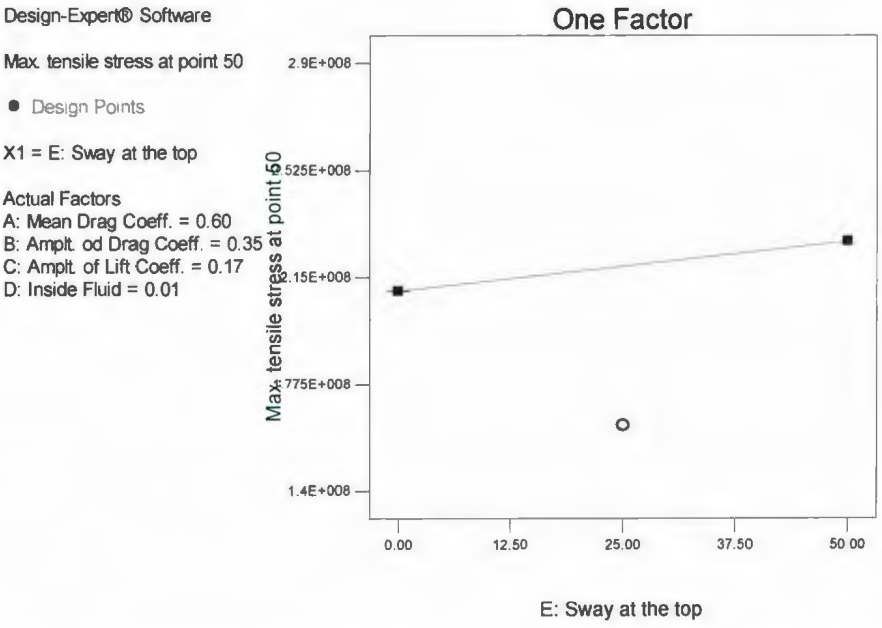

Figure 5.2.9: Influence of change in riser top-end position on max. tensile stress at lumped mass 50

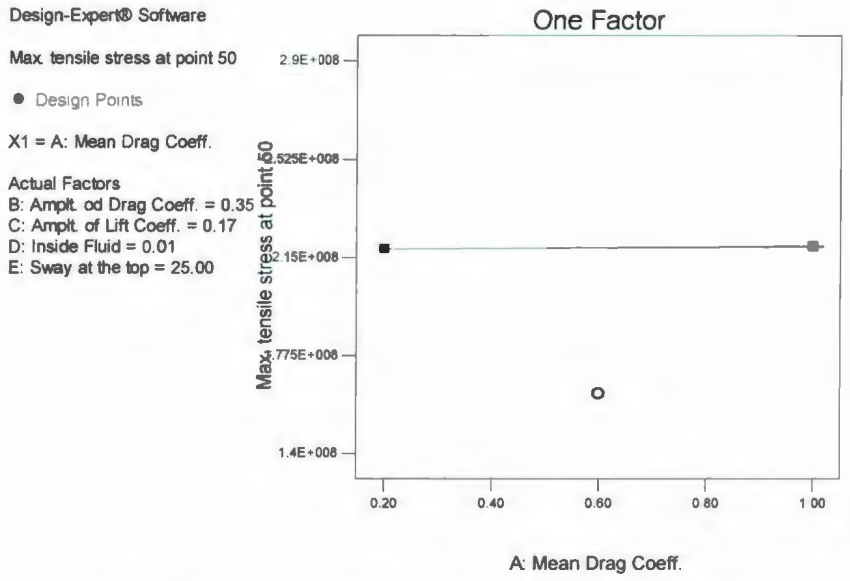

Figure 5.2.10: Influence of mean drag coefficient on max. tensile stress at lumped mass 50

Among the force coefficients, mean drag force coefficient increases the maximum tensile stress along the riser length as shown in figure 5.2.10.

ii. At the mass 99, there exists the combined effect of factors such as mean drag and internal fluid flow, mean drag and riser top-end movement AD, and AE. The effects of AD and AE remain constant on either range of factor levels (figure 5.2.11). Like the case for the tension, the curvature was significant due to the variation in current with water depth.

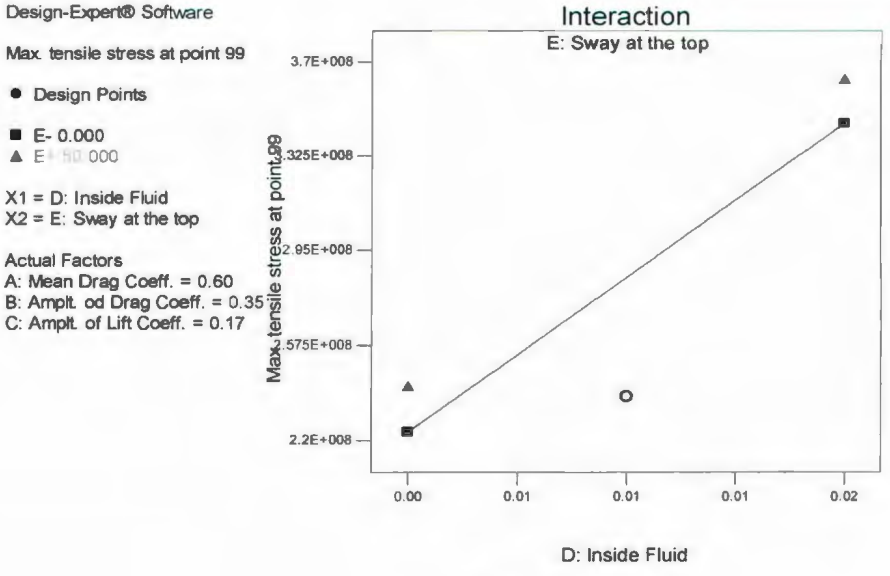

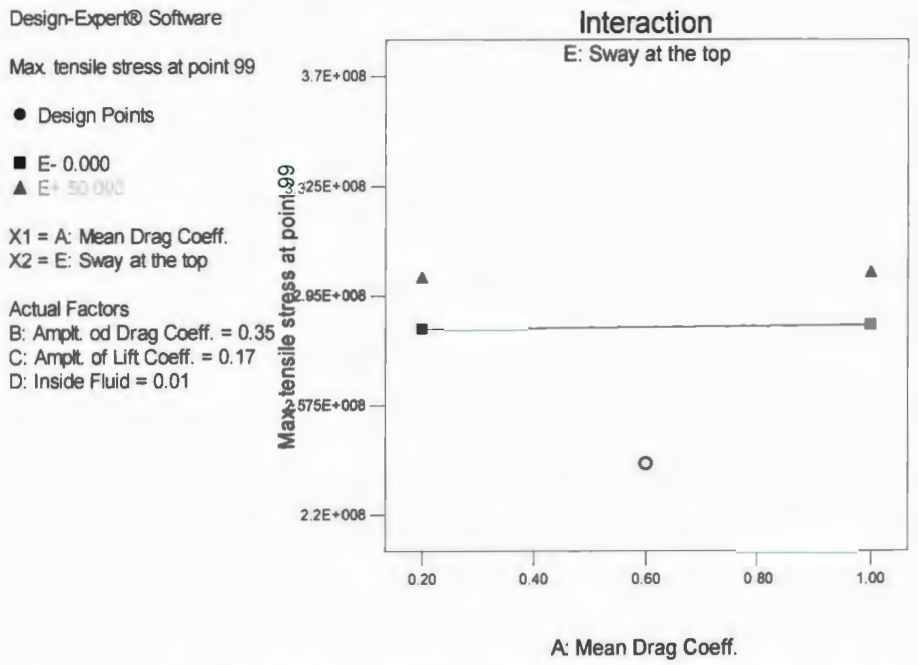

Figure 5.2.11: Effect Influence of change in riser top-end position with fluid flow and mean drag force coefficient on max. tensile stress at lumped mass 99.

5.2.4 Cross flow Displacement

i. Cross flow displacement is affected by the lift force coefficient. With an increment of lift coefficient, cross flow displacement increases. The mean drag force coefficient decreases the cross-flow displacement. A riser carrying the fluid inside of it experiences a high cross flow displacement. While the movement of top end of the riser in the inline direction decreases the cross flow displacement.

ii. There exists a combined effect of factors in affecting the cross flow displacement. For the point 5, AC, BD, AD, BD, CD and AE jointly affect the response. All the interaction of factors decrease the cross flow displacement for either of their levels except for BD and CD. With BD, oscillating drag force coefficient increases the cross flow displacement if the riser is carrying internal fluid flow (figure 5.2.12). However, oscillating drag force decreases the cross flow displacement if the riser is without

internal fluid. The lift force coefficient increases the cross flow displacement for low and high levels of internal fluid discharge.

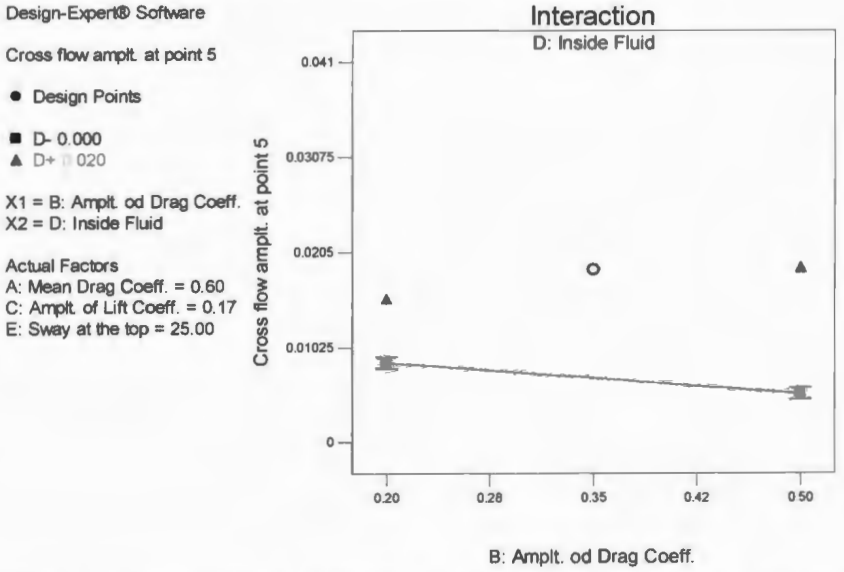

Figure 5.2.12: Influence of internal fluid flow and oscillating drag force coeff. on cross flow displacement

5.2.5 In-line Displacement

i. Mean drag force coefficient decreases the in-line displacement. The oscillating drag force coefficient increases the in-line displacement as shown in figure 5.2.13. Risers with internal fluid flow experiences less in-line displacement. A riser without internal fluid has less mass per unit length, for which in-line displacement can be higher than for the case when the riser is carrying fluid.

ii. At masses like 5 and 99, there exists a combined effect of oscillating drag force and internal fluid discharge. Oscillating drag greatly increases the in-line displacement for the lower level of discharge, while in-line displacement is reduced for the riser with high discharge in it (figure 5.2.14).

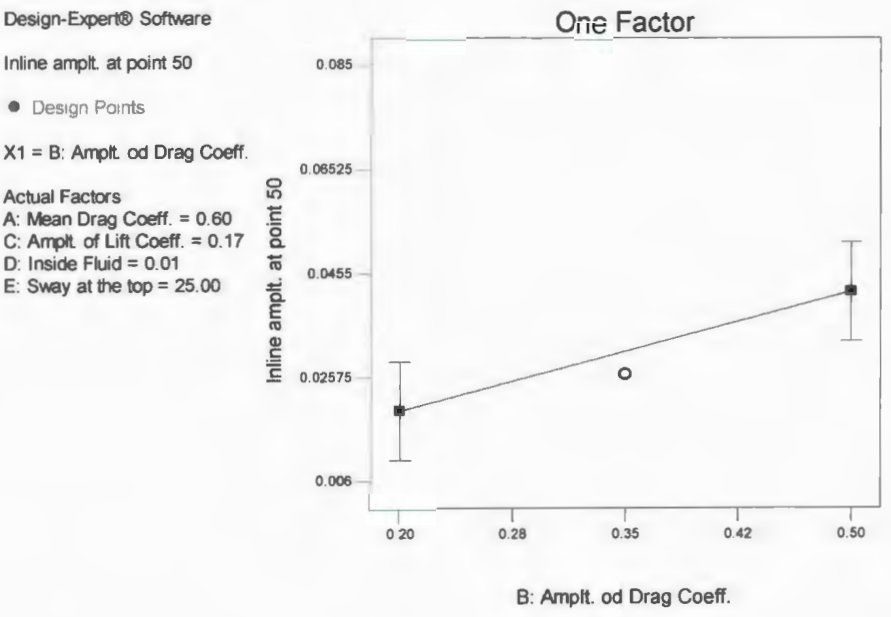

Figure: 5.2.13: Influence of oscillating drag coefficient on in-line displacement at lumped mass 50

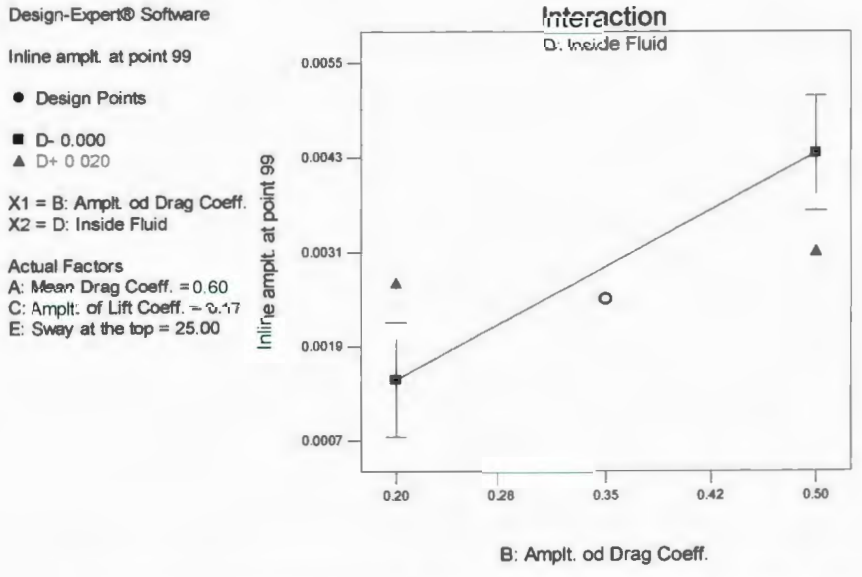

Figure 5.2.14: Influence of internal fluid and oscillating drag on in-line displacement

From the above analysis, it can be concluded that, bending moment is affected by the drag force coefficients, while the lift force coefficient has almost negligible effect. The maximum tensions and tensile stresses are highly affected by the drag force among the three force coefficients. Cross-flow displacement is affected by the lift force coefficient mostly, and at some lumped masses it was found lift force affecting the in-line displacement. The same relationships were found for the influence of the force coefficients irrespective of the type of current loading on the riser. After identifying the significant parameters, it was of interest to see whether there existed any significant changes in the riser responses with the changes of parameters within the expected ranges. For example, for the mean drag coefficient of 0.2, final maximum bending moment at lumped mass 1 was $3.63x10^2$ Nm, while for the value of 1, BM decreased to a value of $3.44x10^2$ Nm. So, with the increment of drag force coefficient from 0.2 to 1 (increment of mean drag coefficient by 400%), the bending moment magnitude decreased by 5.20 %. Also, oscillating drag force coefficient decreased the bending moment at the touchdown zone. For its value of 0.2, the bending moment at lumped mass 1 was $3.54x10^2$ Nm, and for the value of 0.5 (increment of oscillating drag by 150%), maximum bending moment decreases to 3.5310^22 Nm, showing a 0.38% fall in the magnitude.

Similarly, for other masses, change in the parameters within the expected range, showed the variation in the riser responses. The following tables (5.1 and 5.2) show the variation in bending moment at the top-end of the riser with the drag force coefficients.

A. Variation of maximum bending moment with drag force coefficients

Table 5.1: Variation of maximum BM with the mean drag force coefficient at lumped mass 1 for uniform flow

Mean-drag coefficient	***Bending Moment (Nm)***	***Increment in BM***
0.2	1.11×10^5	-
0.6	1.13×10^5	1.76%
1	1.14×10^5	0.87%

Table 5.1 shows the variation of maximum bending moment (after the transient state) with the mean drag force coefficient. It shows that with the change of mean drag force coefficient from 0.2 to 0.6 to 1 (changes by 200% and 67%), the bending moment changes just by the order of 1-1.5%. This variation of bending moment with mean drag force is for the case when oscillating drag is set at 0.35 and the lift force coefficient at 0.17. Similarly, for the case of mean drag force coefficient set at 0.6 and the lift force coefficient at 0.17, maximum bending moment at lumped mass 1 varies with the changes of oscillating drag force coefficient as shown in table 5.2

Table 5.2: Variation of maximum BM with the oscillating drag coefficient at lumped mass 1 for uniform flow

Oscillating drag coefficient	***Bending Moment (Nm)***	***% Increment in BM***
0.2	1.12×10^5	-
0.35	1.13×10^5	0.89%
0.5	1.135×10^5	0.45%

It can be seen from above table that changes in the oscillating drag coefficient (changes by 75% and 42%) leads to the variation of bending moment by order of only 0.5-1%.

B. Variation of maximum tension low with drag force coefficients

1) Tension on a riser segment is increased with the increment of mean drag coefficient. For example, tension measured at the top-end of the riser (at mass 100) at uniform flow for the mean drag coefficient of 0.2 was 1.203×10^7 N, while for the mean drag of 1, the measured tension was 1.230×10^7 N, showing 2.245% increment in the magnitude of tension as shown in table 5.3.

Table 5.3: Variation of maximum tension with mean drag force coefficient at lumped mass 100 for uniform flow

Mean-drag coefficient	***Tension (N)***	***% increment***
0.2	1.203×10^7	-
0.6	1.218×10^7	1.23%
1	1.230×10^7	0.98%

3) Similarly, oscillating drag coefficient increases the tension on a riser segment. Tension magnitude increases by 0.37% when the oscillating drag increases from 0.2 to 0.5 (increment of 15%) as shown in table 5.4.

Table 5.4: Variation of maximum tension with the oscillating drag coefficient at lumped mass 100 for uniform flow

Oscillating drag coefficient	***Tension (N)***	***% increment***
0.2	1.215×10^7	-
0.35	1.218×10^7	0.24%
0.5	1.219×10^7	0.12%

C. Variation of maximum tensile stress with drag force coefficients

1) Drag force coefficient increases the maximum tensile stress on a riser segments. Increasing the mean drag coefficient from the range of 0.2 to 1 causes tensile stress measured at lumped mass 99 of the riser to increase by 2.465% as illustrated in table 5.5.

2) In the same manner, oscillating drag coefficient increases the tensile stress on a riser. With the increment of oscillating drag from 0.2 to 0.5, the maximum tensile stress at lumped mass 99 increases by 2.45% only as shown in table 5.6.

Table 5.5: Variation of maximum tensile stress with mean drag coefficient at lumped mass 99 for uniform flow

Mean-drag coefficient	***Tensile stress* (N/m^2)**	***% increment***
0.2	1.754×10^8	-
0.6	1.776×10^8	1.24%
1	1.797×10^8	1.17%

Table 5.6: Variation of maximum tensile stress with oscillating drag force coefficient at lumped mass 99 for uniform flow

Oscillating drag coefficient	***Tensile stress* (N/m^2)**	***% increment***
0.2	1.772×10^8	-
0.35	1.776×10^8	0.22%
0.5	1.779×10^8	0.18%

D. Variations of the cross-flow displacement with lift force coefficient

Cross flow displacement for the riser is mainly affected by the lift force coefficient. Table 5.7 shows the variations of the cross-flow displacement measured at the lumped mass 99, when mean and oscillating drag force coefficients are set at 0.6 and 0.17 respectively.

Table 5.7: Variation of cross flow displacement with oscillating lift force coefficient at lumped mass 99 for uniform flow

Oscillating lift coefficient	***Cross-flow displacement (m)***	***% increment***
0.05	0.000911	-
0.17	0.00283	210%
0.3	0.003305	16.78%

Changing the lift force coefficient from 0.05 to 0.17 (by 240%) causes cross flow displacement to increase by 210%, which is significant variation with respect to the changes in the lift force coefficient (table 5.7). Also, changing the lift from 0.17 to 0.3 (changes by 77%) causes the cross-flow displacement changes by 16.78%. It shows the lift force coefficient changes the cross flow displacement of a riser by significant order.

E. Variation of in-line displacement with mean drag force coefficient

In-line displacement is affected by factors like mean drag coefficient and also the interaction of mean drag and lift force coefficient (for lumped mass 99). Different lumped masses respond differently for the in-line displacement. For the lumped mass 50, the combined effect of oscillating drag and lift force exists. However, mean drag force coefficient decreases the in-line displacement at the top-end of the riser. Table 5.8 shows variation in the in-line displacement at the lumped mass 50, for the lift force coefficient of 0.17 and oscillating drag of 0.35.

Table 5.8: Variation of in-line displacement with mean drag force coefficient at lumped mass 50 for uniform flow

Mean- drag coefficient	***In-line displacement***	***% decrement***
	(m)	
0.2	0.0654	-
0.6	0.032	51.04%
1	0.0192	40%

For the case of in-line displacement, the main factors along with the interaction of the factors exist in affecting the magnitude of the response. However, over some portions of the riser, the drag force coefficient decreases the in-line displacement. From the above table, it shows there is a significant change in the in-line displacement with the higher levels of change in the mean drag coefficient.

F. Variation of maximum bending moment with position of top-end of riser

Besides the force coefficients, factors like internal fluid flow and change in the top-end of riser position affect the structural responses of a riser. Moreover, these factors dominate force coefficients in affecting responses like tension and tensile stress on riser segments.

For example, bending moment at lumped mass 50 was varied when the riser top-end was moved from its original position. Drifting the riser position from 0 to 50m decreases the maximum bending moment by 12.29%. Table 5.9 shows the variation in bending moment when the riser is moved to 50 meter away from its original position.

The riser top-end position also changes the maximum tension and tensile stress on a riser segment.

Table 5.9: Variation of maximum BM with position of the riser top-end at lumped mass 50 for sheared flow

Movement of the riser (m)	***Bending Moment (Nm)***	***% decrement***
0	1.09×10^5	-
25	1.02×10^5	5.76%
50	9.56×10^4	6.29%

Also, increasing the level of riser top-end position, maximum tensile stress on riser segments increases by significant order.

G. Variation of maximum tension and tensile stress with internal fluid flow

With the increment of internal fluid flow, the tension on riser segments increases significantly. For mean drag coefficient of 0.6, oscillating drag of 0.35 and lift force coefficient of 0.17, and the riser top-end at 25m from its original position, the following table shows the variation in the maximum tension at lumped mass 50 with the variation of internal flow discharge.

Table 5.10: Variation of maximum tension with the internal fluid flow at lumped mass 50 for sheared flow

Internal fluid flow (m^3/s)	***Tension (N)***	***% increment***
0	1.012×10^7	-
0.02	1.872×10^7	84.91%

This shows the higher variation of maximum tensions on riser segments, with position of the riser top-end. Similarly, internal fluid increment highly increases the maximum tensile stress on riser segments as is shown in table 5.11.

Table 5.11: Variation of maximum tensile stress with internal fluid flow at lumped mass 50 for sheared flow

Internal fluid flow	***Tensile stress***	***% increment***
(m^3/s)	**(N/m^2)**	
0	1.580×10^8	-
0.02	2.796×10^8	76.96%

Chapter 6

Conclusion and Recommendation

6.1 Summaries and conclusions:

The lumped mass model of the riser adopted in the code used in this study was useful in understanding the structural responses of various segments of the riser. The primary deformations of the riser were assumed to be due to longitudinal and flexural vibrations and torsional or shear deformations were not considered. The code was validated partially by conducting dynamic simulations of the riser under known constant loads, starting from non-equilibrium initial conditions. The sensitivity of the model to parameters such as drag and lift force coefficients and internal fluid flow, was studied considering a steel catenary riser pinned at both ends. The Design of experiment method was found to be an effective statistical methodology in understanding the parametric relationships of the riser during VIV. Using this methodology, significant parameters were determined in affecting riser responses, which in turn reflected the sensitivity of the riser responses with changes in the parameters. Full factorial simulations were carried out to study the sensitivity of force coefficients on the riser responses, measured in terms of its maximum bending moment, maximum tension and tensile stress, cross flow displacement and in-line displacement, where the riser was subject to uniform flow. The selection of ranges for the force coefficients were based on Reynolds number only. Other factors such as internal fluid flow and the change in riser top-end position were included along with force coefficients, where the riser was subjected to a sheared flow.

The following is a summary of the results, which shows the sensitivity of the parameters considered on the riser responses.

A. Force coefficients

i. Mean drag force coefficient affects the bending moment of the riser highly in comparison with other force coefficients. Depending upon the riser position,

the drag force coefficient increases or decreases the bending moment. For expected ranges of the mean drag force coefficient (0.2-1), the bending moment changes by order of 1-1.5%. Similarly, changing oscillating drag force coefficient from 0.2 to 0.5 causes the bending moment increase just by 0.5-1%. Mean drag force coefficient causes a larger influence on bending moment compared to oscillating drag and lift force.

ii. Maximum tension and tensile stress on a riser is highly affected by the mean drag force coefficient followed by the oscillating drag. Lift force coefficient doesn't have significant effect. Within the expected ranges of changes in the force coefficients (mean drag from 0.2 to 1 and oscillating drag from 0.2 to0.5), maximum tension and tensile stress on riser segments change only by the order of 0.5-2%.

iii. Variations of force coefficients, mainly mean drag and lift force, within the expected ranges, affect widely the in-line and cross-flow displacement of a riser. Changing the lift force coefficient from 0.05 to 0.3 increases the cross-flow displacement by the order of 50-200%. Hence, attention should be given in the selection of the proper force coefficients for the case of displacements.

The behavior of riser responses with the force coefficients remains the same irrespective of the current loading (uniform or shear). Mean drag force affects riser responses such as bending moment, maximum tension and tensile stress highly in comparison to other coefficients. Lift force coefficient increases the cross-flow displacement more highly than other coefficients and affects in-line displacement depending on riser positions.

B. Riser top-end movement and internal fluid flow

i. A change in the riser top-end position with respect to its original position highly affects the bending moment. For example, moving riser top-end by 25m to right direction (away from anchor) from its original position increases

the bending moment by order of 6.7%. Movement of riser top-end increases the bending moment more highly than the internal fluid flow, while, it has little effect in variations of maximum tension and tensile stresses.

ii. Increasing the internal fluid flow causes a significant increase in maximum tension and tensile stress. However, it doesn't influence the bending moment highly as by the riser top-end movement.

6.2 Recommendations

This study was made for a parametric study on a long, elastic and flexible catenary riser configuration. The riser considered in this study was long and flexible and was divided into 100 lumped masses for which analyzing responses of all the lumped masses were not possible. The study was for a certain configuration of a riser and with certain boundary conditions. It is recommended to carry out parametric study on other riser configurations such as vertical riser with different boundary conditions.

During the validation of the code, proper experimental data were not available, for which there were problems in setting up parameters for the simulation to match the setup parameters in the experiments. The ability for the program to simulate a real experiment and produce comparable results was a very encouraging finding, but it is difficult to find tests that clearly state their setup parameters and/or results clearly. It is recommended to set up own tests to compare the riser program against. This way the testing parameters are known and specific properties can be changed.

Riser-sea bed interaction is a challenging aspect in the riser design and analysis. The code can be modified to account for riser-sea bed interaction to study the parametric relationships of riser responses in detail.

References

Allen, D.W., Koop, E.H. F., Langer, C.G., Phifer. and Swanson, R.C. (1994). Design and installation of Auger steel catenary risers. Paper OTC 7620, presented at the Offshore Technology Conference, Houston.

Anagnostopoulos, P. (2000). Numerical study of the flow past a cylinder excited transversely to the incident stream. Part 1: Lock-in zone, hydrodynamic forces and wake geometry. Journal of Fluids and Structures 14 (6), 819–851.

Baddour, R.E. and Nair, Raman, W. (2003). Three-Dimensional Dynamics of a Flexible Marine Riser Undergoing Large Elastic Deformations.Multibody System Dynamics. (10), 393-423.

Baek, S.J., Lee, S.B. and Sung, H.J. (2001). Response of a circular cylinder wake to superharmonic excitation. Journal of Fluid Mechanics 442, 67–88.

Banerjee, A.K. and Nagarjan, S. (1997). Efficient simulation of large overall motion of beams undergoing large deflection, Multibody System Dynamics. 1(1), 1997, 113-126.

Bearman, P.M. (1984). Vortex shedding from oscillating bluff bodies. Annual review of Fluid Mechanics. (16), 195-222.

Bearman, PW., Chaplin, J.R., V.F.J. and Pattenden, R.J. (2004). Laboratory Measurements of Vortex-Induced Vibrations of a Vertical Tension Riser in a Stepped Current Flow Induced Vibration. (21), 3-24.

Bishop, R.E.D. and Hassan, A.Y. (1963). The lift and drag forces on a circular cylinder oscillating in a flowing fluid. Department of Mechanical Engineering, University of College London.

Blake, W.K. (1986). Mechanics of Flow-Induced Sound and Vibration, (1). Academic Press, New York.

Blackburn, H.M. and Melbourne, W.H., (1996). The effect of free-stream turbulence on sectional lift forces on a circular cylinder. Journal of Fluid Mechanics 306, 267–292.

Blackburn, H.M. and Henderson, R.D., (1999). A study of two-dimensional flow past an oscillating cylinder. Journal of Fluid Mechanics 385, 255–286.

Blackburn, H.M., Govardhan, R.N. and Williamson, C.H.K. (2001). A complementary numerical and physical investigation of vortexinduced vibration. Journal of Fluids and Structures 15 (3–4), 481–488.

Blevins, R.D. (1990). Flow-Induced Vibration, 2nd edition, Van Nostrand Reinhold, New York.

Bloor, M.S. (1964). The transition to turbulence in the wake of a circular cylinder. Journal of fliud Mechanics. (19), 290-304.

Coast, Oc. Engrg, Port. and Wtrwy, J. (2004). Experimental Study on Vortex Induced Vibrations of Highly Flexible Immersed Pipe Subjected to Top End Oscillations. (130), 207-214.

D. Hawkins and L. M. Lye. (2006). Use of DOE methodology for Investigating Conditions that Influence the Tension in Marine Risers for FPSO Ships. Flexible Design Ltd, St. John's, NL.

Easton, J. Valerie. and Coll. John. (1997). Statistics Glossary. Volume 1. STEPS . www. Stats.gla.ac.uk.

Fredsoe, Jorgen. and Sumer, B. Mutlu. (1997). Hydrodynamics Around Cylindrical Strucutres, Advanced Series on Ocean Engineering. World Scientific Publishing Co.Pte.Ltd. (12).

Gerrard, J.H. (1978). The mechanics of the formation region of vortices behind bluff bodies. Journal of Fluid Mechanics. (25), 401-413.

Govardhan, R., Jauvtis, N. and Williamson, C.H.K. (2002). Multiple Modes of Vortex-Induced Vibration of a Sphere. Sibley School of Mechanical and Aerospace Engineering, Upson Hall Cornell University, Ithaca, NY.

Govardhan, R. and Williamson, C.H.K. (2004). Vortex-Induced Vibrations. Annual Review of Fluid Mechanics. (36), 413-455.

Graham, R., Michael, J. and Willden, H.J. Richard. (2003). Multi-modal Vortex-Induced Vibrations of a vertical riser pipe subject to a uniform current profile. European Journal of Mechanics B/Fluids. (23), 209–218.

Griffin, O.M. (1971). The unsteady wake of an oscillating cylinder at low Reynolds number, Journal of Applied Mechanics. (38), 729-738.

Griffin, O. M. (1984). Current-Induced Loads on Marine Structures Due to Vortex Shedding. Proceedings of the 1984 Ocean Structural Dynamics Symposium, 457-471, Oregon State University, Corvallis, Oregon, September 11-13, 1984.

Griffin, O.M. (1984). Hydrodynamic Drag On and Vibration of Marine Risers and Cables. Fiscal Year 1984 Progress Report, Naval Research Laboratory, Washington, D.C.

Griffin, O.M. and Ramberg, S.E. (1974). The vortex shedding from a cylinder vibrating in line with an incident uniform flow. Journal of Fluid Mechanics. (66), 553-76.

Griffin, O.M. and Ramberg, S.E. (1982). Some recent studies of vortex shedding with application to marine tubulars and risers. ASME Journal of Energy Resource Technology. (104), 2-13.

Guesnon, J.C. Gillard. and E. Laval. (2000). A riser for ultra-deepwater drilling. World Oil. 221(4), 90.

Guilmineau, E. and Queutey, P. (2002). A numerical simulation of vortex shedding from an oscillating circular cylinder. Journal of Fluids and Structures 16, 773–794.

Hatton, Stephen, A., Willis, Neil. and 2H Offsshore Engineering Limited. (1998). Steel Catenary Risers for Deepwater Environments. Offshore Technology Conference, (2), 29-42.

Hong, Y.P., Koterayama, Wataru. and Nakamura, M. (2002). An Experimental and Numerical Study on Dynamics of Flexible Free Hanging Riser. Nakamura and Wataru Koterayama Kyushu University H. Osawa Japan Marine Science and Technology Huston, R.L. (1990). Multibody Dynamics. Butterworth-Heinemann, Boston, MA. 350-357.

Huse,E. (1996). Experimental Investigation of Dee Sea Riser Interaction. Offshore Technology Conference, Houston, May 1996.

Irvine, Max. H. (1981). Cable Structures. The MIT Press, Cambridge, Massachusetts, and London, England.

Kozicz, John, and Newman, Steven, (2005). Reconfigurable Riser Enabling Drilling Solutions for the Future. AADE 2005 National Technical Conference and Exhibition.

Jong, Jen-Yi, and Vandiver, J. Kim, (1981).Response Analysis of the Flow Induced Vibration of Flexible Cylinders tested at Castine, Maine. Department of Ocean Engineering, Massachusetts University.

Jordan, S.K. and Fromm, J.E. (1972). Oscillatory drag, lift, and torque on a cylinder in a uniform flow. Physics of Fluids 15, 371–376.

Kwok, K.C.S. (1986). Turbulence effect on flow around circular cylinder. Journal of Engineering Mechanics, ASCE. 112(11), 1181-1197.

Ladopoulos, E.G. (2005). Non-linear dynamic analysis by three-dimensional ordinary differential equations. Journal of Engineering Computations, (22) Issue: 4 Page: 453-479.

Liao, Jung-Chi. (2002). Vortex-Induced Vibration of Slender Structures in Unsteady Flow. Massachuetts Institute of Technology.

Lighthill, J. (1986). Fundamentals concerning wave loading on offshore structures. Journal of Fluid Mechanics. (173), 667-81.

Montgomery, D. C. (2005). Design and Analysis of Experiments. 6th Edition. John Wiley and Sons, Inc.

Mourelle, M.M., Petrobrass, S.A., Ribeiro, E.J.B. and Roveri, F.E. (1998). Dynamic Compression Buckling in Flexible Riser. Offshore Technology Conference, (2), 19-27.

Panton, R.L. (1996). Incompressible Flow. New York. John Wiley & Sons, INC.

Phifer, E.H., et al. (1994). Design and Installation of Auger Steel Catenary Risers. OTC Paper No. 7620. Proceedings of the 26th Offshore Technology Conference, Houston, Texas, USA.

Posdziech, O. and Grundmann, R. (2000). A systematic approach to the numerical calculation of fundamental quantities of the twodimensional flowover a circular cylinder. Journal of Fluids and Structures 1–25.

Ribeiro, J.L.D. (1992). Fluctuating lift and its spanwise correlation on a circular cylinder in a smooth and in a turbulent flow: a critical review. Journal of Wind Engineering and Industrial Aerodynamics 40, 179–198.

Sarpkaya, T. (2004). A critical review of the intrinsic nature of Vortex Induced vibrations. Journal of Fluid and Structures. (19), 389-447.

Sarpkaya, T. (1995). Hydrodynamic damping, flow induced oscillations, and biharmonic response. ASME journal of offshore mechanics and arctic engineering. (117), 232-238.

Schewe, G. (1983). On the force fluctuations acting on a circular cylinder in cross flow from subcritical up to transcritical Reynolds numbers. Journal of Fluid Mechanics. (133), 265-285.

Schlitching, G. (1979). Boundary Layer Theory. 7.ed. McGraw-Hill Book Company.

Schulz, K.,and Kallinderis, Y.(1998). Numerical Prediction of Flow-Structure Interaction for Cylinders Undergoing VIV. Offshore Technology Conference, Houston, Texas, May 4-7.

Sparks, Charles P. (2007). Fundamentals of Marine Riser Mechanics: Basic Principles and Simplified Analysis. PennWell Books.

Sumer, B.M. and Fredose, J. (1997). Scour around a Large Vertical Circular Cylinder in Waves. Proc. 16th International Offshore and Arctic Engineering Conference. 13-18.

Sumer, B.M. and Fredose, J. (1997). Hydrodynamics around cylindrical Structures. Eorld Scientific.

Vandiver, J.K. (1992). Dimensionless Parameters Important to the Prediction of Vortex-Induced Vibration of a Long Flexible Cylinders in Ocean Currents. Department of Ocean Engineering, Massachusetts, USA.

West, G.S. and Apelt, C.J. (1993). Measurements of fluctuating pressures and forces on a circular cylinder in the Reynolds number range. Journal of Fluids and Structures. (7), 227-244.

Williamson, C.H.K. (1988). The existence of stages in the transition to three-dimensionality of a cylinder wake. Physics of Fluids. (31).